Alma Mater Studiorum – Università di Bologna

DOTTORATO DI RICERCA IN

Biologia Cellulare e Molecolare

Ciclo 34

Settore Concorsuale: 03/C1- CHIMICA ORGANICA

Settore Scientifico Disciplinare: CHIM/06 - CHIMICA ORGANICA

ADVANCED CELL CULTURE PLATFORMS: METHODS FOR DRUG TESTING WITH MICROFLUIDICS AND MICROSTRUCTURED DEVICES

Presentata da: Ottavia Tartagni

Coordinatore Dottorato

Prof. Vincenzo Scarlato

Supervisore

Prof. Giampaolo Zuccheri

Esame finale anno 2022

Advanced cell culture platforms: methods for drug testing with microfluidics and microstructured devices

Ottavia Tartagni, Bologna - January 2022

University of Bologna
Department of Pharmacy and Biotechnology (FaBiT)
ottavia.tartagni3@unibo.it

INDEX

Abstract

Advanced cell culture systems are developing rapidly in biomedical research. Drug pharmacokinetics and metabolism have traditionally been assessed using traditional cell culture techniques. Current *in vitro* models frequently fail to capture human tissue architecture, necessitating a solid dependence on *in vivo* testing in preclinical species with metabolic pathways, disease processes, and toxicity patterns distinct from humans. Nowadays, various approaches and technologies are being used to challenge the difficulty of recreating the complexity of entire tissues *in vitro*. However, these culturing systems present limitations from requiring high costs, providing not easily scalability and customization. Here, we present two versatile and cost-effective methods for developing culturing systems that integrate 3D cell culture and microfluidic platforms.

Firstly, for basic studies and therapeutic applications, a large number of high-quality cell spheres of homogeneous size and shape are required. Conventional approaches usually have a dearth of control over the size and geometry of cell spheres and require sample collection and manipulation. To overcome this difficulty, we prototyped microstructured cell culture inserts to generate highly homogeneous spheroids from different cell lines. The prototype device was designed to contain more than 400 microwells with the purpose of providing a robust and effective tool for *in vitro* drug testing. We demonstrated the use of this platform to generate size-controlled microtumors from a variety of human cancer cell lines. Using a human colorectal cancer cell line was investigated the drug response of spheroids cultured in our device. Compound effects were successfully observed through viability, growth, and morphologic investigations. Low-melting-point agarose inclusion provided a useful way for immunostaining and microscopy analysis.

Furthermore, we fabricated a microfluidic device suitable for selective cell culture treatments. The microfluidic device was utilized to reproduce and confirm *in vitro* investigations carried out using normal culture methods. The device layout and the syringe pump system, entirely designed in our laboratory, successfully allowed culture growth and medium flow regulation. The platform can be fully compatible with different cell lines; we chose to test the microglia cell line (N9) in cell communication and neuroinflammation research. The designed fluidic chip hosted two separated culture chambers that can be put in communication. Also, through fluid dynamic simulation, solution flows can be finely controlled, and it is possible to perform treatments and immunofluorescence in one single chamber selectively. Our microfluidic system appeared as a promising *in vitro* platform for drug screening and cell interaction investigations.

To conclude, we propose the development of two culturing platforms, which are the result of separate scientific investigations but have the primary goal of performing drug treatments in a reproducible manner. Our devices shall improve future studies on drug exposure testing, representing adjustable and versatile cell culture systems.

1. INTRODUCTION

1.1 Scaling up from standard 2D monolayers to advanced cell culture techniques

Two-dimensional (2D) cell culture has been the method used to culture cells since the early 1900s (Ferreira et al. 2018). Cell culture investigations have traditionally been carried out with multi-well plates, petri dishes, and tissue culture flasks, in which the cells are plated onto a rigid planar surface. These traditional 2D substrates have significantly advanced our understanding of basic cell activity due to their ease of use and high cell viability. They are, however, unable to accurately mimic the cellular milieu *in vivo*, resulting in not physiologically relevant cell responses in the vast majority of situations. Many important discoveries have been achieved using traditional 2D cultural methodologies, however, many research works have frequently proven the drawbacks of 2D flat platforms (Barralet et al. 2005; J. Lee et al. 2009).

At all length scales, cells intrinsically respond to chemical (e.g., surface chemistry and material composition) and physical (e.g., mechanical and structural qualities) stimuli from their surroundings (Lukashev and Werb 1998; Geiger, et al. 2009). Nearly all cells live in a complex three-dimensional (3D) fibrous structure known as the extracellular matrix (ECM) in their natural habitat (Lee et al. 2008; Wang et al. 2011). The ECM's 3D nanostructure, which is unique to each cell type, supports and guides the cell functions. In 2D cell culture, disordered cell–cell interactions, high oxygen tension, and high growth factor concentrations can significantly change inter and intracellular behavior (El-Ali et al. 2006). Furthermore, when cells are cultured on a flat 2D substrate, they dramatically adapt and change their morphology, proliferate abnormally, and frequently lose their differentiated phenotype, resulting in abnormal cellular behavior. It is well understood that alterations in gene transcription and protein translation, as well as cytoskeleton remodeling and abnormal cell signaling, can occur because of such structural changes to the physical environment. This reductionist approach to comprehending basic biological processes has merit, but it is limited since cells growing on 2D substrates do not always mimic their native counterparts in real tissues. The development of more robust *in vitro* models capable of reproducing *in vivo* solid tumors could improve the efficacy of anti-cancer drug discovery and screening. Moving from simple technologies to sophisticated approaches, the development of such models may help to reduce the number of false-positive results produced during preclinical validation of novel compounds, as well as improve the *in vitro/in vivo* correlation (***Figure 1***).

The principal advanced culturing technologies include scaffold-free/scaffold-based spheroids generation; organoids; microfluidic platforms for culturing 2D and 3D cells; organ-on-chips to

7

simulate tissue and organ function and 3D bioprinting which combines cells, growth factors and biomaterials to fabricate complex organs for regenerative medicine purposes (Mirbagheri et al. 2019).
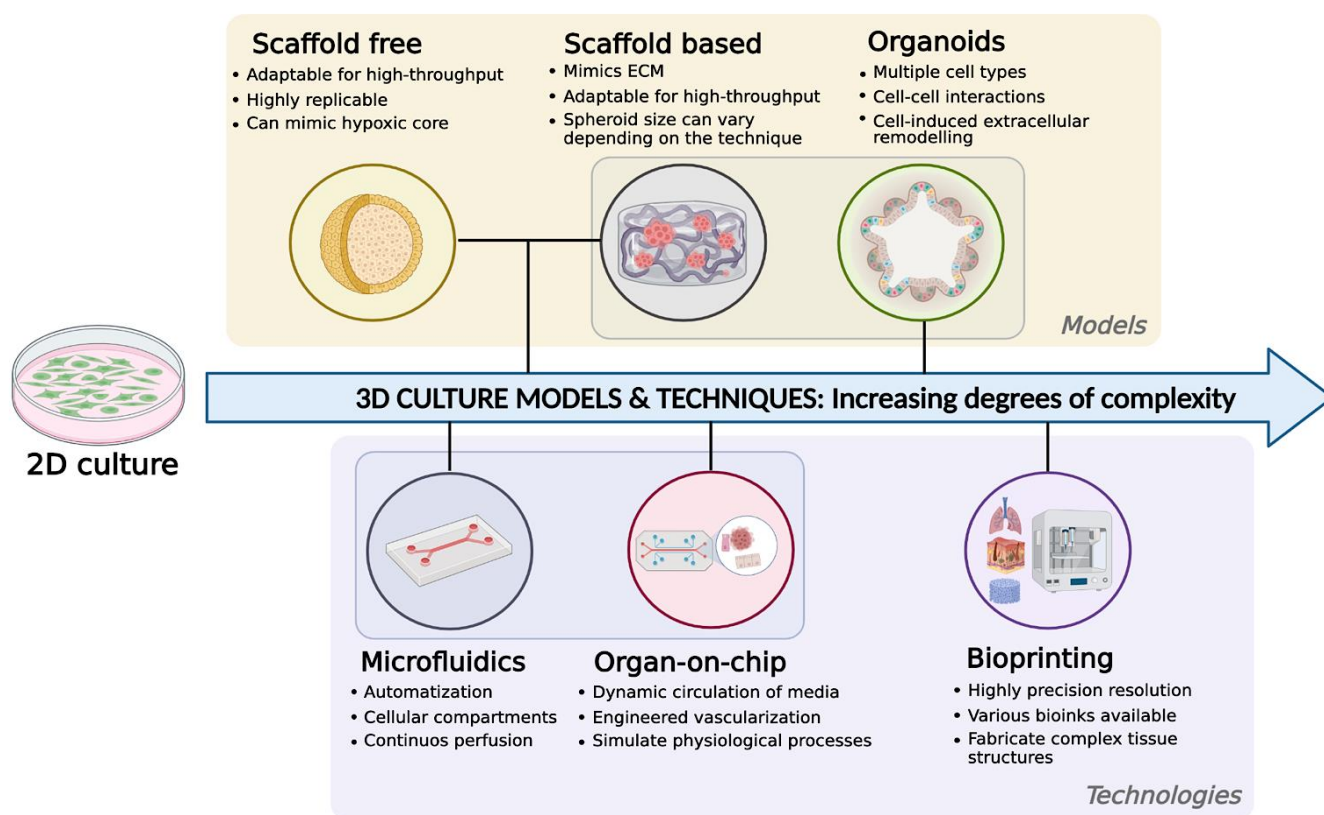
Figure 1: The wide range of 3D models and technologies exhibit increasing degrees of complexity. There are many advanced cell culture methods and platforms including multicellular spheroids, scaffold hydrogels, organoids, microfluidics, organs-on-chips, and 3D bioprinting. Small rectangles surrounding organoids/scaffold-based models and microfluidics/organ-on-chip represent natural overlap between the two topics. *Created with BioRender.com*

Researchers now have the ability to grow cells in 3D, which increases the benefit of cell-based assays and allows for the generation of more precise and physiologically relevant data. The dynamic system created by the formation of tissue-like structures in 3D combined with medium perfusion/circulation moves cell-based models even farther towards the reconstruction of more 'in vivo like' situations. Maintaining a cell natural 3D architecture is thus one of the most important aspects in improving the value of cell-based assays. Several technologies are now accessible that support 3D cell culture solutions. Experimental models must depict the various aspects of the same tissue in a reproducible, measurable, and reliable manner, which is not always easy, straightforward, or attainable. Rather than being a one-size-fits-all solution for *in vitro* cell culture, this is a case of utilizing various aspects of 3D cell technology, depending on the biological question being investigated. There is not a unique answer for all 3D culture requirements. Because these technologies are now available from commercial sources, researchers can now choose the best appropriate method for their research needs. Furthermore, new breakthroughs

in dynamic media perfusion are frequently integrated with 3D cell culture technology to further boost cell proliferation and the physiological relevance of the model. Culture medium perfusion is enabled by a variety of modern technologies, including intelligently constructed devices and mini-benchtop bioreactors. The pharmaceutical industry is extremely focused on expanding innovative ways to identify and develop new compounds, and 3D culture has been designated as a key topic. These new methodologies will be useful alternative approaches to animal research, cell biology, tissue engineering, cancer biology, etc. Similarly, contract research organizations are now employing 3D culture methodologies to provide more data to their clients (Law et al. 2021).

1.1.1 Cell spheroids

Spheroids are dense, three-dimensional (3D) self-aggregates of cells that exhibit extensive cell-cell adhesion and closely resemble *in vivo* characteristics of tissue counterparts. Despite the fact that scientists have been cultivating cell aggregates for decades (Moscona, 1957), the term "spheroid" was not used until 1971 (Sutherland et al. 1971). Additionally, there is further terminology for models formed from the brain or mammary stem cells, such as neurospheres and mammospheres, which refer to original organs, whether normal or tumor. Other common examples of spheroids include embryoid bodies (group of embryonic cells that proliferate and develop into 3D colony aggregates in 3D non-tumor cells), multicellular tumor spheroids (MTSs or MCTS) and hepatospheres.

Cell aggregation can be explained using the same physical principles that govern the interaction of immiscible fluids, such as the tendency to form spherical shapes to reduce surface area and free energy in the system (Yu et al. 2018). The phenomenon of self-aggregation leads to 3D structures that are often essential to various biological processes, regardless of cell status (healthy or tumor). Furthermore, during advanced stages of development, cytoskeleton integrins and proteins emerge as principal elements responsible for cell aggregation and compaction of 3D structures. In fact, in compact spheroids, cells are firmly connected to one another, making it difficult to identify single cells. Cells clumped together in a tight or loose aggregation cannot form a full sphere and disintegrate easily. Integrin-mediated attachment to ECM molecules initiates cell aggregation, which is then compacted by E-cadherin mediation (Lu and Stenzel 2018). Cell lines that formed compact spheroids had high levels of E-cadherin, whereas tight aggregates had accelerated N-cadherin expression (Ivanov et al. 2017). When cells lose their ability to aggregate into a sphere, they also lose their adhesion molecules. Aggregates undergo an exponential evolution from a looser, more deformed, and elongated beginning state to a circular and compact shape.

Due to their spherical conformation, spheroids are considered the most adaptable model among the 3D structures formed from cells in suspension reported in the literature (Weiswald et al. 2015). As a result, culturing spheroids has become a strong technique for *in vitro* experiments, and has been the subject of numerous studies in drug discovery, oncology and tissue engineering (Fennema et al. 2013). Spheroids can be made up of just one cell type or can include numerous cell types in a single co-culture spheroid. Multicellular co-culture spheroids have been demonstrated to be particularly effective at simulating the morphology and polarity of *in vivo* cell-cell adhesions (Laschke and Menger 2017).

Scaffold based and scaffold-free systems are the two most common types of technology platforms for 3D cell culture. The cells are cultured in 3D artificial matrices or in hydrogels in scaffold-based culture. Because the scaffold simulates the ECM, it provides mechanical support and allows cells to interact with the ECM. Various biomaterials, including natural and synthetic compositions, can be used as scaffolds. Because of their biocompatibility, natural polymers such as gelatin, alginate, collagen, and Matrigel are usually chosen (Wang et al. 2016). In 3D scaffold manufacturing, synthetic polymers such as poly (lactic-co-glycolic) acid (PLGA) or polycaprolactone (PCL) and poly (ethylene glycol) (PEG) are utilized. Synthetic polymers are readily available; they may be manufactured in large, consistent quantities and adapted to specific purposes (Naz et al. 2017; Taghavi et al. 2017).

On the contrary, in scaffold-free culture, different techniques are available for spheroid formation. The use of attachment-resistant cell culture surfaces, such as 96 and 384-well spheroid microplates with ultra-low-attachment (ULA) surface or retaining the cells as suspension cultures in medium are two common matrix-free approaches for generating spheroids (i.e., hanging drop technology, agitation-based techniques, and bioreactors). In addition, low-adherent surfaces are used as an alternative strategy to induce spheroid formation and growth by replicating the original microenvironment of cells. In conclusion, perfusion flow culture systems are another division of three-dimensional cell culture. These systems, which can include 3D spheroids, are designed to replicate the continuous flow of nutrients and waste through cells and tissues. Culture in microfluidics and 3D bioreactors systems are used to simulate dynamic biological processes and the effects of *in vivo* factors including shear stress and fluid turbulence. In terms of culture type, microfluidics and bioreactors are frequently identified in the literature as a scaffold free platform, because they create floating 3D cultures supported by constant agitation that keeps cells in suspension (Cui et al. 2017). Several morphological parameters can be tracked over the course of spheroid formation. Firstly, spheroid size is determined by the cell type(s) from which spheroids are produced, as well as the culture conditions in which they are grown. Several hundred cancer cells have been used to test the suitability of MTSs creation. Some cancer cells had a high

spheroid formation efficiency, whereas others had a low or no spheroid formation efficiency. The effectiveness of MTSs formation varied depending on cell lines, even for the same tumor type. They usually range in size from 100 μm to > 500 μm (Huang and Gao 2018). Spheroids larger than a few hundred micrometers, on the other hand, show activation of hypoxia-induced survival factors, such as HIF-1α, and a loss of cell viability at their cores since their oxygenation is dependent on diffusion. Larger tumor spheroids (500 μm of diameter) generate nutritional and oxygen gradients that replicate their natural equivalents, making this feature of spheroids helpful for the study of solid tumors (Groebe et al. 1996; Bhang et al. 2011) (**Figure 2**).
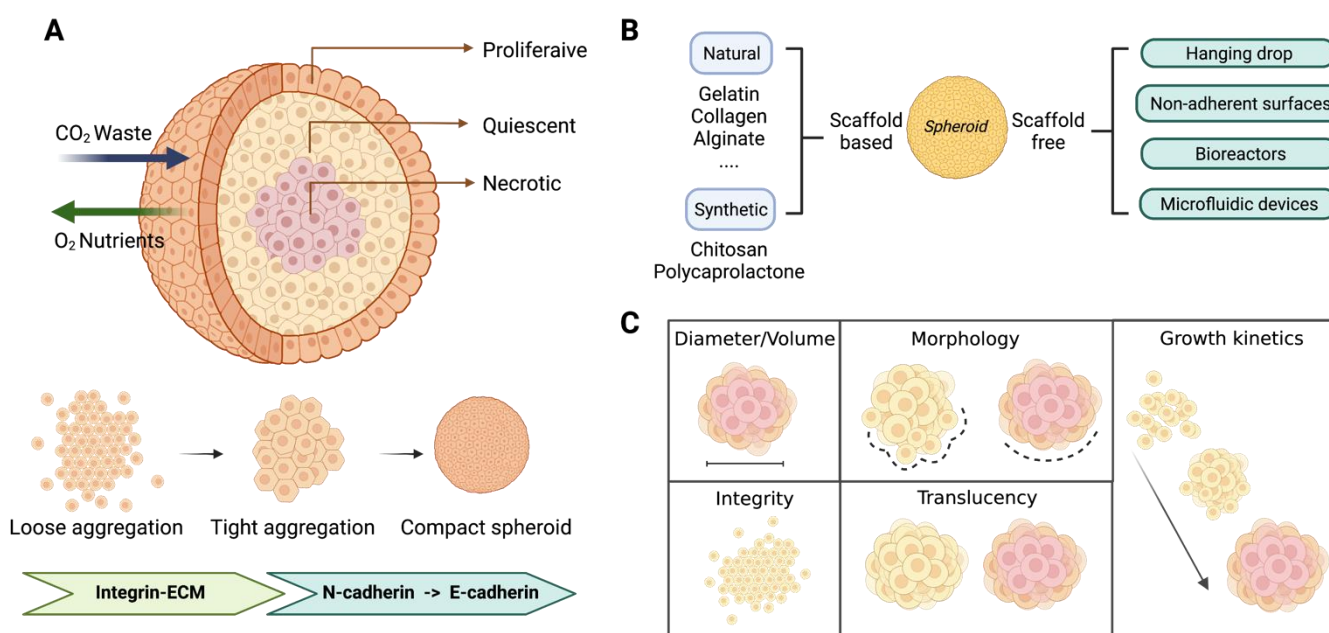
Figure 2: Spheroid structure, generation process and morphological parameters. (A)The structure of MTSs is divided into three layers: a proliferative outer layer, a quiescent inner layer, and a necrotic core. Like *in vivo* solid tumors, MTSs exhibit a gradient in oxygen, carbon dioxide, and nutrient content. MTSs formation process. Cells initially aggregate by loose bonds between integrin and ECM and then form close contact through N-cadherin to E-cadherin interactions. (B) There are two types of spheroids culture methods: scaffold-based and scaffold-free cell culture methods. Each group develops several techniques (C) Examples of different spheroid properties that can be assessed using label-free brightfield and phase-contrast microscopy. Created with BioRender.com

Before and after anticancer drug treatment, several approaches are available to define spheroids in a viable, fixed, or dissociated form. These techniques allow for the analysis of anticancer drug-treated spheroids architecture, size, shape, gene and protein expression, metabolic status, migration, and invasion. In general, standard biological assays used for 2D culture can be applied to spheroids, with some drawbacks as outlined in the following **Table 1.**

Technique	Description	Staining/Marker	Features	Advantages/Limitations	References
Phase contrast microscopy **Bright field microscopy**	Monitoring of morphology and spheroids growth Light is transmitted through the sample, and denser areas attenuate light transmission, originating contrast	e.g., hematoxylin and eosin	Size/volume, Monitoring spheroid disaggregation and/or morphological disruption in response to an anticancer treatment. Nuclei and cytoplasmatic structures	↑ Non-invasive, low cost method ↑ Long term monitoring ↓ Not detailed data from complex 3D spheroid structures ↓ Requires spheroid processing for histological sectioning	(Zanoni et al. 2016) (Clayton et al. 2018)
Fluorescence microscopy	Fluorescent dyes for specific specimen structures; Stained or immunostained spheroid or spheroid sections	Hoechst/DAPI; Phalloidin/ tubulin/actin; Ki67 staining; Caspase staining; Annexin V+ Propidium iodide (PI); Calcein or FDA +ethidiumhomodimer1 (EthD1)	DNA, nuclei Cytoskeletal arrangement Cell proliferation Cell death/apoptosis Live/dead assays	↑ Monitoring a wide range of features ↓ Large samples require sectioning ↓ The histological procedures using spheroid fixation restricts the investigation of dynamic modifications in the spheroids over time	(Virgone-Carlotta et al. 2017) (Yakavets et al. 2019)
Confocal laser microscopy	This technique uses a focused laser spot that passes through the sample to create an image, using a pinhole to remove out-of-focus light	Same markers described for fluorescence microscopy	Spheroid architecture	↑ 3D reconstruction (stacks) ↓ Restricted to small spheroids, the penetration depth is usually less than 100 μm ↓Scattering in thick tissues.	(Durymanov et al. 2019) (Leary et al. 2018)
Light sheet fluorescence microscopy (LSFM) **Two-photon microscopy (TPM)/multi-photon microscopy (MPM)**	This technique uses a thin plane of light to optically section the sample and to allow the visualization of thick specimens; The illumination is done perpendicularly to the direction of observation These techniques use two photons (TPM) or pulsed long-wavelength light (MPM) to excite fluorophore	Same markers described for fluorescence microscopy	The innermost layer of live and fixed spheroids	↑ Higher spatial resolution than confocal; ↑ 3D reconstruction ↑ The penetration depth is greater than 1 cm; ↑Reduced light exposure and phototoxicity ↓ LSFM implies high processing time and memory to produce high-resolution 3D images ↓ Complex technology, laborious sample mounting; ↑ Allows 3D reconstruction using a series of images ("stack") ↑ Low photobleaching; ↑ Penetration depth goes from 500 to 800 μm; ↓ Low acquisition speed	(Pampaloni et al. 2014) (Bruns et al. 2012) (Rane et al. 2016) (Pratiwi et al. 2021) (H. Lin et al. 2019)
Electron microscopy (SEM-TEM)	The surface of the structures in the sample are scanned with a beam of electrons (SEM); A beam of electrons hits the sample, part of the beam is transmitted through the specimen and used to generate high resolution images (TEM)		Cellular protrusions; Integrity of cell–cell interactions; Integrity of cellular membrane after anticancer drug treatments; Cell junctions and ECM deposition; Drug treatment outcomes such as apoptosis, cell shrinkage; Distribution of drugs or nanoparticles in the spheroid	↑ High resolution. ↓ In some cases, specimen collapse and morphological alterations can be associated with the steps of procedures	(Uroukov et al. 2008) (Chelobanov et al. 2020)

Table 1: Methods currently used to characterize spheroids and to evaluate drug effect

Method	Description	Reagents/Readout	Application	Pros/Cons	References
Flow cytometry	Physical and chemical properties of spheroids single cells. Required mechanical or enzymatic disaggregation of spheroids	AnnexinV/PI; PI/ribonuclease; 5-bromo-2'-deoxyuridine (BrdU) + PI (or analog); Hoechst 33342; Fluorescent staining of specific cellular proteins.	Cell death, apoptosis Cell cycle analysis, Live/dead cell analysis	↑ Quantitative analysis ↓ Required disaggregation ↓ A large number of spheroids are required	(Trumpi et al. 2015) (Wang et al. 2018) (Bauleth-Ramos et al. 2020)
Spheroids flow-based method	Monitoring a sample when free-falling, driven by gravity, into a flow-channel where the analysis medium is at rest.		Gathering precise information on mass density, shape, size and weight of cell aggregates	↑ Physical characterization of spheroids ↑Diameter range 20-500 um ↓Measures only one spheroid at a time	(Cristaldi et al. 2020) (Sargenti et al. 2020)
Molecular biology methods for quantification of gene expression	qRT-PCR Western Blot analysis	Quantification of gene expression at mRNA level Quantification of gene expression at protein level		↑ Accurate and well-known methods ↑ After disaggregation, samples can be manipulated similarly to 2D cultures. ↓ Mechanical disruption and association with chemical buffers are required to extract proteins and RNA from the cells.	(Norberg et al. 2020) (Pignatta et al. 2015) (Joshi et al. 2018)
Methods for quantitative cell viability analysis	MTT: Reduction of MTT tetrazolium salt by NADPH dehydrogenases, present in the mitochondria of metabolically active cells, into an insoluble formazan product Lactate dehydrogenase (LDH) quantification: conversion of lactate to pyruvate via the reduction of NAD+ to NADH. Then, diaphorase uses NADH to reduce a tetrazolium salt to a formazan product Alamar blue:Metabolically active cells are able to reduce resazurin to resorufin mainly through mitochondrial enzymes (NADH dehydrogenase or NADPH dehydrogenase) Acid phosphatase activity:Based on the quantification of cytosolic APH p-nitrophenyl phosphate is hydrolyzed by viable cells to p-nitrophenol via intracellular acid phosphatase Cell Titer-Glo 3D: method for determining the number of viable cells in culture based on the quantification of the ATP present, an indicator of metabolically active cells	Colorimetric, tetrazolium salt reduction for evaluation of the metabolic activity LDH release quantification, cytotoxicity evaluation Fluorometric, evaluation of the metabolic activity through ATP measurement by resazurin reduction Colorimetric, cytotoxicity evaluation through measurement of assay ACP activity Luminescent, evaluation of the metabolic activity with ATP measurement by luciferin oxydation		↑ Well-known methods so far implemented for 2D culture approaches. ↓ Limited efficacy in 3D spheroids and microtissues, due to difficulties of reagents to cross cell–cell junctions and/or 3D matrices. ↑ Highly sensitive. ↑ Does not require spheroid dissociation ↓ Complete removal of culture medium is required, which may not be practical and increases spheroid damage risk. ↑ Better penetration of the reagents into the spheroids. ↑ Enables higher accuracy and reproducibility in large spheroids. ↑ Does not require removal of culture medium. ↓ ATP output may be affected by several factors and is not always proportional to cell number	(Walzl et al. 2014) (Ho et al. 2012) (Rolver et al.2019) (Vinci et al. 2012) (Raghavan et al. 2015) (Shi et al. 2018)

One of the techniques most frequently used for spheroid characterization is morphometric analysis. Label-free brightfield or phase-contrast microscopy, which is cost efficient, easy to use, and prevents specimens photodamage, can be employed to analyze spheroid morphology. Additionally, once images are obtained, they can then be processed in analysis software that allows measurement of properties such as diameter, area, perimeter, solidity, roundness, and sphericity. All of these measures are relatively quick and low-cost and may be done manually or through process automation in the case of large-scale spheroids examination (Ivanov and Grabowska 2017). This system can track a variety of morphological factors over the duration of spheroid formation in a semi-automated manner.

The integrity of the spheroid, volume, diameter, shape, translucency (a measure of spheroid compaction), and development dynamics (including growth delay) can all be evaluated. All of these tests are suitable for drug screening, drug response, and toxicity testing (Friedrich et al. 2009). Specifically, when imaging analyses are used to track spheroid growth, the focus is usually on how their size and shape change over time. This provides indirect data on spheroid compactness, which is frequently highlighted by a change from a loose to a tighter cell aggregate (Weiswald et al. 2014). However, because spheroids undergo distinct compaction processes throughout time, based on factors such as cellular variety, growth *milieu*, and compound treatments, this approach is not fully representative of 3D models (Lin and Chang 2008; Vinci et al. 2012). Aggregates of similar dimensions, for example, can have different compositions depending on the metabolic/proliferative cell state and the extracellular matrix. Because cell growth is characterized by changes in mass density and volume, determining these values with accuracy is a critical obstacle to solve. Nevertheless, cells regulate density more finely than size, and measuring cell weight and mass density directly can help monitor cell responses to external events (Bryan et al. 2010). With the invention of nanomechanical resonators or electrokinetic microfluidic chips, several methods for assessing cell weight and mass density were established. These approaches, however, are not designed nor validated for reaching the average size of spheroids and organoids (Zhao et al. 2014; Neurohr and Amon 2020; Xie et al. 2019). Currently, technology for fine measurement of the weight and mass density of individual spheroids has been developed (Cristaldi et al. 2020).
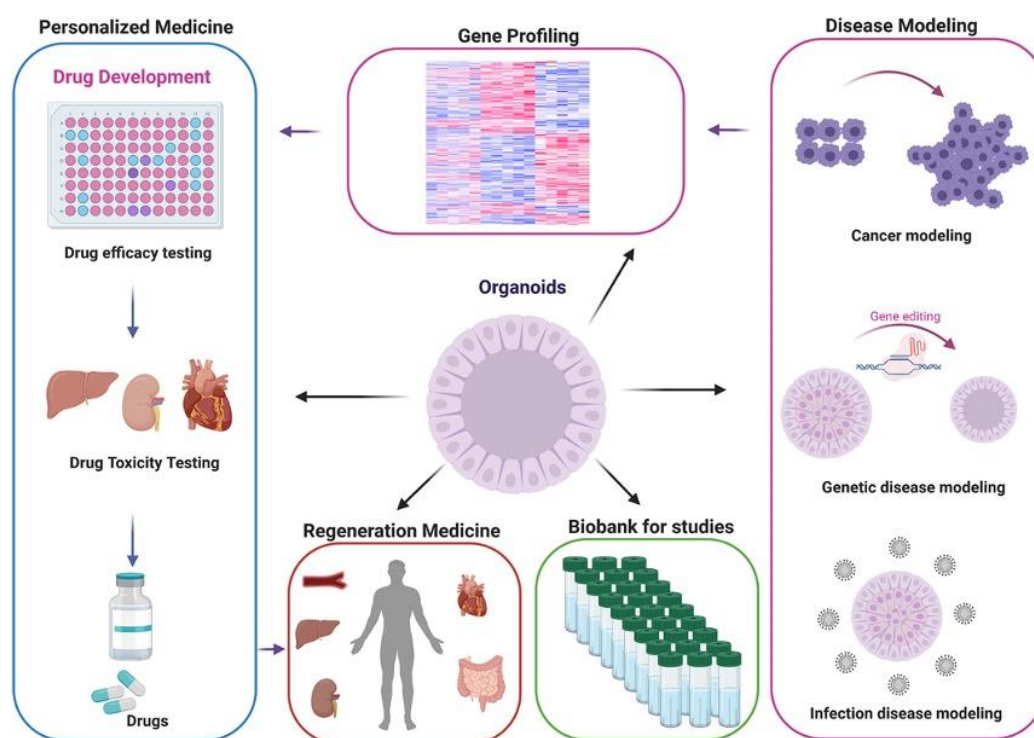
1.1.2 Organoids

Organoids are valuable tools for studying individual disorders and developing personalized treatments. This new method has increased drug translatability for preclinical therapies and the ability to imitate the complexity of organs, opening up several new possibilities for human disease

modeling, tissue engineering, drug development, diagnosis, and regenerative medicine (***Figure 3***). Organoids are three-dimensional structures that are composed of multiple cell types, self-organized to recapitulate embryonic and tissue development *in vitro* (Turksen, 2019). The adoption of 3D cell culture methods has resulted in remarkable advancements in the cultivation and development of stem cells and committed progenitor cells. Initially, different organ-specific cell types (ESCs, iPSCs, and adult stem cells) are required to self-organize and sort together through adhesion proteins and imitate some of the functional properties of native organs in order to form organoids. Pluripotent stem cells (PSCs) have a wide range of potential applications for producing pure populations of any cell type in the body (Hockemeyer and Jaenisch 2016). Drug discovery, cell treatment, and tissue regeneration could all benefit from pure populations of progenitor or terminally differentiated cells, particularly those that are difficult to separate from tissues. Major improvements in stem cell differentiation have recently been made employing 3D culture techniques that mimic *in vivo* development and time regulation of signaling pathways. These cells must be cultured in a 3D media with matrices that replicate the extracellular matrix scaffolding structure of native tissue (ECM). The Engelbreth-Holm-Swarm (EHS) matrix, also known as Geltrex, Cultrex BME, and Matrigel, is commonly employed in the organoid development process and provides a complex environment for cell growth (Kratochvil et al. 2019).

The use of human organoids in the modeling of human diseases is one of the main goals of this method. Moreover, drug/genome screening and the creation of living biobanks are used to assess the efficacy of individualized treatments, such as cell and organ replacement therapies, for specific diseases. The intestinal 3D organoids of cystic fibrosis (CF) were the first human disease to be modeled in organoids (Firth et al. 2015). CF is caused by a number of mutations in the CF transmembrane regulator (CFTR) gene, which is found in epithelial cells throughout the body. Dekkers et al produced primary CF patient-derived intestinal organoids *in vitro* to simulate the disease (Dekkers et al. 2013). More recently, 3D hepatic organoids were formed from iPSCs to the human genetic disease, encompassing both functional hepatocytes and cholangiocytes (Guan et al. 2017). Cerebral organoids were also used to assess genetic abnormalities in the brain (Bershteyn et al. 2017).

Additionally, in recent years, establishing tumor organoid models for drug discovery and personalized medicine applications is becoming more popular. Patients' tumor cells can be implanted in an immune-deficient or humanized mouse under ectopic and/or orthotropic circumstances, resulting in patient-derived xenografts (PDXs). Due to their ability to simulate the physiological and biochemical effects of cancer treatments on a customized patient's tumor, these models presented a viable alternative to prior tumor models. Unfortunately, not all tumor models are compatible with PDXs and it is a time-consuming and costly procedure that only allows

screening very few potential drugs (Tentler et al. 2012). Researchers have attempted to circumvent these limitations by developing 3D tumor organoid models for personalized cancer therapy. Indeed, unlike conventional tumor models (e.g., 2D tumor cell culture and PDX models), patient derived tumor organoids (PDTOs) might be cultured from a small sample size acquired from biopsies and better mimic the environment of a tumor in the body. The preservation of tumor heterogeneity in culture, on the other hand, is a significant aspect of the successful development of tumor organoids. PDOs are three-dimensional in vitro models that have been shown in multiple studies to closely resemble basic characteristics of primary tumors, such as histological complexity and genetic heterogeneity in human cancer. According to hematoxylin and eosin staining, PDOs share morphological characteristics with the original tumor, and immunohistochemical markers used in the identification of certain tumors show that the tumor's expression pattern is maintained in PDOs. The outcomes of PDOs for predicting treatment are promising, suggesting that PDOs might be a good platform for identifying and evaluating the efficacy of anticancer compounds.

Figure 3: Three-dimensional (3D) human organoids applications (Shariati et al. 2021) Image under Creative Commons Attribution 4.0 International license

Furthermore, PDOs retain the genetic and transcriptome properties of their original tumors. These organoids, additionally, could be a formidable model for precision medicine testing with an appropriate 3D high-throughput screening (HTS) strategy (Boehnke et al. 2016; Phan et al. 2019). However, the maintenance of heterogeneity of tumor in culture is a critical factor for the successful designing of tumor organoids and also, PDOs generated in published studies have mostly lacked

essential elements, such as blood vessels, immune cells and other stromal cells. It is well known that angiogenesis is one of the most important biological characteristics of cancer. Thereby, microfluidic technology can facilitate the complex nature of 3D organoid culture through organoid-on-a-chip and organ-on-a-chip models.

1.1.3 Microfluidics

The field of microfluidics involves both science and technology of systems that manipulate and process low volumes of fluids (in the range of microliters (10^{-6}) to picolitres (10^{-12}), generated in small-scaled cells and microchannels with dimensions of around < 1 µm to > 500 µm (Dixit and Kaushik 2016). For over two decades, the application of micro technologies for biomedical research has led to the development of miniaturized platforms for *in vitro* experiments. Nowadays, a variety of fabrication methods for microfluidic systems have been used, including etching, photo and *e-beam* lithography, embossing, *replica molding* (REM), laser photoablation, and 3D printing techniques, given its recent accessibility. Specifically, in M. Madou's work all fundamentals of microfabrication techniques are summarized (Madou 2002). The selection of the correct manufacturing method is mainly determined by the equipment technology, manufacturing speed, desired resolution, and materials. The development of these technologies has allowed a great improvement of microfluidic devices and their rapid diffusion in laboratories all over the world. Microfluidic devices are mainly manufactured with elastomers, plastics, or paper. Synthetic polymers like polydimethylsiloxane (PDMS) are the most frequent platforms for microfluidic systems, and they have been used in cell culture models because of their high oxygen permeability (Zaremba and Smoleński 2003), distensibility (Huh et al. 2010) and ease of manufacture. The fabrication of PDMS devices is a well-developed and straightforward process. The PDMS allows rapid replica molding (**Figure *4)*** from silicon or photoresist molds, as it adapts to substrates with micrometric structures. The devices are cast and peeled from a micro-structured mold, then the *inlet* and *outlet* ports are created. PDMS devices are typically attached to a glass slide or other bonding material. As a flexible, optically transparent, gas permeable, and biocompatible polymer, PDMS provides advantages that have made it the most popular material for lab-on-chip studies (Porto et al. 2016).
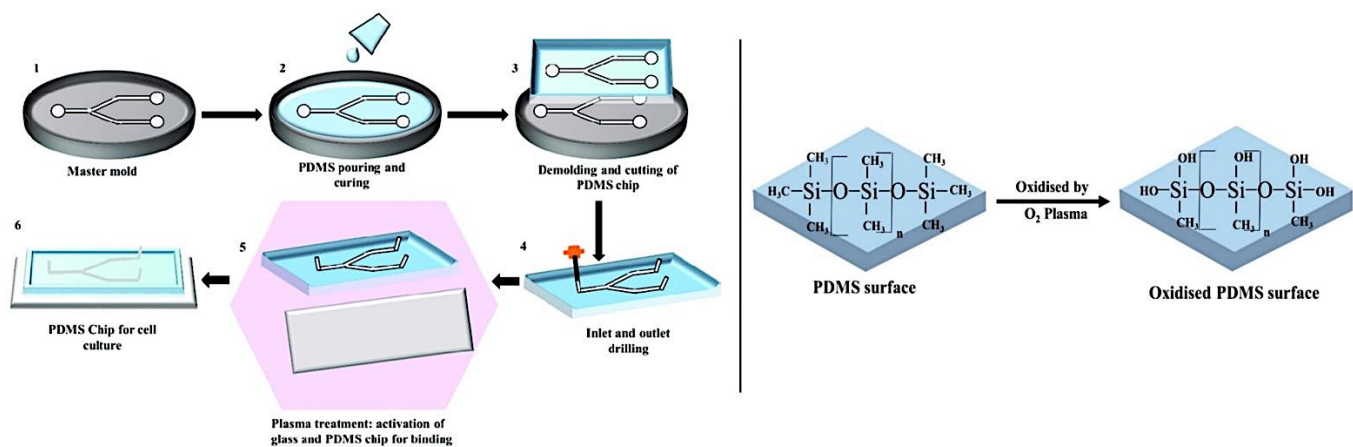
Figure 4: Illustration of the step-by-step fabrication process of a PDMS chip by replica molding. (1) Device design (2) Pouring a mixture of PDMS prepolymer and curing agent into the master mold and allowing it to solidify; (3) Peeling the solidified PDMS from the master mold and cutting it into an appropriate shape; (4) Punching the inlet and outlet holes; (5) Activating the PDMS and glass surface with plasma treatment to facilitate bonding; (6) Binding and curing of PDMS chip bonded on glass ready to use. On the right, surface modification of PDMS using oxygen plasma. The hydrophobic -CH_3 groups are replaced by the hydrophilic silanol groups (SiOH) during oxidation, which improves wettability (Akther et al. 2020). Image under Creative Commons Attribution 4.0 International license

Depending on the application, microfluidic cell culture systems are designed to incorporate scales ranging from millions of cells to single cells, providing a level of flexibility not possible with conventional well plates. The use of channels, membranes, and other elements incorporated into microfluidic devices may be designed to enable spatial control over cell behavior, and interactions between cell populations may be regulated by the use of these systems' structural features. Furthermore, microfluidic devices frequently enable constant fluid flow, which is a crucial physiological condition that is not present in static standard culture methods. Microfluidic flow conditions are important for applying fluid mechanical stresses to cells, forming gradients of oxygen, growth factors, and other biochemical signals, and maintaining cell–cell interactions.

1.1.4 Organ-on-chip

Several organ-on-chip models have been created using microfabrication and microfluidics technology. These are essentially miniature 3D organ models with *in vivo* capability that could be highly valuable for toxicity assessment. Moreover, organ chips resolve many issues that spheroids and organoids generated in ECM gels present (Sontheimer-Phelps et al. 2019). Despite spheroids and organoids being useful tools for modeling a variety of diseases, they have a dearth of tissue-tissue interactions and organ-level features. These devices culture living cells in constantly perfused chambers to mimic tissue and organ function. Researchers can use these devices to examine tissue formation, organ physiology, and disease pathogenesis, as well as discover and test new compounds (Bhatia et al. 2014). Huh et al., in their publication "lung-on-a-

chip" in 2010, introduced the model of "organ-on-a-chip" as microfluidic *in vitro* cell culture systems that replicate the physiology of the essential functional components of an organ (Huh et al. 2010). Due to the high expectations of recreating essential parts of the human physiology environment and the potential for replacing animal models, organ-on-a-chip has become a prominent technology for biological research (***Figure 5***).
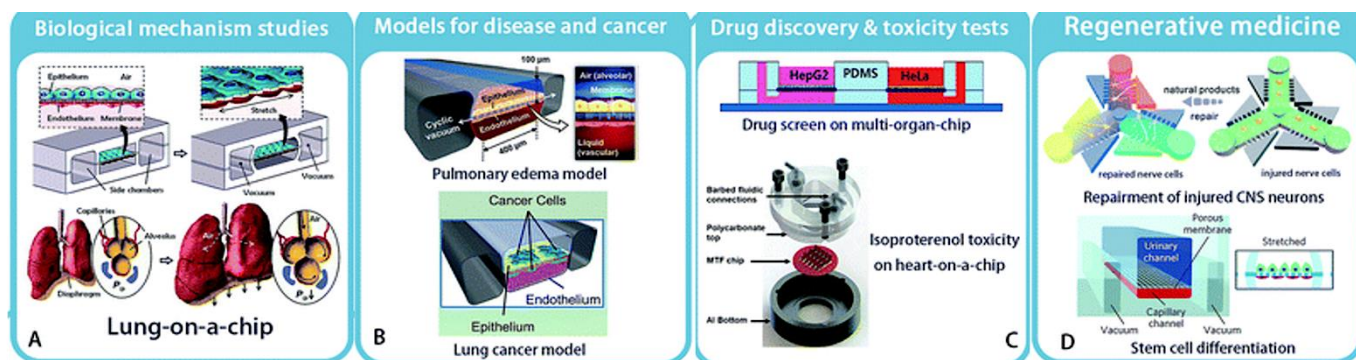
Figure 5: Organ-on-chip technologies and their application areas. (A) lung-on-a-chip, biological mechanism. (B) Disease model – organ-on-a-chip model for lung cancer. (C) Devices used for drug discovery and toxicity tests. (D) Regenerative medicine as neuron recovery and differentiation of stem cells (Quan et al. 2020). Image under Creative Commons Attribution 4.0 International license

Organ on chip applications include a wide variety of biomedical science and technology uses. For example, Hassell and colleagues constructed a lung-on-a-chip containing non-small-cell lung cancer and tracked tumor cell proliferation in a controlled microenvironment. They detected therapeutically relevant mechanisms such as tumor dormancy and tyrosine kinase inhibitor responsiveness. The function of mechanical strain in altering cancer sensitivity to therapies was also highlighted, thanks to the mechanical movement on the chip (Hassell et al. 2017). Moreover, models are increasingly being used for drug screening as organ-on-a-chip technology advances. Agarwal et al. used a heart-on-a-chip model to recreate the therapeutic effect of isoproterenol (Agarwal et al. 2011). Multi-organ chips were recently developed to identify anti-angiogenic and anti-tumor compounds, as well as to demonstrate anti-cancer action of luteolin, a flavonoid, in liver and cancer tissues (Jeon et al. 2021). For the pharmaceutical and biotechnology industry, the greatest utility of organs-on-chips may be in the validation and prioritization of lead drug candidates (rather than high-throughput screening) as well as the investigation of molecular mechanisms of action and toxicities.

Human organs-on-chips with advanced features may potentially help in the discovery of new indicators of therapeutic efficacy, toxicity, or disease response, which could be useful in clinical trials. In conclusion, organs-on-chips approach should also overcome a number of obstacles. Technical robustness is the main key issue. To ensure optimal performance of organs-on-chips over a month or more, several components must come together, including the cells, ECM

coatings, fluidic controls, bubble removal, and gradient maintenance. A "universal blood substitute"—a single culture medium that nourishes all tissues, just as blood supplies all organs in the body—is required for systems consisting of several, linked organ chips. Because existing culture media have been adjusted for each cell type, this remains a substantial challenge, especially if some tissues are grown in serum-containing medium while others are cultured in serum-free medium.

1.2 Strategies for spheroid generation and drug screening applications

1.2.1 Multicellular tumor spheroids generation: principal techniques

There are various popular approaches for realizing 3D cell culture, each technique possesses certain advantages and limitations, as summarized in *Figure 6*. Because of its simplicity and low cost, the hanging drop is one of the most widely used procedures, in which gravity and surface tension are exploited to produce spheroids in Petri dishes. Specifically, with the hanging drop method, cells can be cultivated in a drop of medium suspended on the lid of a cell culture dish. Because there is no surface to allow cell attachment, cells gather at the bottom of hanging droplets to form spheroids. Furthermore, hanging drop plates are protected from evaporation by a lid, ensuring a humid and sterile environment.

However, these suspension cultures are time consuming and often do not provide compact and uniform spheroids. Another disadvantage of the hanging drop method is that the cell culture environment is completely exposed to the external environment, resulting in medium evaporation from the drops. Additionally, the rise in osmolarity caused by a change in medium concentration is detrimental to cell viability and the total number of hanging drops that can be used in a particular area is limited. Furthermore, media exchange is difficult. The number of spheres and their size scaling are further limited by the need to pipette additional medium into each droplet manually. The hanging-drop method is more suitable for cells that can quickly grow in a non-adhesive environment and have a high propensity for aggregation (Raghavan et al. 2015; Thomas et al. 2014).

Another approach consists in using superparamagnetic iron oxide nanoparticles (SPIONs) as patterning agents to direct cell self-assembly into spheroids using magnetic forces, known as magnetic levitation. SPIONS are incubated overnight with semi-confluent adherent cells to facilitate cellular absorption (Whatley et al. 2014). The magnetically tagged cells are trypsinized, counted, and re-seeded in low attachment plates after the excess SPIONS are washed away. Following that, a magnet is placed on top of the plate lid and the SPION tagged cells are dragged

up or down by magnetic forces, accordingly. Within a few hours, the cells self-assemble into spheroids (Tseng et al. 2015; Leonard and Godin 2016).
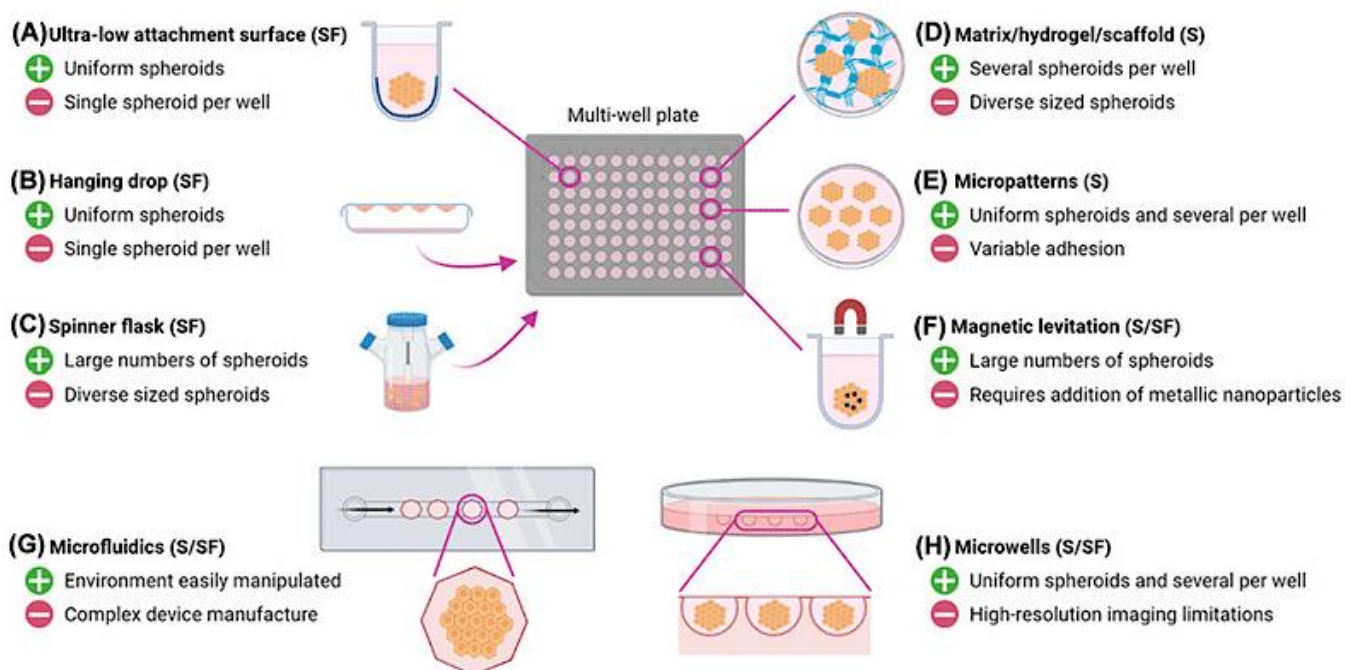
Figure 6: Depending on the cell type and downstream application, spheroids can be generated using a number of scaffold (S) and scaffold-free (SF) approaches. The most popular approaches for using a multi-well plate format are (A) ultra-low attachment surfaces, (B) hanging drop, (C) spinning flasks, (D) adding an extracellular matrix material, (E) micropatterning, and (F) magnetic levitation. Using this approach, the spheroids can be created directly in the multi-well plate, while the arrows indicate procedures that require the spheroids to be transferred into the multi-well plate after assembly. Microfluidic devices (G) and microwells in a variety of dish types (H) are two other configurations. One key advantage and disadvantage are listed for each strategy (Mysior and Simpson 2021). Image under Creative Commons Attribution 4.0 International license

Cultivating cells in suspension in bioreactors is another mechanical stimulus for obtaining spheroids. This dynamic device encourages cell collision controlled by gentle convective forces supplied by an impeller for aggregate formation. The diameters of the spheroids described by the authors varied between 80 and 300 μm, depending on the cell line, mixing rate, and culture duration (Santo et al. 2016). Changes in the tumor fluid microenvironment promote tumor growth and metastasis, according to Huang et al. with fluid shear stress (FSS) being a key contributor (Huang et al. 2018). Because FSS is the product of shear rate and fluid viscosity, understanding the behavior of cancer cells at various shear rates may aid in elucidating the tumor microenvironment's development. However, multiple cell lines and culture settings, combined with non-homogeneous shear stress in the spinner flask and a lack of data on impeller design, make it challenging to compare cell culture experiments and develop satisfactory and standardized results culture techniques.

The biologically active scaffolds, in scaffold-based methods, not only support cancer cells 3D architecture, but also operate as a source of external cues that stimulate cell-cell and cell–matrix interactions and influence tumor cell activities. ECM-based natural hydrogels, synthetic hydrogels, and designed hydrogels that imitate native ECM are all common scaffolds in 3D culture systems (synthetic hydrogels with integrin binding motif). Hydrogels are a network of cross-linked synthetic or natural polymers having tissue-like elastic characteristics that are insoluble in water. Because of the interconnecting microscopic pores, hydrogels have a high water retention capacity, allowing for simple movement of oxygen, nutrition, metabolic wastes, growth, and other soluble elements through the porous channels. Hydrogels are made up of designed polymers that are either natural, synthetic, or semi-synthetic (Kleinman and Martin 2005).

As previously mentioned, Matrigel is a standard ECM-based natural hydrogel that is commercially available. Laminin, collagen, heparin sulfate proteoglycans, entactin, and numerous soluble substances are abundant in Matrigel. Endogenous chemokines and growth factors are present in hydrogels made from natural polymers, contributing to their vitality and growth-promoting qualities. Endogenous soluble factors, on the other hand, introduce unpredictability into the culture conditions, making it difficult to achieve repeatable assay results. Moreover, hydrogels made of synthetic polymers [poly (ethyl glycol), poly (vinyl alcohol), poly (2hydroxy methacrylate)], poly-2-hydroxyethyl-methacrylate, are physiologically inert but have excellent tensile strength, customizable mechanical properties, and consistent assay findings. External stimuli can be used to control the swelling and permeability of synthetic hydrogels (Ahmed 2015). Techniques based on the use of polymers are also available. The direct addition of methylcellulose to the culture medium, for example, enhances the viscosity of the medium and causes cell aggregation.

Another method for impairing cell attachment to surfaces and stimulating cell aggregation is to coat multiwell plates with non-adherent polymer hydrogels (Amaral et al. 2017). In this regard, ultra-low-attachment (ULA) well plates are commercially available, providing a simple method of generating spheroids at a cost that falls somewhere between the old hanging drop approach and more complex approaches (Vinci et al. 2012). However, methods using low-attachment ULA plates ideally only carry one spheroid per well and have limited automation and final assay capabilities. Recent methods involve the use of more complex technology tools and equipment and have gained worldwide attention. The first is based on the development of microfluidic systems, which are beneficial in cases where system miniaturization is required and allows fine control of liquid elements and shear stress for spheroid formation (Bauer et al. 2017). The second strategy is based on additive manufacturing, often known as 3D printing, which allows for finer control of the platform desired shape and diameter (De Moor et al. 2018). In comparison to

previous methods, producing cell spheres within enclosed microfluidic channels is appealing since evaporation is minimal and a reduced media volume per sphere can be used. A single device *inlet* can also provide media to all of the enclosed microwells, making simultaneous media exchange to all spheres possible with a single pipetting operation. Two primary 3D printing strategies have been investigated in the last decade. The first relies on creating architecture-specific micro molds using computer-aided design (CAD) software, which are then printed using non-adhesive materials and into which the cells are then placed for spheroid formation (Mehesz et al. 2011). The second technique is based on 3D bioprinting, in which cells are mixed with biocompatible hydrogels and then deposited in microchambers within a scaffold or on a surface capable of facilitating or encouraging in situ spheroid formation (Jiang et al. 2018). 3D bioprinting can also be employed to produce microtissues directly, without the need for a previous stage of spheroid development (Fedorovich et al. 2012). In the following chapter we will focus on 3D printed micro mold technologies for obtaining spheroids. Specifically, methods for producing mold with a large number of micro-cones will be described. These methods are used to cast microwells with well-defined dimensions and forms.

1.2.2 The challenges of micropatterned surface technology

Despite the development of various 3D cell culture techniques, producing uniformly sized spheroids that can be individually addressed with drug compounds remains a challenge. In fact, the population of spheroids produced by 3D cell culture techniques is often fairly dispersed in terms of size and shape, which can strongly influence the outcome of drug efficacy and toxicity studies. The production of such characteristics is significant for medical applications for various reasons. Firstly, it allows for reproducible and robust drug screening results and a deeper understanding of tumor biology. In most cases, compact spheroids are more drug-resistant than aggregated cells, whereas smaller spheroids are more sensitive to chemotherapy and radiotherapy (Däster et al. 2017; Gencoglu et al. 2018). Second, homogeneous MTSs can be mass-produced in large quantities, allowing high-throughput drug testing. The development of standardized spheroid fabrication procedures could potentially reduce data variability and enhance the clinical significance of experimental data derived from spheroid systems. To generate size-controlled spheroids, microfabrication of microstructured devices has been investigated. The process focuses on creating a mold with a numerous array of micropillars (or micro-cones) that will be employed to cast microwells with well-defined dimensions and shapes in a biocompatible material. Micro patterned master molds are typically made with soft lithography and 3D printing technologies. This method is based on the application of CAD software, which collects specific input of the dimensions, diameters, areas, and volumes of the micro-cones printed on the material that will be used as a

mold. Therefore, the master mold is constructed in terms of dimensions and geometry to allow the formation of spheroids within microwells with determined size and shape properties. In a 3D printer, the CAD design is converted in the master mold with quality and resolution suitable with the designed dimensions, which can range from less than 1 μm to more than 500 μm. Reusable primary molds can be successfully obtained within a few hours thanks to the layer-by-layer deposition of material.

Acrylate-based photopolymers, Polymethylmethacrylate (PMMA), polystyrene (PS), photopolymerized polyethylene glycol dimethacrylate (PEGDMA) and acrylic resins are among the synthetic polymers most employed in mold manufacturing. For what concerns the components for device production, PDMS is one of the most employed materials. Specifically, PDMS is found to be an appropriate material for both spheroid formation and long-term perfusion culture with minimal cellular attachment due to its hydrophobic nature, optical transparency, and gas permeability. Although PDMS can prevent cell adhesion for specific cell types, some highly adherent cells can still adhere on this substrate, especially in the serum rich culture media which can contain many adhesion factors. Reliable non-adherent coatings are critical to avoid adhesion, which can alter the behavior of cells and prevent sphere formation. In fact, a crucial aspect for correct spheroids formation is providing a non-adhesive surface, so cellular attachment occurs exclusively between cells and not between cells and the surface of the device.

Coating treatments with various chemical compounds are routinely utilized to improve the hydrophobicity of PDMS. These materials include surfactants (F-127; F-108), Polyvinyl alcohol (PVA), bovine serum albumin (BSA). Spheroid production has also been found to be improved by coating microchannel walls with a layer of poly (hydroxyethyl methacrylate) hydrogel. PDMS, on the other hand, can be made hydrophilic by plasma treatment, as necessary for certain applications (Huang et al. 2013; Chen et al. 2015; Luk et al. 2008). Moreover, natural polymers such as collagen, gelatin, alginate, and agarose generate hydrogels that are often cast into microstructured molds and used for spheroids culture (Zhang et al. 2018; De Moor et al. 2018; Ivanov and Grabowska 2017).

Because the transfer of mechanical energy in microstructured device wells is low and the culture media is static, the only pressure applied on the cells is due to the short column of culture medium above the spheroid. As a result, this method is superior to the traditional stirred bioreactor technique in terms of shear stress. Precisely, the usual shear associated with microstructured well culture happens only during cell inoculation, culture medium exchange, and spheroids removal from the culture system, which are needed procedures in all types of culture systems. Indeed, when compared to alternative spheroid culture procedures, the use of this technology has a significant distinctive feature. Micro molding is regarded as a reliable and repeatable manufacturing approach,

with a wide range of applications and customization for generating microscopic 3D structures. The number of cavities and dimensions of the microstructured non-adhesive device will thus determine how large the spheroid production scale can be expanded.

Spheroids generated in microstructured devices are more uniform in size than those cultured using conventional procedures such as scaffold-based and hanging drop techniques. Because the cells are spatially constrained and the microwells act as foci of cell attachment for self-aggregation, altering microwell dimensions can easily adjust the size of spheroids. The use of micro-molds resulted in more diameter homogeneity than the hanging drop approach, according to a study of 600 spheroids created using both procedures (Mehesz et al. 2011). Furthermore, the authors demonstrated a 40-fold increase in productivity employing the microstructure process in terms of pipetting time and the number of spheroids created. 3D cell culture in microstructured devices competitiveness is evident in a variety of measures, including lower shear stress, improved reproducibility and quality control of the spheroids obtained in terms of mean size and size distribution, and culture medium volumes used per spheroid.

In contrast, less cell manipulation is required in stirred bioreactors, more effective mass transfer is observed, easier spheroid harvesting can be achieved by gravity, and process scale-up is preferred. Although spheroid formation is gradual in both systems, cell to cell communication is significantly faster in the micro molded well method. However, while bioreactors require significant investments in high-quality tanks with temperature, pH, nutrients, and metabolite concentration control devices, as well as a robust stirring system and other accessories, the microstructured systems only requires a 3D printer and molding materials, as well as cell suspension and culture medium dispensing systems and incubators. Additional costs are linked to aseptic manipulation during all process phases for both systems. To conclude, despite the difficulties in direct imaging methods for single spheroid analysis, microstructured devices offer potential use in a wider set of cell-based assays. Nevertheless, complete image analysis of the entire spheroid population remains challenging, and spheroids need to be recovered from culture devices for many procedures.

1.2.3 Spheroid-based drug screening

The development and application of three-dimensional cell cultures in drug discovery are becoming more widespread. Academic laboratories and pharmaceutical/biotechnology industries are currently working to develop new, more relevant in vitro models for drug development. In the last several years, a number of innovative approaches with compound screening platforms using 3D cell culture systems have been developed, particularly for cancer research (Chatzinikolaidou 2016). Multicellular tumor spheroids, as previously said, closely recapitulate the 3D cellular

environment and recreate essential pathophysiological gradients in *in vivo* tumors, which are critical for assessing the therapeutic success of anti-cancer medications. As a result, developing efficient ways to create high-quality tumor spheroids and incorporate them into existing biological screening protocols is crucial. Despite its many benefits, employing MTSs in the preclinical stage to screen new anticancer drugs has a few drawbacks. The primary concern is homogeneity and reproducibility in generating MTSs of uniform shape and size. The second problem is determining how to create a reliable method for assessing MTS development and drug efficacy. Also, significant for the 3D platform is the ability to adapt to high-throughput screening. In fact, the development of high-throughput MTSs culture for drug screening techniques is a critical component for commercial applications. The size of MTSs is influenced by cell type, culture duration, and seeding density, which is an essential parameter in tumor biology and drug screening. The diverse cell layers are determined by the MTS's size and providing nutrition and oxygen inside the spheroid becomes more problematic as it grows larger. As a result, optimizing or regulating the spheroid size is important, but it is indeed difficult. Even though the size of the MTSs created is determined on a variety of parameters, the size of the spheroids formed is frequently significantly different, even when the conditions are the same. Consequently, it's essential to design standardized and reproducible techniques for 3D cell culture of comparable size and morphology. However, the more sophisticated the developed systems, the more difficult it will be to implement them in high-throughput platforms.

Researchers are still working on reproducible scalability of these systems in 96- to 384-well plates so that they may be incorporated into an automated screening system that is compatible with existing assays and analysis procedures. Nonetheless, high-throughput platforms are critical, particularly for screening new drug candidates, as both academia and industry need increasingly strong, predictive, and repeatable 3D culture models for this reason (Edmondson et al. 2014; P. Joshi et al. 2018). Spheroid form and size, in particular, can have an impact on drug delivery and efficacy. As a result, in order to reduce inaccuracy and improve reproducibility, it is essential to regulate the concordance of spheroid morphological features. The ideal spheroid diameter for cytotoxicity testing is a hot topic in the literature, and no agreement has been achieved yet. Spheroids with a diameter of up to 200 μm have been shown to be able to model 3D cell-cell and cell-matrix interactions, and they are often used in drug testing. (Lambert et al. 2006; Fehlauer et al. 2005; Friedrich et al. 2009). On the contrary, larger spheroids present a hypoxic core and are more heterogeneous, containing cells at various stages of proliferation (Nath and Devi 2016). The presence of a necrotic core might be advantageous for some drug testing methods but troublesome for others. Because passive diffusion of nutrients and oxygen is insufficient, large tumors in vivo necessitate the establishment of capillaries that allow blood perfusion in order to

maintain cell activities at the core (Alemany-Ribes and Semino 2014). Spheroids with a diameter more than 500 μm develop a secondary necrosis core in the absence of a perfusion system in vitro, complicating pathophysiological conditions and making them harder to manage, lowering the accuracy of the cytotoxicity assay (Inamdar and Borenstein 2011; Wan et al. 2016). For these reasons, a number of researchers choose to deal with spheroids with diameters ranging from 200 to 500 μm (Hardelauf et al. 2011; Patra et al. 2016; Chen et al. 2015; Ivanov et al. 2014; Dadgar et al. 2020). In conclusion, choosing a spheroid formation technique is very important because they are not equivalent to forming spheroids. Many limitations, such as cost and reproducibility, have restricted the use of tumor spheroids. Different spheroids' culturing techniques will influence the shape, size, surface features, inner textures, and density. However, there is still no consensus on which model best depicts the biology of distinct tumor forms and, as a result, should be used for screening purposes. Further technological advancements, personalized medicine, and model development will undoubtedly solve these limitations.

1.2.4 Challenges in thick specimen imaging

Although 3D cell culture is one of the most extensively used *in vitro* models, it presents some basic obstacles, such as spheroid size and morphology variability, poor light scattering, and poor antibody penetration inside the spheroid structure which makes imaging challenging. In spheroids, cell size, cell number, and cell density have a significant impact on the development of pathophysiological gradients, as well as their pharmacological response. Spheroids composed of loosely structured cells, on the one hand, need special care in handling because they tend to disintegrate. In contrast, densely packed spheroids provide issues in imaging and compound distribution. Standard fluorescence microscopy techniques cannot image deep into the spheroids. Live spheroid microscopy at a cellular or even subcellular resolution is complex using standard techniques such as widefield fluorescence microscopy and laser-scanning confocal microscopy because of their size in lateral and axial directions (Schneckenburger and Richter 2021).

A wide variety of microscopic approaches are available for studying 3D cellular models. While not adequate for deep sample imaging, widefield fluorescence microscopy can be employed as a starting point for quantitative analysis. Widefield imaging can even offer considerable advantages over more complex approaches in circumstances when only the size of the spheroid or the global level of fluorescence is relevant due to its fast image collection and low phototoxicity. Moreover, large spheroids (>150 μm) imaging is quite challenging with confocal microscopy. Poor light, antibody penetration and attenuation of fluorescent signals due to light scattering are the main drawbacks. Firstly, for 3D sample imaging, Light Sheet Fluorescence Microscopy (LSFM)

is extensively used. LSFM is a widefield approach that involves optical sectioning with the specimen illuminated from the side (at 90 degrees to the microscope axis) by a cylindrical lens or laser scanning (Pampaloni et al. 2013). The principal advantage of light sheet is that only specific sample planes are illuminated and simultaneously recorded, resulting in significantly lower light exposure than other approaches. However, light-sheet microscopy, which has been successfully applied to imaging large samples (i.e., larvae, embryos) cannot be used as a universal tool for 3D cell model imaging. In fact, LSFM requires special equipment for sample preparation (clarification), mounting, and generates large datasets that need to be stored and processed. The use of optical clearing techniques on scaffold-free self-assembled spheres can have a variety of effects on sample size and opacity and protocols should be chosen in a sample-dependent fashion. Light dispersion is caused by refractive index mismatches between biological components, making fluorescent signal collection difficult in thick tissues. Optical clearing agents have been developed to address this issue, reducing scattering by better matching refractive indices within tissues or removing scatter-inducing cellular components (Becatti et al. 2020). Furthermore, two-photon excitation microscopy (TPM) allows noninvasive and deeper quantitative imaging with low phototoxicity and sufficient resolution of thick samples, as 3D spheroids. Compared to confocal microscopy, two-photon microscopy uses longer excitation wavelengths to reduce scattering and absorption while also lowering photodamage to the sample. For example, we included images of the same spheroid (200 μm of diameter) imaged with the confocal and two-photon microscope at the *Molecular Imaging and Photonics Lab*, KU Leuven (**Figure 7**).
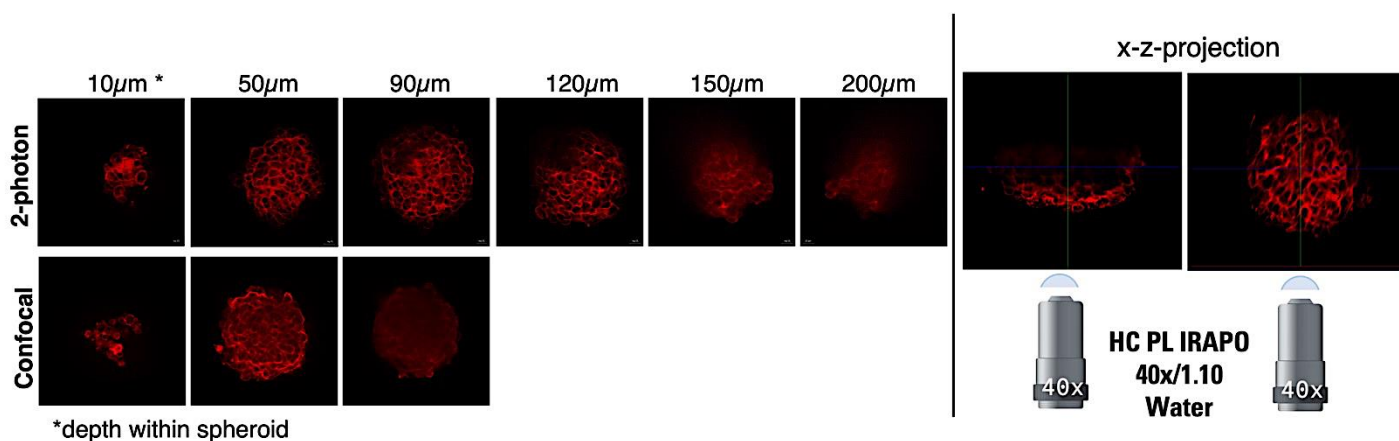
Figure 7: Imaging penetration depth comparison between confocal and two-photon microscope: Z-scans of the same sample were acquired with the two microscopes**.** While images with sufficient signal intensity can only be obtained from the outer 50μm in confocal images, penetration depth exceeds 150μm for 2P-excitation at a wavelength of 1294 nm. HCT116 spheroid stained with phalloidin 647 (red) and mounted with agarose LMP 0.5%. Images obtained at MIP laboratory, KU Leuven University

Cellular resolution can only be obtained in areas less than 50-100μm away from the surface in the majority of applications. In 2-photon microscopy, the dye is excited by the simultaneous

absorption of two photons of longer wavelengths. In this approach, the necessity for near-simultaneous absorption of two photons leads to single-point excitation with low background noise and minimized photobleaching. Specifically, the lower excitation volume is another significant advantage of 2-photon excitation over single-photon excitation. The 2-photon effect can only happen at the objective's focal spot, where the photon flux is extremely strong. However, in single-photon microscopy, stimulation occurs both above and below the focal plane, resulting in far increased phototoxicity. This advanced microscopy technique is also used for localizing nanoparticles within thick samples (Pratiwi et al. 2021; Rane and Armani 2016). To conclude, the use of modern fluorescent microscopes in association with optical cleaning technologies has considerably improved the imaging of large biological samples (penetration depth, image contrast, and spatial resolution) as 3D spheroids.

1.3   Microfluidics applications for advanced cell culture

Microfluidic devices provided powerful tools for biological and chemical studies. Microfluidic systems for cell culture are suitable for drug discovery and toxicity assessment in ways that go beyond traditional static culture models (Rothbauer et al. 2018). Integrated systems that combine microchannels with pumps, valves, filters, and sensors are referred to as "lab-on-a-chip" (LOC) or "micro total analysis systems" (µTAS). The introduction of microfluidics in the life sciences has made it possible to face, and often overcome, the crucial limits present in standard analysis systems, allowing the control of temperature, gases, geometry, regulation of nutrient supply, removal waste management, compound treatments, and dosage parallelization, as well as culture automation (Reichen et al. 2013). Cell-based microfluidics was initially developed for cell counting and analysis in miniaturized flow cytometers, which are commercially available systems today (Schrum et al. 1999). Microfluidic devices for cellular studies have also been fabricated to study cell transport and culture in the absence and presence of concentration gradients, temperature or shear force conditions (Andersson and Van den Berg 2003). Other applications include cell sampling, cell entrapment, sorting, patterning, capture, drug delivery and multiparametric cell analysis. These systems can provide defined and reproducible simulation scenarios that allow the investigation of cellular behavior in an environment that mimics the mechanical forces within living tissues (Rothbauer et al. 2018). Furthermore, microfluidic devices for cell culture help study drug effects, supplements and potentially toxic agents thanks to improved response times and reduced costs (Auner et al. 2019). High throughput multiplexed microfluidic devices could be used to test compounds more quickly and under more conditions. For drug development and testing, microfluidic culture models have been employed to imitate the liver (Kamei et al. 2019; Wang et

al. 2010) kidney (Jang et al. 2013), lung (Ruzycka et al. 2019), blood vessels (Nie et al. 2018), and gastrointestinal tract (Xiang et al. 2020).

Moreover, microfluidic cell culture systems have a wide range of applications as *in vitro* platforms for disease and damage simulation. Injury (Kim et al. 2012) celiac disease (Moerkens et al. 2019) Alzheimer's disease (Park et al. 2018), and, most notably, cancer (Mathur et al. 2020) have all been studied using microfluidic devices. Finally, microfluidic based 3D models of cancer are catching up fast. Recent advances in microfluidics have contributed significantly to 3D spheroid research, by incorporating spheroids in microfluidic systems with different methods. Lee et al. observed that cell viability of hepatocyte spheroids was lower in static condition when compared to dynamic culture conditions in microfluidic platforms after days of culture (Lee et al. 2013). Furthermore, Ruppen et al. observed that cancer spheroids exposed to continuous drug perfusion had higher drug resistance than spheroids in static conditions (in a microwell plate) (Ruppen et al. 2014). Continuous perfusion culture does, in fact, improve cell oxygen and nourishment delivery. In addition, considering the growing impact of personalized medicine, patient material can be used to grow highly standardized tumor spheroids in microfluidic devices on a massive scale before testing drug potency. The impacts of the tumor microenvironment might be considered in this way. Combining these approaches will result in very efficient workflows for determining the best treatment option for each patient, while also supplementing the limited information on predictive genetic indicators (Stockslager et al. 2021).

1.3.1 Microfluidic culture platforms in neuroscience research

The following chapters of this work will focus on the development of a microfluidic platform applied to the study of microglia activation and communication mechanisms in the context of neuroinflammation.

In the field of neurology, microfluidics technologies have been used to investigate cellular/molecular mechanisms and complex interactions that occur among neural cells, bringing crucial insights to nervous system research (Park et al. 2006). Traditional research methods, such as co-culturing neurons and glial cells, are insufficient to preserve biochemical and physiological axon–glia interactions in culture. This approach fails to study the axon-glia communication network and the processes that influence different regions of the neuron in neuronal damage and neurodegenerative disorders (e.g., spinal cord injury and Alzheimer's disease) (Gross et al. 2007). On the other hand, microfluidics is characterized by compartmentalized platforms that may be used to isolate axons from neuronal cell bodies and explore interactions between different cell types using controlled flows. Indeed, this method allows for the co-culture of multiple cell

populations in close proximity, making it an ideal tool for neurons-glia co-culture. The Campenot chamber, a three-chamber culture device for neuritic isolation, was one of the earliest microfluidic platforms produced for neuronal research (Campenot 1977). This method allowed the division of axons from neuronal cell bodies. Further studies using the Campenot chamber have led to significant breakthroughs in axonal growth, degeneration, and regeneration in the peripheral nervous system (PNS) (Raff et al. 2002; Zweifel et al. 2005). However, the method required a lengthy operation, and the system was unsuitable for live cell imaging, necessitating the removal of the chamber and cell fixation. Later, various novel platforms made it possible to examine the axonal and neuronal environment at a deeper level. Microgrooves, in particular, housed axon extensions of neurons in close proximity to the microchannels, allowing for precise separation of axons from respective cell bodies (Taylor et al. 2003; J. Park et al. 2009; Rhee et al. 2005). Hosmane et al. used a circular microfluidic device to explore axon–microglia interactions in a fascinating study. The created PDMS device was made up of separate microchambers with microchannels that separated axons and neuronal cell bodies (Hosmane et al. 2010). Microglia were also directly placed into areas of interest in the axonal compartment using patterned microstenciling. Microglial response to degenerating axons was studied, as well as glia migration towards wounded axons. In addition, the coculture technique allowed researchers to investigate microglia activation by looking at gene expression associated with M1 (iNOS and CD32) and M2 (Arg1 and SRB1) states. Moreover, combining 3D culture techniques and microfluidics platforms, more appropriate human brain models can be generated. Park et al. created a three-dimensional (3D) microfluidic system that replicated the interactions between neurons, astrocytes, and microglia in the context of Alzheimer's disease (AD). This tri-culture platform featured a core chamber and numerous peripheral chambers connected by microchannels to the central one. Microglia recruitment and phenotypic modifications were studied via migratory channels in the Matrigel-coated central chamber, which housed neurons and astrocytes differentiated cells. This platform application offers a significant improvement over current in vitro human AD models, allowing us to investigate the function of human microglia in neuroinflammatory molecular pathways and neuron/astrocyte destruction, which could be important in AD pathophysiology (Park et al. 2018). To conclude, microfluidic platforms have shaped new perspectives on how we handle biological samples and matrices. When compared to traditional macroscale approaches, microfluidics allows for the manipulation of cellular microenvironments, the investigation of interactions of different chemical agents on individual neurons and glia, and the targeted analysis of cell-to-cell connections and single cell projections.
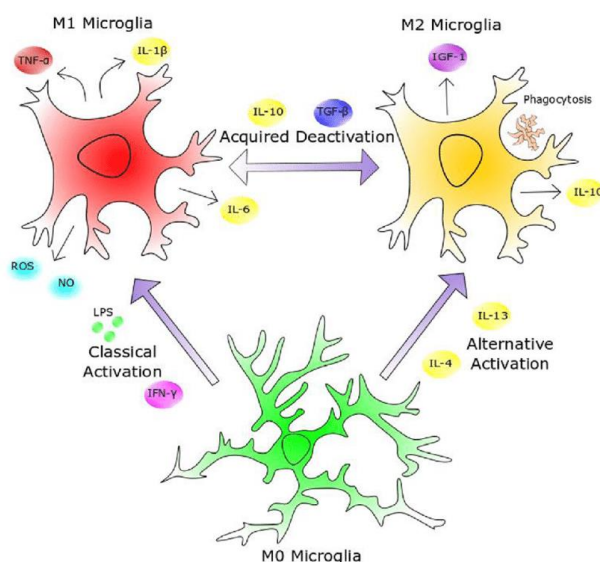
1.3.2 Microglia and neuroinflammation

Central nervous system (CNS) diseases remain a prevalent and persistent clinical problem due to our incomplete understanding of their pathogenesis. In the past, the relevant part of CNS disease research focused on neurons. In the last decade, a large number of studies in continuous and rapid growth indicate that microglia, as the representative of immune cells in the CNS, plays a key role in neuropathic and neuroinflammatory diseases (Dai et al. 2015). Neuroinflammation is an important feature shared by various neurodegenerative diseases such as Parkinson's disease (PD), Alzheimer's disease (AD) and amyotrophic lateral sclerosis (ALS). Activation of microglia is the primary component of neuroinflammation in the central system (CNS), providing the first line of defense whenever injury or disease occurs. Neuroinflammation is now seen as a double-edged sword that can bring both harmful and beneficial effects to neuronal cells. Microglia mediates host defense against infectious pathogens, self-harmful proteins such as β-amyloid (Aβ), aggregated α-synuclein, mutant huntingtin, mutant, or oxidized superoxide dismutase (SOD), prions, as well as primary or metastatic tumors of the SNC. In response to these stimuli, microglia can initiate a neuroinflammatory response which, like peripheral inflammation, includes the production of cytokines (e.g., TNF and IL-16,27) and chemokines (Ccl228) to recruit additional cell types necessary for the maintenance of brain homeostasis. Neuroinflammation, however, unlike peripheral inflammation, can also be limited to microglia without recruiting circulating leukocytes. The persistence of this state can induce neurotoxicity, which leads to neurodegeneration. Sensing, cleaning and protection functions keep microglia cells constantly engaged, the deregulation of any of these functions causes an imbalance that initiates neurodegeneration (Hickman et al. 2018).

1.3.3 Microglial phenotypic diversity: M0 and M1 phenotypes

The resting microglia cells (M0) in the adult brain have a morphology characterized by a small cell body and numerous protrusions, characteristics that distinguish these cells from macrophages and dendritic cells. As part of their homeostatic functions, microglial cell bodies remain stationary, but their processes continuously scan the surrounding extracellular space and communicate directly with neurons, astrocytes and blood vessels. This state of perpetual motion allows them to respond quickly to damage or infection, expressing an activated phenotype by transforming and performing inflammatory or anti-inflammatory functions. Microglia is, therefore, an extraordinary plastic cell, able to respond to a wide range of stimuli.

Once specific factors generated by parenchymal lesions, degeneration or infection are detected, the microglia undergo morphological transformations to overcome and repair the insults

suffered by the CNS. Shifts in morphology, phenotype and microglial functions are observed during almost all neuropathological conditions (e.g., degenerative diseases, infections, strokes, tumors, brain injuries) (Wolf et al. 2017). Activation of microglia can be divided into two distinct types: the classic one (M1) and the alternative one (M2) (*Figure 8).* M1 activation is the most explored activation state in animal models and has been characterized by studies on the immune response of peripheral macrophages. This type of activation is characterized by a response stimulated by microorganisms with consequent expression at high levels of pro-inflammatory cytokines and a greater microbicidal capacity. Interferon-γ (IFN-γ) causes activation in the M1 phenotype, a response usually associated with host defense from intracellular pathogens. Recent evidence suggests that the macrophage cell itself has the potential to adopt M1 or M2 profiles based on the type of stimulus (e.g., aging, injury or chronic disease).

Figure 8: Microglial activation pathways: Upon stimulation with LPS or IFN-γ microglia polarize to M1 pro-inflammatory phenotype (up, left), M1-microglia releases cytokines and chemokines such as IL-1β and IL-6. These molecules mediate in neuroinflammation and pathogen removal. On the other hand, IL-4 and IL-13 enhance the M2 anti-inflammatory state (up, right) M2-microglia releases cytokines and chemokines. They mediate inflammation attenuation and homeostasis reestablishment (Gray et al. 2020). Image under Creative Commons Attribution 4.0 International license

Microglia cells, like peripheral macrophage cells, acquire states of "classical activation", "alternative activation" and "acquired deactivation", depending on the environment in which they are activated and the factors that lead to their stimulation. The classic M1 activation state, stimulated by lipopolysaccharides (LPS) and IFN-γ, induces the pathways of inducible nitric oxide synthase (iNOS) and NF-κB and the consequent production of various pro-inflammatory cytokines such as TNF-α, IL-1β and IL-6, as well as superoxide, reactive oxygen species (ROS) and nitric oxide (NO) (Petralla et al. 2021). The M2 phenotype includes the states of alternate activation and acquired deactivation, which is induced by IL-4/IL-13 and IL-10/TGF-β, respectively. M2 microglia facilitates the phagocytosis of cellular debris, promotes ECM reconstruction and tissue

repair, and supports neuron survival via neurotrophic factors (Tang et al. 2016). When compared with circulating macrophages, the typical morphology of microglia is characterized by short and fine processes, which allows them to effectively perceive and monitor even small changes in the local brain environment. Their large surface allows fine communication with the surrounding environment, which is necessary for monitoring the cerebral microenvironment in healthy parenchyma. The morphology of branched microglia is strikingly similar between humans and mice, suggesting highly conserved functions of the microglia between species. To adopt an active state in response to pathophysiological cerebral insults, during cerebral inflammation, it assumes the characteristic amoeboid morphology with attenuated motility of processes. This morphology is often thought of as a transformation towards a macrophage phenotype. Interestingly, changes in morphology may correspond to alterations in microglial function and these changes are related to brain damage or repair (Xiong et al. 2016). Furthermore, Toll-Like Receptors (TLRs) allow microglia to respond to both exogenous and endogenous threats (Janova et al. 2016). TLR activation ensures immediate host responses to infection and tissue damage, regulating innate and adaptive immune functions in several steps. TLRs recognize viral and microbial RNA, DNA, glycolipids and glycopeptides, classified as pathogen-associated molecular patterns (PAMP)(Gay et al. 2014). It is known that LPS, as a component of the outer membrane of gram-negative bacteria, is recognized by Toll-Like receptors. It has also been observed that this recognition causes the activation and consequent change of state of the microglia from M0 to M1, developing a proinflammatory phenotype (Dai et al. 2015).

All neural cells, including neurons, astrocytes, oligodendrocytes and microglia, release extracellular vesicles (EVs) which include exosomes and ectosomes, under normal or pathological conditions. Recently, more attention has been paid to the ability of EVs to transfer genetic information between cells, in particular mRNA and microRNAs (miRNA). The intercellular communication based on these functional RNAs requires their selective compartmentalization in an appropriate vesicle, which guarantees protection from circulating RNAs and therefore the maintenance of their ability to control gene expression. The expression of various miRNAs, which are involved in numerous cellular processes, can characterize the "resting" state of microglia as well as the M2/M1 activation states. For these reasons, EVs represent an optimal candidate for genetic exchange between cells by modulating the behavior of recipient cells. The EVs are therefore essential for cellular communication in the CNS and beyond, they provide a fine regulation tool for the various cell types, allowing the remote transfer of complex molecules and genetic material. For these reasons, several studies promote their involvement in the spread of the inflammatory state also among microglia cells (Bonafede and Mariotti 2017; Dabrowska et al. 2019).

2.   AIM OF THE STUDY

This research work aimed to develop two innovative methodologies designed for the optimization and standardization of advanced *in vitro* cell culture models. Micro-technologies, such as microstructured devices or microfluidic platforms are powerful tools in biomedical research, in principle able to provide more advanced physiologically reliable results without involving the use of laboratory animals.

Firstly, we wanted to design a microwell-based device allowing the cultivation of hundreds of spheroids to conduct drug experiments and characterization analysis. Part of our purpose was to fabricate a customizable 3D model cultivation tool to be used for drug screening on highly homogeneous spheroids, minimizing cell loss and preventing the escape of spheroids during device handling. In parallel, we wanted to validate the system with different cell lines and verify it to be an all-in-one platform for microscopy analysis as well. The focus of this study was to help expand the use of spheroids in drug screening platforms by filling the unmet need for an easy one-step method adaptable to various standard analyses and producing multiple, homogeneous, image-compatible 3D structures. We concentrated on the characterization of this method and proving its suitability as a cultivation system, aiming to implement it as a drug screening platform.

The second goal, towards developing a microfluidic system, was to explore advanced methods of culture manipulation to improve standard *in vitro* experiments. Microfluidic technology has enormous applications in every field of life science, allowing culturing cancer and non-cancer cells. We chose to fabricate an innovative microfluidic platform and face different approaches regarding culturing mouse microglia cell line (N9) within the system to conduct growth and viability analysis. We wanted to design new strategies to put into communication cell cultures grown separately through regulated flows. The opportunity to perform cell culture and molecular investigations in an automated and highly adjustable system was the first step to achieving in-depth studies on cellular environment and interactions. About this, the goal was to provide a new and alternative approach to overcome the common cell culture limitations in relation to studies on the role of microglia in neuroinflammation spreading.

To conclude, the presented Ph.D. work mainly concerned the development of advanced cell culturing methods. Consequently, an essential aspect of the project regarded protocol documentation. Standard Operating Procedures (SOPs) have been written, describing in detail the various methodologies developed to achieve uniformity and efficiency of the experimentations.

2.1 Structure of the Thesis

This work will present the development of two advanced culture platforms. The Thesis is organized into two parts, each relative to a specific culturing system. *Material and methods* and *Results and Discussion* chapters will mention the fabrication processes and the results related to each topic separately.

The first platform consisted of a microstructured device for highly uniform spheroids generation. A key contribution of this work over state of the art in this field is to demonstrate how our microstructured device will be fully functional as an all-in-one platform for several characterization analyses. The proposed architecture is fully scalable and flexible, offering even the possibility of *in situ* immunofluorescence. In recent years, there have been very few examples of immunostaining protocols that have used a similar approach in the literature.

The second culture system consisted of a microfluidic device suitable for selective cell culture treatments. The microfluidic device was used as an alternative means by which to replicate and confirm *in vitro* experiments performed with standard culture methods. We propose the innovative aspect of choosing and developing the most suitable technology to achieve scientific results.

In conclusion, an important aspect should be pointed out. The two platforms result from different scientific investigations, which aim to solve different problems, but nevertheless have the primary purpose of performing drug treatments on cells in a reproducible fashion (including chemotherapy medications, chemical compounds, nanostructures, endotoxins etc.).

Finally, our recently developed system that combines a microfluidic system with a microwell array for three-dimensional cell culture will be mentioned as a future prospect.

3. MATERIALS AND METHODS

3.1 Fabrication of microstructured devices for 3D cell culture

An essential starting point for the formation of a culturing system for homogeneous spheroid generation was the fabrication of the master mold that can be used to make multiple casts. The positive mold (with convex shapes, like cones for microwells formation) must present several characteristics to ensure that the negative mold (final cast with microstructured surface) had a minimum distance between the microwells and that they are deep enough to allow spheroid formation after seeding. Thanks to the collaboration with Prof. Attila Bonyár from the Department of Electronics Technology of Budapest University-Hungary, several master molds have been produced (**Figure 9**). Different models were designed with *OpenSCAD* (https://openscad.org/) and *Autodesk Inventor 2010* (https://www.autodesk.it/). Further modifications have been made regarding cones geometry. In previous mold versions, the cones were packed in a looser arrangement, but then mold design was modified to result in the least number of flat areas between the cones. Before selecting the final mold for devices production, various designs were used to test spheroid generation with different cell lines.
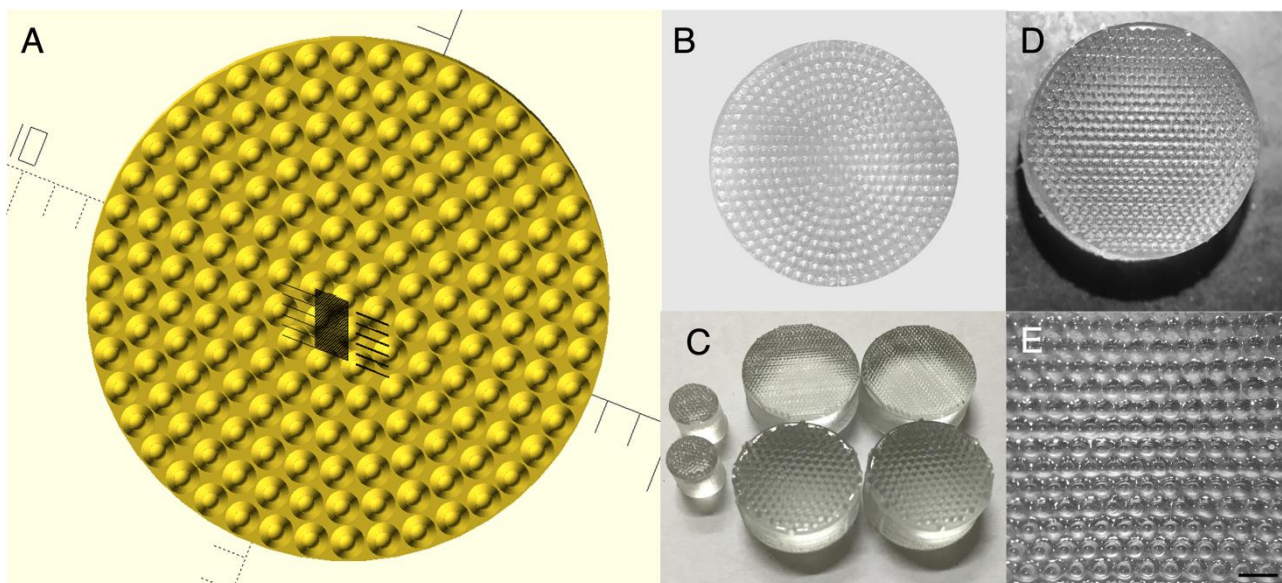
Figure 9: Examples of master molds fabrication design. (A) OpenSCAD model with 170 cones. (B) PDMS positive mold example. (C) Master mold with different dimensions and cones arrangement made with 3D printing technique (D) Master mold chosen for device production (E) Details of cones array on mold surface (scale bar: 1mm)

3.1.1 Microwell surface manufacturing

Microstructured wells were made by fitting thin microstructured poly-dimethyilsiloxane discs (PDMS, 15 mm in diameter) on the bottom of commercially sourced multi-well plates. The PDMS discs were replica-molded on microstructured resin molds. The positive mold surface was characterized by a packed hexagonal arrangement of 429 *micro-cones* of 0.35 mm of height, 0.15 mm of spacing and 0.5 mm of base diameter. To fit in 24-well plates, molds had a cylindrical shape with a base diameter of 1.5 cm. The design is scalable and can be extended to obtain molds for a 6- or 12-well plate, or reduced for fitting in 96-well plates, if desired, with a change in the total number of microstructures in each well. The molds were fabricated with *3D* printing technique using an *Objet Geometries Eden 250 printer* with FullCure 720 base material and FullCure 705 support material. This set-up has a lateral printing resolution of 40x80 µm. After printing, all the produced structures were treated with a 7% NaOH for 30 minutes to remove any residual support material. To ensure homogeneity and control over devices thickness, the cylindrical molds were placed within dedicated holders and ~1 ml of PDMS (Sylgard184® 1:10 ratio of curing agent:base, DOW Chemical Company) was poured over their surface. Molds were degassed for 10 minutes under vacuum, then the top surface was covered with a glass slide to provide the devices with a flat base. Devices were then cured at 60 ºC for at least 1 hour and then peeled off from the mold and occasional excess silicone was removed with a scalpel. Devices were rinsed in 70% ethanol and dried under a stream of nitrogen gas. To fix on the multi-well plates, a small drop of uncured PDMS was poured on the bottom of a well and let it spread on the well surface. One PDMS device was then gently laid on the bottom of the well and left to cure at 60ºC for at least 60 minutes. The final PDMS device consisted of a microstructured surface where each microwell had an approximate diameter of 400 µm and a depth of 350 µm. Similar microwell devices can be made in agarose using the same molds. For this procedure, sterile 2 % agarose (Sigma-Aldrich) in 0.9% (w/v) NaCl was poured on master molds and a glass slide was then placed on top to provide device flat surface. After removing the master template, the agarose scaffold with highly ordered micro-wells was placed on the bottom of a culture well.

3.1.2 Device inserts sterilization

The microwell inserts were made non-cell-adhesive by overnight incubation at room temperature with a sterile solution of 1% Polyvinyl alcohol (PVA) in water (Trantidou et al. 2017). Care was taken in ensuring complete wetting of the surfaces and in getting rid of any air bubbles. Then, the wells were rinsed with PBS and sterilized with 1 mL of 70% ethanol/water for 60 min at room temperature. The wells were then washed twice with 1 mL of PBS, and, for sterilization, the

plate was kept under UV light present in a standard biosafety cabinet for 50 minutes. The wells were left overnight in PBS to ensure complete extraction of residual ethanol from the PDMS. When the plates were prepared for later use, sterile water was used instead of PBS, and the plates were then dried. Prior to use, 500 µl of cell culture medium was added to each well and the plate was kept in an incubator at 37°C before cell seeding.

## 3.2 Spheroid formation and characterization

3.2.1 Multicellular tumor spheroids culture

Different cancer cell lines were tested for the generation of 3D tumor spheroids. They were generously provided by Prof. Anna Maria Porcelli (*FaBiT, Bologna University*) and were obtained from the American Type Culture Collection (*ATCC*). HCT116 (colorectal cancer cell line); UOK257 (human renal carcinoma cell line); SKOV-3 (ovarian cancer cell line) were cultured in DMEM High Glucose (EuroClone®) supplemented with 10% fetal bovine serum (FBS) plus 1% penicillin/streptomycin (P/S) in 5% CO_2 at 37°C. HRT-18 cell line (Ileocecal colorectal cancer) was cultured in MEM (Gibco) 10% fetal bovine serum (FBS) plus 1% penicillin/streptomycin (P/S). TPC1 cell line (human papillary thyroid carcinoma) was cultured in RPMI medium (Gibco) 10% fetal bovine serum (FBS) plus 1% penicillin/streptomycin (P/S). Neurospheres (consisting of mouse subventricular-zone isolated neural stem cells), generously provided by Prof. Barbara Monti (*FaBiT, Bologna University*), were cultured in DMEM F12 serum-free medium (EuroClone®), supplemented with insulin (10 µg/mL), 1% N2, 1% B27, 20 ng/mL EGF, 20 ng/mL FGF, 2 mM glutamine and 10 units/mL penicillin and 10 ug/mL streptomycin (Sigma-Aldrich).

Before cell seeding, devices were washed twice in PBS, 500 µl of medium were added in each well and the plate was centrifuged at 110 x g for 5 minutes in order to remove the air bubbles trapped in the microwells. For the seeding passage, the desired cell concentration was diluted in 300 µl of medium and added to each well. Then, multi-well plates were centrifuged at 70 x g for 4 min to facilitate the aggregation of the cells into the microwells. For maintenance, medium was exchanged every 48h. During the medium exchange, care was taken not to aspirate the microaggregates by carefully pipetting on the well side without tilting the plate.

Medium was added and subtracted from the same point in the well during each exchange (*Figure 10*). All cells were propagated at 37°C in standard cell culture conditions (5% CO_2, 95% humidity), the outermost wells of the destination plate were filled with sterile PBS to limit media evaporation and avoid fluctuations in drug concentrations and media osmolality during the testing period. For characterization, spheroids were harvested by gently pipetting medium on microwells

with a p1000 micropipette. To prevent spheroids attachment, the pipet tip was previously coated with *faCellitate* (Biofloat ™ Flex, coating solution).
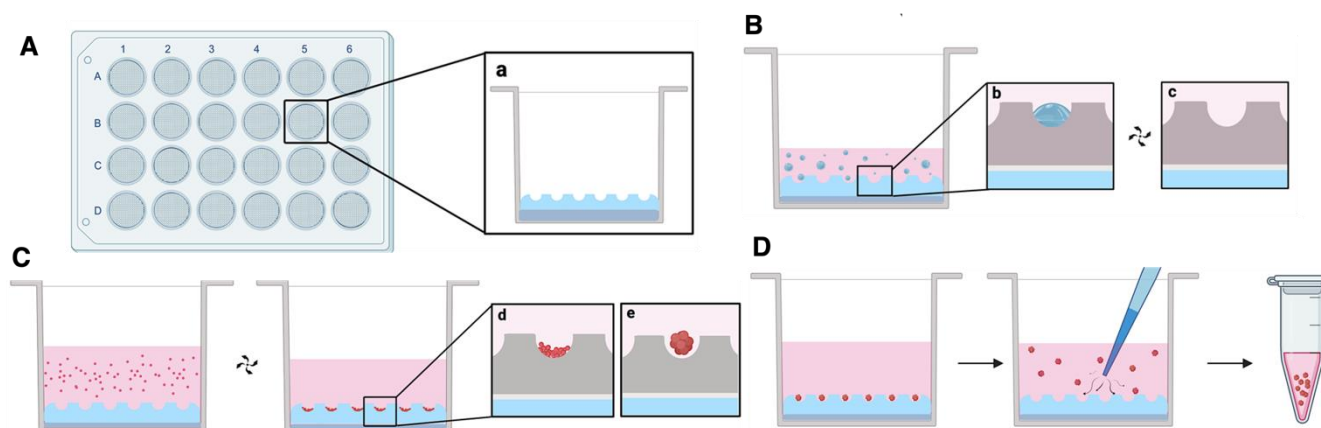
Figure 10: Schematic representation of prototype device workflow. (A) 24-wells plate with devices positioned on wells bottom (a) Schematic cross-section of one well showing PDMS layer for device adhesion; each device presents >400 microwells (B) Air bubbles trapped within microwells (c) air removal after centrifugation step at 70 g. (C) Cell seeding and sedimentation after centrifugation, cells correctly positioned on microwells bottom (d) and spheroid formation afterwards (e). (D) Spheroids can be harvested for further procedures. Created with BioRender.com

3.2.2 Growth kinetics

Phase contrast images of multicellular tumor spheroids were taken using a Zeiss Axio Vert A1 inverted microscope with a high-resolution camera (AxioCam MR CCD) ahead of the start of the experiments up to the end of the treatments with antitumor drugs, which commonly lasted 72 hours. To measure the spheroids diameters, the images were examined using ImageJ software (National Institutes of Health, Bethesda, MA). The volume of spheroids was estimated with the assumption that they had a spherical shape. The same spheroids number per condition (n=28) was monitored and the treatment time was the same for every experiment. Images were analyzed with ImageJ software and the polygon tool was used to outline spheroids. The difference between the volume of spheroids at the end with respect to the beginning of each treatment was used to generate a growth rate parameter (k_c). Similarly, the growth rate (k_0) was computed for spheroids that were not treated. The difference in growth rates of control spheroids (k_0) against treated spheroids (k_c) was divided by k_0 to compute growth inhibitory effects at the end of day 3, i.e., Growth inhibition = (k_0-k_c)/k_0.

3.2.3 Viability assay

Cell viability was measured using an MTT (3-(4,5-dimethylthiazol-2-yl)-2,5-diphenyltetrazolium bromide) colorimetric assay. At the end of the treatments, the spheroids were harvested and resuspended in 100 µl of culture media, then transferred in a new 24-well plate and incubated with 10 µl of MTT 1 mg/mL (Sigma-Aldrich). Tetrazolium substrate was added to

each well and plates were incubated for an additional 4h at 37°C. The spheroids were then solubilized in 800 µl of DMSO and the absorbance was measured at 570 nm using a microplate reader. The viability of the treated spheroids was expressed as a percentage with respect to untreated control spheroids. Data were analyzed with GraphPad Prism 8.

3.2.4 Prototype device comparison with commercial culture plates

3D cell spheroid production of prototype device was compared with commercial products Elplasia® 24-well round bottom plate ULA surface (#441; Corning Life Sciences, 554 microwells per well) and Sphericalplate5D, 24-well plate (Kugelmeiers®,750 microwells per well). HCT116 cells were cultured in growth media until 70% confluency was reached. Cells were trypsinized and counted using a hemocytometer. Because these two commercial plates are different in microwell design and number (Sphericalplate 5D presents pyramidal shaped microwells with round bottom), the required cell seeding densities were also different. As described in 3.2.1, for our prototype device and even for commercial plates residual bubbles may influence cell seeding as well as cell distribution. Therefore, an additional step was required to remove air bubbles before cell seeding. According to the manufacturer's recommendations, microwell inserts were wetted with medium and air bubbles were removed by centrifugation at 1000 x g for 1 min. Cell dilutions were adjusted in such a way that a 500 µl volume contained around 150 cells per microwell in order to generate cell clusters of 100-150 µm of diameter after 24h. Culture plates were placed on a metallic tray and cultured in an incubator under 5% CO_2 at 37°C. During a 7-days culture period, phase contrast images of the cell spheres within the devices were acquired. All plates were incubated for 7 days following initial seeding. Medium was supplemented every other day to maintain proliferation and viability in all plates. Additionally, newly seeded spheres were treated with PTX 25 nM, viability analysis of control and treated spheroids was performed with MTT assay (3.2.3).

3.2.5 Scaffold-based 3D culture

Cell suspensions of 80.000 cells/well (for 200 cells/microwell) were prepared in sterile eppendorf tubes for MCF-7 and HeLa cell lines. Then, the samples were centrifuged for 6 minutes at 250 x g. The supernatant was discarded and a solution with culture media and Geltrex® at a final concentration of 2.5% was added to the cell suspension to obtain a final volume of 100 µl for seeding. 24-well plates containing the PDMS microstructured devices were previously kept at 4°C, and a thin layer of cell culture media was added to each well. Cell suspensions were then seeded in each well and plates were centrifuged at 70 x g for 4 minutes. After 20 minutes at 37°C,

500 µl of cell culture media were added to each well. Spheroid formation and diameter measurements were assessed with a light microscope and compared to spheroids generated in parallel with the usual seeding method for PDMS inserts. As above mentioned, images were analyzed with ImageJ and the circularity of the spheroids was measured as $(4\pi\times[Area])/[Perimeter]^2$, and ranges from 0 for infinitely elongated polygon to 1 for perfect circle.

3.2.6 Chemicals and Treatments

Briefly, HCT116 cells (80.000 cells/well) were seeded into 24-well plate with microstructured PDMS inserts (i.e., about 200 cells/microwell), following the same protocol described above. Three different compounds were tested and incubated for 72h: Paclitaxel (PTX; Sigma-Aldrich; 25, 50, 100, 250 nM), Doxorubicin (DOX; Sigma-Aldrich; 250, 500nM, 1, 2 µM), Suberoylanilide Hydroxamic Acid, also known as SAHA (Sigma-Aldrich; 500nM, 1, 2, 5 µM). Paclitaxel and SAHA were solubilized in dimethyl sulfoxide (DMSO) and the final concentration of DMSO in each cell culture was 0.1% in all cases. Doxorubicin was solubilized in distilled water. Four different concentrations of each compound were prepared by serially diluting a stock solution in cell culture media. Two wells were seeded for each concentration (about 400 spheroids each) after confirmation of the homogeneity of spheroid size in each well.

3.2.7 Live and dead assay and automatic analysis

Live spheroids were labeled directly while in the microstructured PDMS microwells, after removing most of the culture medium. Staining was performed with fluorescein diacetate (FDA, Sigma-Aldrich, 10 µg/ml, ex/em 490/520nm) and Propidium Iodide (PI; Sigma-Aldrich, 8 µg/ml, ex/em 536/617nm) diluted in cell culture medium without FBS. FDA labels the viable cells cytoplasm in green, PI labels the nuclei of dead cells in red. Prior to the live and dead labeling, were added 150µl of a 0.5% low melting temperature agarose solution were added to the microwells to avoid cell dispersion, especially in the loose peripheral layer all around the spheroids. The double staining was performed by incubation in a dark room at 37°C for 1h before epifluorescence microscope analysis (Nikon Eclipse 80i with Hamamatsu Flash 4 sCMOS digital camera). Four different device areas were acquired with 5X objective (Nikon, 0.15 NA) with at least 20 spheroids each, in order to analyze > 60 spheroids per condition. Images were captured by acquiring Z-stacks of the samples using FITC (FDA) and Cy5 (propidium iodide) and merged. A customized software tool was developed to manually select each spheroid and automatically process the acquired images. The implementation of the algorithm was carried out in MATLAB 2020b (MathWorks, MA, USA) using the Image Processing Toolbox^{TM}. It was characterized by

spheroid identification and picture segmentation algorithms were used to automatically separate the multicellular spheres from the background (6). The segmented spheroid masks were then utilized to extract the desired characteristics. In addition, a circular segmentation was performed in order to estimate the radial distribution of the fluorescence. Data were normalized to spheroids analyzed before treatment (t0).

3.2.8 Immunofluorescence and image acquisition

First, spheroids cultured in 24-well plates with PDMS microstructured inserts were washed twice with PBS for 5 minutes, then, they were fixed with methanol-free 4% PFA for 20 minutes at room temperature. After fixing, samples can be stored at 4°C or immunofluorescence can be performed immediately. Samples were incubated with a blocking solution containing 0.3% Triton X-100 in PBS and 5% goat serum for 1h at room temperature. Primary antibodies (rabbit monoclonal anti beta-actin 1:200 dilution and mouse monoclonal anti alpha-tubulin 1:2000 dilution, Abcam) were diluted in PBS- 0.3%Triton X-100, 1% BSA. The next day, spheroids were washed 3 times for 10 min. each time with PBS-0.1% Triton X-100, incubated with goat anti-rabbit Alexa 488-conjugated antibody 1:1000 (Abcam) and anti-mouse Alexa-555 1:1000 for 2 hours at room temperature in PBS-0.3% Triton X-100, 1% BSA. Spheroids were then washed 3 times for 10 min. each time in PBS-0.1% Triton X-100, 10 min in PBS and then incubated for 10 minutes in Hoechst 33258 (2 µg/ml; Sigma-Aldrich). Samples were then washed 5 min. in PBS. A 3 mm layer of 2% of low-melting-point agarose (Sigma-Aldrich) was carefully laid on the bottom of the wells to cover and embed the spheroids while maintaining their original microwell arrangement. Once firm, the agarose replicates the microstructure of the device. The spheroids are embedded at the apex of the agarose micro-cones. The agarose stub was then separated from PDMS device and positioned face-down on a microscope coverslip. Image acquisitions of spheroids were carried out with a confocal microscope (Nikon A1-R) using either a 20X objective (NA=0.75) or a 40X objective (NA=0.95). Image acquisitions in the Z direction was performed using a 1 µm z-step. Automatic mosaic acquisitions for a large number of spheroids were performed.

Additionally, the generated 3D spheroids were imaged with state-of-the-art two-photon microscopes at the Molecular imaging and Photonics Lab (MIP) at KU Leuven University, Belgium. The MIP lab was equipped with a Leica TCS SP8 X with a tunable MaiTai DeepSee femtosecond laser (tuning range of 690-1040 nm). This laser was used to excite phalloidin 488 (Phalloidin CruzFluor™, Chemcruz®) at 976 nm of wavelength. Moreover, a Leica MP TCS SP8 DIVE with a multi-photon Insight X3 laser with a tuning range of 680-1300 nm was used. This laser allowed to excite phalloidin 647 (Phalloidin CruzFluor™, Chemcruz®) at 1294 nm of

wavelength. Vario Beam Expander (VBE) provided tuning for best depth penetration and best resolution. For imaging single spheroids >150 µm of diameter, a HC PL IRAPO 40x/1.10 W CORR objective was used. For each spheroid, a Z stack spanning 300 µm was acquired, collecting one frame for every 5 µm distance along the Z axis. For 3D reconstruction, the Leica Application Suite X (LAS X) software was employed.

3.2.9 Data analysis

The software used during the experimentation were: ImageJ, GraphPad Prism8, MS Excel and MATLAB 2020b for image and statistical analysis. Results represent the mean values of 3 independent experiments, each performed with 3 biological replicate cultures, unless mentioned otherwise. Error bars represent standard deviation (SD) or the standard error of the mean (SEM), as indicated in the figure legends. The statistical significance of data was evaluated using unpaired Student's t test or one-way analysis of variance (ANOVA), where specified, using Prism software, Version 8.0 (GraphPad). P-values for each comparison are represented by asterisks as indicated in figure captions.

3.3 Microfluidic platform for microglial cell culture

3.3.1 Design and fabrication of the microfluidic chip

The first steps for the fabrication of the microfluidic system consist in the design and production of a positive mold. For the design elaboration was used an open-source vector graphic editor: Inkscape (https://inkscape.org/it/). To obtain a positive mold with specific thickness and resolution characteristics, a plotter converted into a cutting plotter and a sufficiently thin sheet of tracing paper (about 100 µm) was used. The file obtained from the graphic editor was converted into format (.plt) and subsequently sorted to ensure a single passage of the plotter blade on the cellulose sheet used to create the positive mold. Depending on the cutting capacity of the plotter, the file can be sent to print several times. Not having a printing software compatible with the operating system of the computer and the plotter used, the file was sent directly from the terminal (DOS), using a small script for repeatedly sending the file. Moreover, the *replica molding technique* (REM) was used to fabricate a positive mold for the fabrication of the microfluidic PDMS device. Once obtained the cellulose sheet with the tailored characteristics, it was attached on a glass slide (previously cleaned and cut in half- 2.5 x 3.5 cm) taking care to remove all traces of

the cyanoacrylate adhesive. Subsequently, the glass slide was washed with soap and water and dried with ethanol, then borders were covered with adhesive tape with height ~0.5 cm to accommodate PDMS (*Figure 11* a, b).
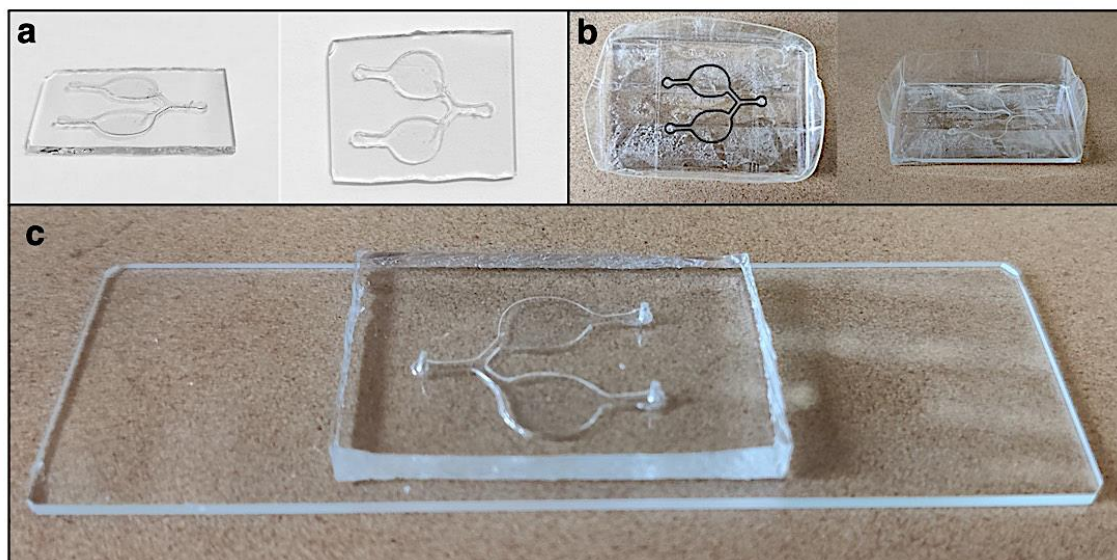
Figure 11: **Fabrication process of the microfluidic device.** (a) Glass slide with designed microfluidic chambers made of cellulose sheet. (b) Mold thickness adjustment with adhesive tape. (c) Ultimate negative mole bonded on a glass slide with holes to accommodate fluidic tubes

Specifically, 10 g of PDMS (prepared as described in 3.1.1) were poured into the cavity. Then, the mold was placed into a degassing chamber for 30 minutes to get rid of air bubbles and incubated (Minib Batt 805, Asal) at 60°C for at least 1 hour to allow fast PDMS cross-linking. The negative PDMS device was then detached from the mold and the edges cut with a scalpel to obtain a parallelepiped of dimensions of 3.0 x 2.2 x 0.5 cm. Subsequently, holes to accommodate tubes for the fluid entry and exit were made with a blunt flat needle. Polytetrafluoroethylene (PTFE) tubes (OD 1.0 mm and ID 0.5 mm, Bohlender, Sigma-Aldrich) were inserted in the holes and a drop of PDMS was poured in tubes junctions to maximize its adherence. Finally, the mold was sealed on a new glass slide. Precisely, slide and device surfaces were activated to obtain a stable and covalent bond throughout plasma surface treatment (Femto, *Diener Electronic*). The plasma machine was set at 50% of the power for about 30 seconds, setting an air flow of 6 L/min. Once the surfaces were activated, the PDMS device was positioned on the slide applying light pressure. To favor the formation of covalent bonds between the two surfaces, the device was placed at 60°C for about 1 hour.

3.3.2 Syringe pump fabrication

The designed system required the use of a syringe pump to regulate the flows inside the fluidic chip, allowing media exchange and treatments. Specifically, fast prototyping tools such as CAD, 3D printer and Arduino were used to design, fabricate and program the syringe pump. The pump was characterized by a spring clutch which allowed the central block to slide when pulled upwards, in order to have a rapid return of the carriage which hosted the syringe pistons. The clutch was made of a coupling nut, cut in half and drilled on the top in order to attach two screws as a lifting lever. The block on the left served as stop for the syringe pump and the two lateral metal bars were the guide for the correct movement of the carriage and the stepper motor. Consequently, the motor turned the large center screw and moved the block that hold the syringe plungers. The block on the right acted as front limit switch, which housed the two guides and the screw terminal part. The main pump body was structured to keep in place the syringes, with a locking lever and an upper plastic bar that hold the syringes with a screw and a spring. The stepping motor operation was therefore controlled by Arduino Nano, the motor turned the central screw and moved consequently the central carriage and the pistons fixed to it. The Arduino Nano customized program performed the reading of the status of 12 switches present on a DIP switch and translate it into moving the stepper motor and therefore of the syringes. Each state of the 12 switches represented a given configuration of the syringe pump: infusion/withdraw, 4 types of usable syringes (1 - 2.5 - 5 - 10) mL, 8 flow rates expressed in µl/ h or µl/ min, 8 different quantities of volume moved, and 4 different volume delivery modes (continuously or with interval pulses of 1, 2 or 4 hours). The system thus obtained was characterized by rechargeable lithium batteries as power supply.

3.3.3 Microglia cell culture seeding and maintenance in device chambers

N9 murine microglia cell line was generously provided by Prof. Barbara Monti (*FaBiT, University of Bologna*). N9 cells were cultured in petri dishes (Corning, treated with poly-L-lysine 10µg/ml, Sigma) with complete medium DMEM High Glucose supplemented with 10% FBS and 1% penicillin and streptomycin at 37°C in an atmosphere of 5% CO_2 and normal O_2 levels. The microfluidic platform was first pre-treated with poly-L-lysine diluted 1:100 in H_2O (10µg/mL, Sigma) to promote cell adhesion to the glass surface. Firstly, the device was filled with pure ethanol with the syringe pump set at a flow rate of 200µl/min. Throughout application of a light pressure on the PDMS device, bubbles trapped into device chambers were eliminated. In fact, ethanol, having a lower density and surface tension than water, allows for better air removal from the system. Once the two chambers were entirely filled, a solution of 70% ethanol in sterile H_2O

was fluxed to gradually hydrate the surfaces of the culture chambers avoiding the formation of air bubbles. Subsequently, the poly-L-lysine solution was incubated into the device for 1 hour. The cell seeding procedure volumes (40 µl) were based on device structure and size. 200-300µl of complete culture medium was flowed into the chambers, previously equilibrated in an incubator at 37°C, with a flow rate of about 200 µl/min. N9 cells were aliquoted at a concentration of 150.000 cells/mL and flowed at a rate of 200 µl/min, for a total volume of 300-500 µl. Later, the microfluidic device connected to the syringe pump was let at 37°C for 2 hours. Cells were let to settle and adhere. Subsequently, the syringe pump was activated, creating a flow that allowed media exchange and providing a continuous supply of nutrients over time. The operating condition for growth/maintenance were as follows: flow rate 200 µl/h per cell, 10 µl of volume for syringe with a pulse every 2 hours. This setting allowed media exchange every 4h, avoiding cell detachment. Cell morphology and distribution were verified after 24h. The operation was repeated every day for the entire duration of the experiment.

3.3.4 Viability staining

To verify cell viability within the microfluidic culture device, a viability assay with fluorescein diacetate (FDA, 490-520ex/em, Sigma) was performed. The microglia cells previously cultured for 24h, were incubated with FDA (5 mg/ml in acetone) diluted in 1X PBS. 200µl of FDA solution were fluxed into each device chamber while maintaining an adequate flow rate, approximately 10µl/min per syringe. Therefore, the solution was flowed for 20 minutes followed by 10 min incubation in the dark.

3.3.5 Inducing LPS mediated activation

Cell line LPS activation was performed in serum-free medium. For this purpose, after counting, the cells were seeded and maintained in DMEM without FBS. A solution of LPS 1000 ng/ml (Sigma) diluted in cell medium was prepared. Additionally, the device must be used to selectively LPS-activate the cells present in a single cell (C1), while maintaining the other as a control cell (C2). For this purpose, keeping all the necessary attention to avoid the entry of air bubbles, the tube coming out of the C1 cell must be closed with a clamp and the position of the pump is changed by inverting the inlet tube with the outlet tube and vice versa. Additionally, this arrangement of flows allows the selective passage of the LPS solution within a single cell. It was also necessary to regulate media flows in order to not cause cell detachment and at the same time perform rapidly a complete and homogeneous replacement of medium. complete with the one containing LPS. With regard to this, a flow rate of 20 µl/min was set. For this purpose,

approximately 100µl of medium + LPS was fluxed into the chamber in order to ensure that the entire cell and the dead volumes of the tubes were filled with the treatment solution. At this point, cells were incubated for 2 hours at 37°C. To eliminate LPS from the device chambers, maintenance flows were re-established for the next 24 hours of incubation. Specifically, 100 µl were flowed at a rate of 20 µl/min to replace LPS containing media with fresh media to rebalance the flows used for maintenance and cell growth.

3.3.6 Activation mediated by conditioned media

In order to simulate activation through conditioned media, it was necessary to use only one inlet tube connected to eppendorf containing media which leads to the activated cells chamber (C1) and use the tube entering the chamber containing the resting cells as outlet. It was therefore necessary to block the tube used as an inlet for the maintenance phase to exploit the micro channel connecting the two chambers to allow media flux. For the following 24 hours the flow entering in C1 and leaving C2 was regulated with the same characteristics of the culture maintenance phase.

3.3.7 Immunostaining

To test immunofluorescence assays within the microfluidic device, a protocol for the staining and detection of β-Actin and α-Tubulin was used. The bonding operation generated covalent bonds between glass and PDMS that prevented the two elements separation without causing them to break. Hence, it was necessary to fix, permeabilize and incubate in the intact chip. A solution containing 4% paraformaldehyde (PFA) in PBS was flowed in the microfluidic chambers (150 µl at a flow rate of 20 µl/min) and incubated for 20 minutes at room temperature. Then, 150 µl of PBS was used for a washing step at the previous pumping speed, the system was then stored at 4°C until the next step. For cell membranes permeabilization, the mechanism of rapid dehydration and thermal shock was used. Specifically, 150 µl of pure methanol (previously brought to 4°C) was flowed at a rate of 20 µl/min, then the microfluidic device was placed at -20°C for 10 min. Then, a washing in PBS was carried out as previously described. Non-specific binding sites were blocked with 150 µl of blocking solution (PBS + 0.3%Triton X100 + 5% goat serum) and incubated for 1h at room temperature. Two different primary antibodies were used, one per cell of the device, in order to evaluate the possibility of keeping the operation separate and having a negative result in the adjacent chamber. One chamber was treated with an antibody directed towards β-Actin (D6A8-Rabbit mAb-#8457-Cell Signaling) diluted 1:200 in the antibody

dilution buffer (PBS + 0.3%TritonX100 + 1%BSA). The other chamber was treated with an antibody directed towards α-Tubulin (DM1A-Mouse mAb -#3873-Cell Signaling) diluted 1:2000 in the antibody dilution buffer. The separate treatment of the two cells was carried out using the inlet and outlet arrangement exploited for differential activation with LPS, setting a flow rate of 20 µl/min for a total volume of 150 µl for both chambers. The incubation was carried out overnight at 4°C. After incubation, the sample was washed with PBS-0.1%Triton. Consequently, secondary antibodies were used (Alexa Fluor 488 anti-rabbit mAb and Alexa Fluor 555 anti-mouse mAb). Secondary mAbs were used simultaneously diluting them 1:1000. The solution was fluxed using the *inlet* and *outlet* maintenance configuration of the device, within both chambers. After washing with PBS-0.1%Triton X100, nuclei were stained with Hoechst 33258 (Thermo Fisher) diluted 1:100 in PBS. Fluorescence microscope observations (Nikon Eclipse 80i with Hamamatsu Flash 4 sCMOS digital camera) were performed after closing all the tubes with a clip for better device handling. Immunofluorescence staining was with FITC and Cy3 filters for Alexa 488 and Alexa 555 respectively.

3.3.8 iNOS immunofluorescence

To detect N9 microglia activation iNOS Rabbit mAb (D6B6S, #13120 Cell Signaling) was used, this antibody recognizes endogenous levels of total iNOS protein which is a molecular messenger induced by cells in response to bacterial endotoxins such as LPS. Immunostaining was performed on fixed N9 cells cultured on glass coverslips; samples were divided into controls and N9 culture previously activated with LPS 1000 ng/ml for 24h. Specimen were blocked with blocking solution (1X PBS/5% normal serum 0.3% TritonX-100), incubated with iNOS 1:200 Ab-I solution (1X PBS/1% BSA/0.3% TritonX-100) overnight at 4°C. Then, samples were rinsed three times in 1X PBS for 5 min each, incubated with secondary antibody Alexa Fluor 555 anti-rabbit diluted 1:1000 in Ab solution (1X PBS/1%BSA/0.3%TritonX-100) for 2 hours at room temperature. Coverslips were then washed for 5 min in PBS and then mounted on glass slides with UltraCruz Mounting medium (Santa Cruz, Dallas, TX, USA), sealed with nail polish and stored at 4°C until used.

3.3.9 Data analysis

The software used during the experimentation were: ImageJ, GraphPad Prism8 and MS Excel for image and statistical analysis. Ansys workbench 2019 R3 (https://www.ansys.com/) was used

for fluid dynamics simulations in the geometric structures developed in CAD. The program carries out numerous operations that require the optimization of some parameters by the operator in relation to the design of the model to be tested, the type of fluid, the flow rate, pumping mechanics and other information such as Reynolds number.

4. RESULTS AND DISCUSSION

4.1 Microstructured device for three-dimensional cell culture

4.1.1 Spheroid formation on prototype device

First, attention was directed on microtumor and microtissues (non-cancer cells) formation deriving from five different human cancer cell lines, one embryotic kidney cell line and mouse SVZ derived neural stem cells. The designed PDMS inserts were tested as a reproducible method for uniform 3D spheroids generation in vitro. Several stages of morphological changes occurred during spheroid development. Individual cells could be easily identified in the early stages when single cells spontaneously self-assemble to create cell aggregates in each micro-well. Cell aggregates then began to merge as a result of intercellular interactions and connections. After those multicellular spheroids developed solid structure with smooth and continuous surfaces. As shown in *Figure 12* successful spheroid formation was observed with different cell lines in our microdevices. It was investigated whether well-controlled tumor spheroids with long-term cell viability could be obtained from the PDMS devices. With the tested cell lines the 3D cell culture production did not require the use of any additional substance (i.e., biological matrices, synthetic hydrogels) since cells naturally adhere to each other and do not depend on matrices or scaffolds for spheroid formation. Microwell arrays allowed the generation of spheroids as well as the control of the size of the 3D cell cultures as it depends on the initial cell seeding density. Cell spheres were found to be solidly inserted into microwells and unwanted transfer of spheroids from one well to another did not occur, generally. To prove so, 500 µl of cell suspensions of different cell types (HCT116, NS, UOK257, SKOV-3, TPC1, HEK293, HRT-18) with different cell concentrations (20000, 50000, 80000, 100000, 150000 and 200000 cells/device) were seeded for characterization. The size of the cell clusters was shown to be strongly correlated with the initial cell seeding density, suggesting that this strategy can create size-controllable cell spheroids from a variety of cell types. Different cell densities resulted in varying sphere sizes, with a high seeding cell density producing a large cell sphere. Moreover, the size of the spheroids, in relation to the different cell densities, varied according to the cell line type. As shown in *Figure 12* B, at low cell density (50 cells/microwell), HEK293 formed a larger tumor size (200 µm in diameter at 200cells/microwell) than TPC1 (120 µm in diameter) and SKOV cells (150 µm in diameter). Neurospheres and SKOV-3 cell lines formed a looser aggregate compared with HCT116 or TPC1 and HRT-18 at the same cell amount. This result indicated that compared with the other two cell types, HCT116 cells were characterized by a tighter spherical structure with less ruffled borders

after spheroid formation. Furthermore, it was observed that even a non-homogeneous three-dimensional culture such as neural stem cells can be grown in the prototype device giving uniformity and control in the size of this type of cell culture type. In order to validate this technology for long-term monitoring of spheroids, the growth of HCT116 spheroids with different cell seeding concentrations (10, 20, 40, 100 cells/microwell) was tracked from day 1 post-seeding up to 13 days (see *Figure 12* C) Several stages of morphological changes occurred during spheroid development. Individual cells could be easily identified in the early stages when single cells spontaneously self-assembled to create cell aggregates in each micro-well. Cell aggregates then began to merge as a result of intercellular interactions and connections. After that, multicellular spheroids developed as solid structures with a smooth and continuous surface. The spheroid borders became ruffled in the final stage, indicating cell proliferation at the spheroid periphery and individual cells were no longer recognizable. The change of mean MCTS diameter of all four cell types, after a slight decrease, increased sequentially. Thereafter, around day 9 the diameter reached a plateau. The growth rate of spheroids with different sizes (5000, 10000, 20000 and 40000 cells/well) was almost independent from cell seeding concentration, about 46%.
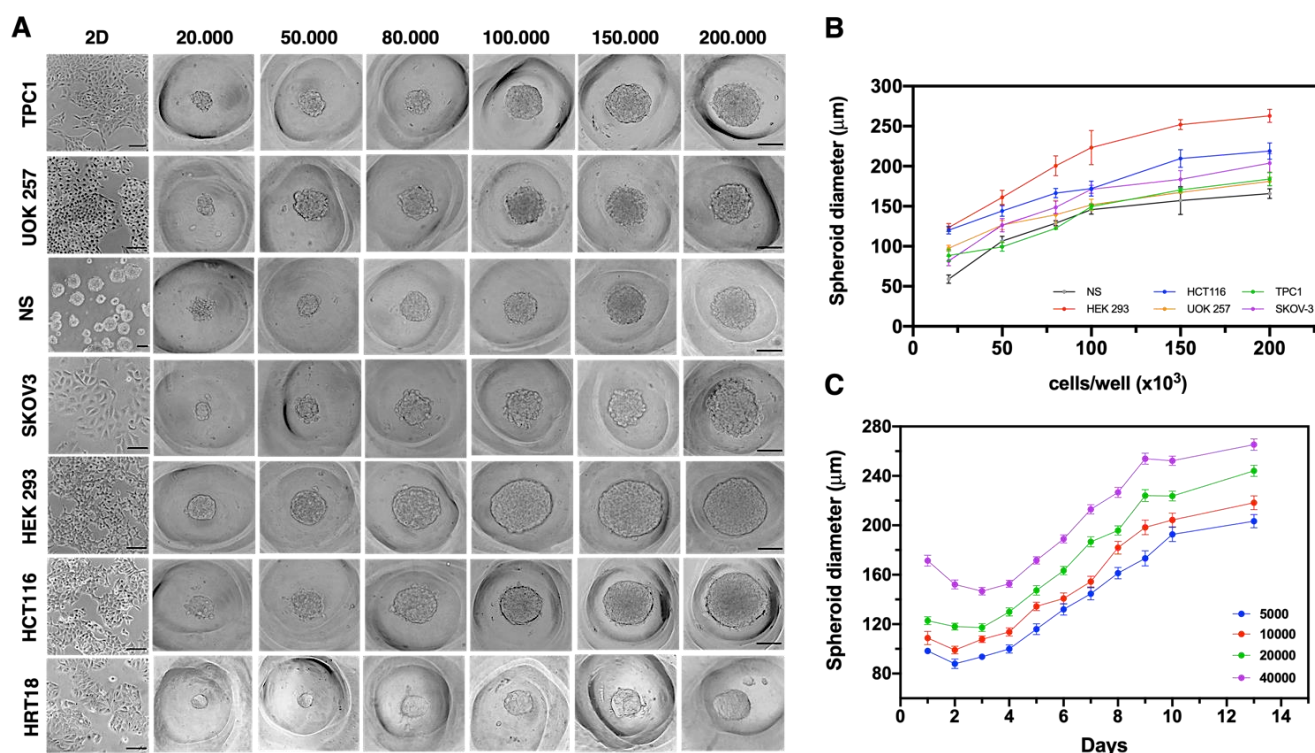
Figure 12: Characterization of multicellular spheroids generation. (A) Representative images of 2D cell culture and derived spheroids plated at different cell densities. Images were acquired 48h post plating. Scale bar: 100 µm (B) The diameter of cell spheroids after two days of culture with a different cell seeding number (n ≥ 28 for each cell line). (C) HCT116 spheroid growth assay, diameter changes from different cell seeding densities

Furthermore, in prototype device the microwells shape allowed to trace the same spheroids over time, thus managing to define the specific growth for different cell lines. Hence, investigations were focused on deepen analysis on specific growth and uniformity of the cell lines used. As

example here the growth monitoring and size distribution evaluations of HCT116 and SKOV3 cell lines are reported (**Figure *13*** A and B respectively).
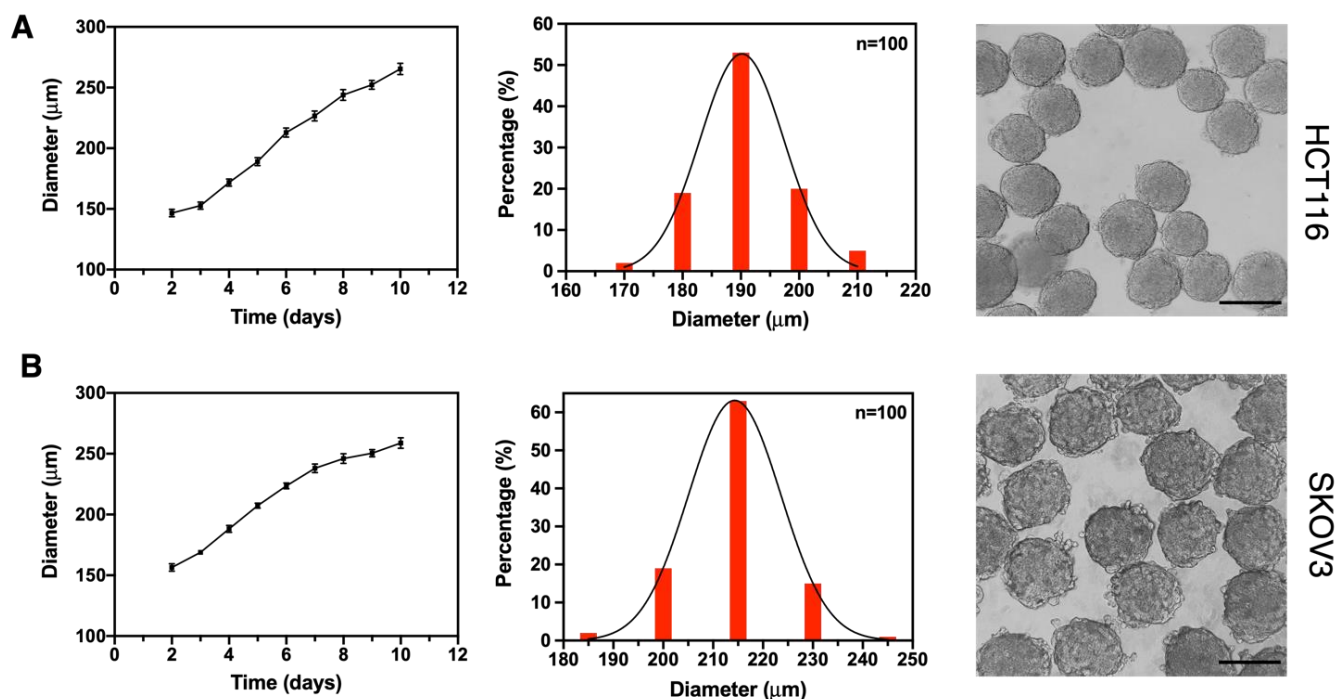

Figure 13: Growth monitoring and size distribution analysis of HCT116 and SKOV-3 spheroids cultured on PDMS devices. Growth curves derive from seeding 100×10^{3} cells mL^{-1} and following growth of same spheroids over 10 days of culture (n=28). Size distribution analysis was obtained from recovering spheroids cultured for 4 days. The average size ($\pm$ SD) of SKOV-3 and HCT116 spheroids on three different devices was 213 ± 9 µm and 190 ± 8 µm respectively (n = 100)

Very homogeneously sized spheroids were obtained: 97% of the HCT116 spheroids had a diameter between 180 and 210 µm at the end of the time of growth, while 99% of SKOV-3 spheroids were between 185 and 230 µm. As shown in phase contrast images, after the harvesting procedure, the spheroids shape and compactness were not altered by the procedure.

4.1.2 Agarose as alternative device material for spheroids production

It is widely known that *in vitro* platforms for three-dimensional cultures may vary for material components to provide a better cellular milieu for solid and reproducible experiments. PDMS is a well-grounded component in biomedical research, the polymer surface properties can be easily adjusted (i.e., short-term exposure to oxygen plasma converts the PDMS surface from its native hydrophobic state to hydrophilic, surface coating with surfactants to prevent cell attachment). However, other biocompatible materials may be used for multicellular spheroids production, depending on the application. The previously described resin molds used for PDMS inserts generation showed application even for agarose device production without any adaptation. We compared spheroid production capacity and uniformity provided by each material. Agarose devices surface perfectly replicated mold morphology, and no device breakage was encountered

during inserts placement on wells bottom. Agarose device production resulted very fast, allowing to assemble many devices in a short time. While using PDMS devices, some air bubbles were formed in the micro-wells when the medium was added into the devices. Air bubbles may affect cell seeding and cell distribution. Therefore, a centrifugation step was required to remove air before cell seeding in PDMS devices. On the contrary, with agarose devices, this step was not necessary. The different materials were compared through monitoring HCT116 spheroids growth, homogeneity, and cell culture viability. As shown in *Figure 14* cell spheres were successfully produced with both techniques. Also, the diameter of 28 spheroids was tracked after spheroid formation from day 3 to day 7.
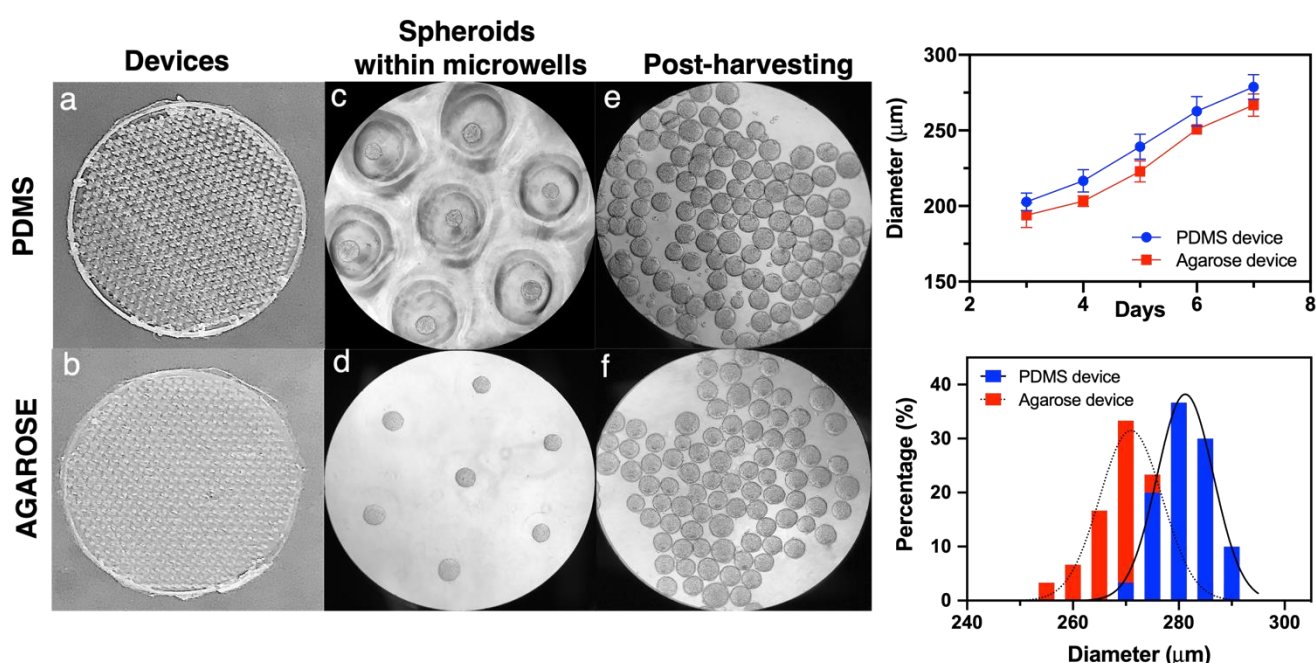

Figure 14: Comparison of cell spheres produced with PDMS and agarose devices. (a, b) Low magnification images of PDMS and agarose devices surface. (c, d) Spheroid array in microwells imaged with X10 lens 24h post seeding. (e, f) The harvested cell spheres were intact and uniform with both device materials. The graphs on the right show growth curves comparison, data relative of 28 spheroids per different device (n=3) and size distribution analysis of spheroids collected after 7 days of culture (n=30; 3 biological replicates).

There were no significant differences in spheroids growth behavior between agarose and PDMS inserts. Moreover, the size distribution was analyzed between the spheroids population cultured in three different PDMS and agarose devices after seven days of culture. Both agarose and PDMS devices produced cell spheres with good uniformity in size and shape. Compared to spheroids size generated with PDMS devices (281±4.6 µm), HCT116 spheroids cultured in agarose were slightly smaller (271±7.0 µm), and size distribution ranged between 260-290 µm of diameter. On the contrary, the diameter of spheroids cultured in PDMS devices ranged between 270-290 µm. This could be due to the fact that in agarose devices it is easier for single cells to

settle on the device edges after seeding or, for formed spheroids, to move from one well to another, thus causing variations in the size of the spheroids in culture.

4.1.3 Use of biological matrices for spheroids generation in prototype devices

Previous results showed successful formation and growth of different cell lines in the fabricated prototype device. Without the use of a supporting scaffold, spheroids were created by allowing cells to self-assemble into clusters. However, another common approach is to produce cell aggregates throughout matrix-assisted procedures, 3D scaffolds made of biological or synthetic polymers and generally provide small, and heterogeneous three-dimensional culture and necessitate a far more precisely controlled environment in terms of temperature and pH, which is time consuming. In fact, certain cell lines require components in their growth media that imitate the extracellular matrix (ECM), such as laminin or collagen IV. These components are important for cell/extracellular matrix interactions and can provide an environment conducive to intercellular connection development (Hughes et al. 2010; Kleinman et al. 2005). For the development of 3D compact cell clusters cultures with MCF-7 and Hela cell lines, the use of an extracellular matrix was investigated. In fact, the use of the PDMS device without matrix led to lose and not uniform spheroids from both HeLa and MCF-7. After a few days of culture, the structure of the formed spheroid showed a detached outer cell layer for HeLa while multiple spheroids in one well, with a poorly defined morphology for MCF7 cell line (*Figure 15* A).
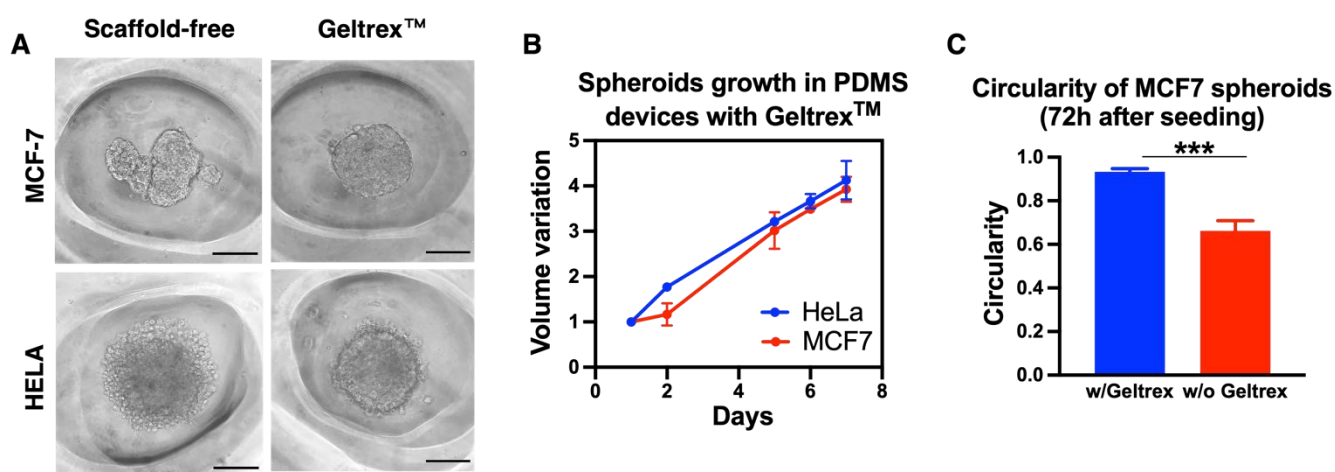

Figure 15: Spheroids assembly in prototype inserts with Geltrex®. (A) Representative phase contrast of MCF-7 and Hela spheroids cultured in PDMS device with and without use of Basement Membrane Matrix. (B) MCF-7 and Hela spheroids growth curves. (C) Mean circularity ($\pm$ SD) of MCF-7 spheroids cultured in three different devices changed significantly depending on the method applied for spheroid generation in three biological replicates (difference between means of 0.27$\pm$ 0.01; n=20). ***P value < 0.001

In order to improve the effectiveness of the proposed technology used in creating compact and homogeneous spheroids with these extensively used cell lines, the inserts' microstructured surface were combined with scaffold technology. For these experiments, Geltrex™ LDEV-Free (Reduced Growth Factor Basement Membrane Matrix, Gibco®) was used as an extracellular matrix. MCF-7 and HeLa cells were seeded at 100.000 cells per well (about 250 cells/microwell) in prototype inserts. Then, several Geltrex™ concentrations and conditioning regimens (i.e., just after cell seeding or 24h after cell seeding; concentrations range 9mg/mL to 15 mg/mL) were tested and compared with a control cell culture without Geltrex™. The results showed that when Geltrex™ was added during cell seeding tightly packed spheroids were detected in the presence of Geltrex™ at a final concentration of 2.5%. This procedure allowed to homogeneously cover micro-wells depth and lead to homogeneous and compact spheroid formation. Additionally, it was observed that a drastic temperature change (from 4°C to 37°C) generated a matrix contraction during gelification that uplifted cell clusters in microwells bottom, a few minutes after seeding and centrifugation. Progressive temperature change proved to be the best way to maintain cell clusters in place, thus spheroid culture morphology and array separation was preserved. (**Figure 15** B). MCF-7 spheroids circularity, calculated from 2D projection images, varied significantly according to the presence or absence of Geltrex™. In fact, the use of matrix provided regular cell clusters with mean circularity of 0.90±0.02. On the contrary spheroids generated with the standard procedure were characterized by a circularity of 0.6±0.1. The low values of circularity observed might be due to the lack of total compactness during the first period of culture. On the contrary, ECM secretions ensured total compactness or "spheroidization" thus, increasing the circularity of the spheroids (**Figure 15** C).

## 4.1.4   Drug response of MTS on prototype device, MTT endpoint assay

As a proof-of-concept of the relevance of our new microwells-based microsystem, the drugs effect on spheroids was investigated using a colorectal cancer cell line: HCT116. Due to their effectiveness and widespread usage in clinical therapies, Paclitaxel and Doxorubicin were employed as model compounds to assess the potential usefulness of this prototype platform for anticancer drug screening. Additionally, previous studies reported that SAHA has a promising anticancer activity. SAHA is a histone deacetylase (HDAC) inhibitor and causes growth arrest and death of some transformed cells both *in vitro* and *in vivo*, with little or no toxic effects on normal cells. The compound significantly inhibited the expression of HDAC proteins in colon adenocarcinoma cells and in tumors of nude mice providing a possible effective treatment for patients (Weichert et al. 2008; Jin et al. 2012). Having established the optimal conditions for spheroid assembly, the effect of Paclitaxel, Doxorubicin and SAHA on preformed HCT116

spheroids was examined. Compounds were used in different concentrations of doped media to treat the spheroids for 72h. The experimental conditions established were based on morphological follow up spheroids' morphology before, during and at the end of the treatments period. Quantitative measurements of the core volume are performed at 0h, 24h, 48h and 72h (*Figure 16*).
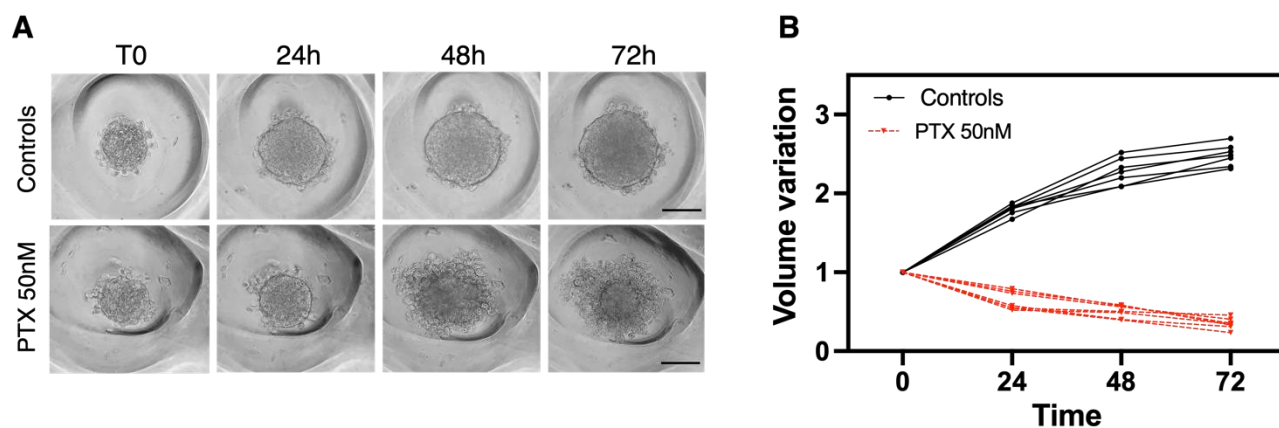

Figure 16: Representative phase contrast images of one control and one treated HCT116 spheroids in PDMS device. Images were used for generating growth curves, tracking the same spheroids over time. Scale bar: 100 um (B) Volume variations of individual control and treated spheroids relative of a device area monitored over time (n=14).

To begin, the time course of changes in spheroid size and shape was tracked starting on preformed spheroids at day 3 of culture. A 3-days initiation interval for spheroid formation was found to reproducibly create spheroids of 160-200 μm at the onset of treatment, this spheroid dimension is usually carried out for drug testing. Mean data representative of the spheroids volume variations derives from tracking over time 28 spheroids per condition (7 spheroids imaged with 10X lens of 4 different areas of each device) as shown in *Figure 16* B. An important aspect to emphasize on growth tracking analysis concerns the fact that for each treatment the same spheroids in PDMS devices have been followed over time, and not a random set of cultured spheroids. MTT cytotoxicity analysis was additionally performed as end-point assay at the end of each treatment to assess the effect of tumor spheroids in response to drug exposure. Because of its simplicity, the MTT assay is one of the most extensively used procedures for cytotoxicity screening. However, for 3D cell cultures alternative colorimetric, fluorometric and luminescent methods are frequently used, as commercial kits and ready-to-use solution (i.e., resazurin, acid phosphatase, AlamarBlue®, CellTiterGlo®). In this work, as described by Ho et al., MTT assay has been adapted to prototype device culture (Ho et al. 2012). In preliminary experiments the correct penetration of the reagent into the spheroids was also verified. Nonetheless, this viability assay is still employed in recent research works (Li et al. 2020; Fontoura et al. 2020). The endpoint MTT assay showed that all drugs suppressed cancer cell growth.
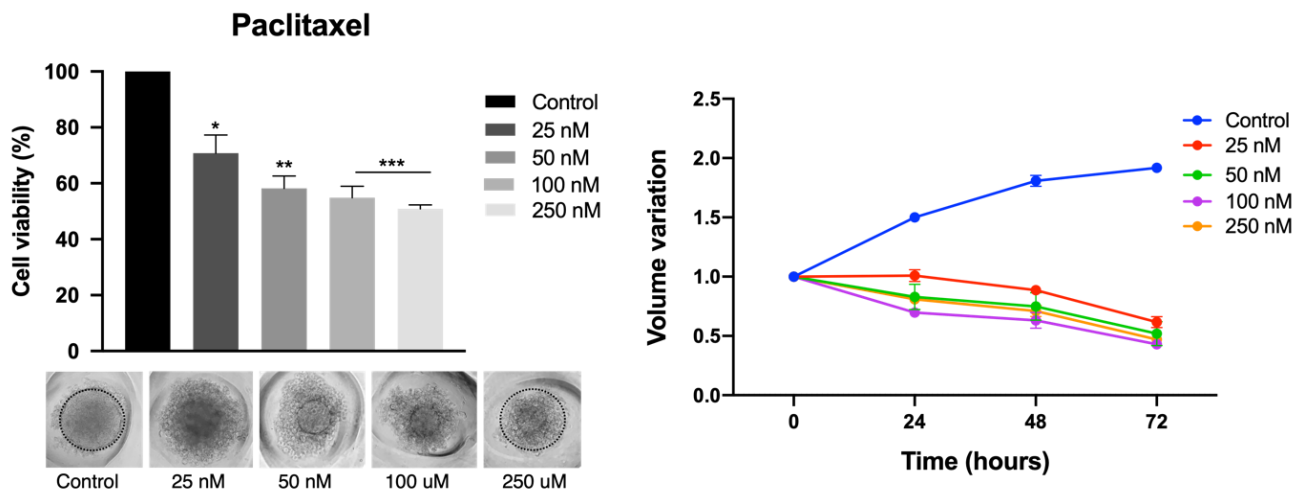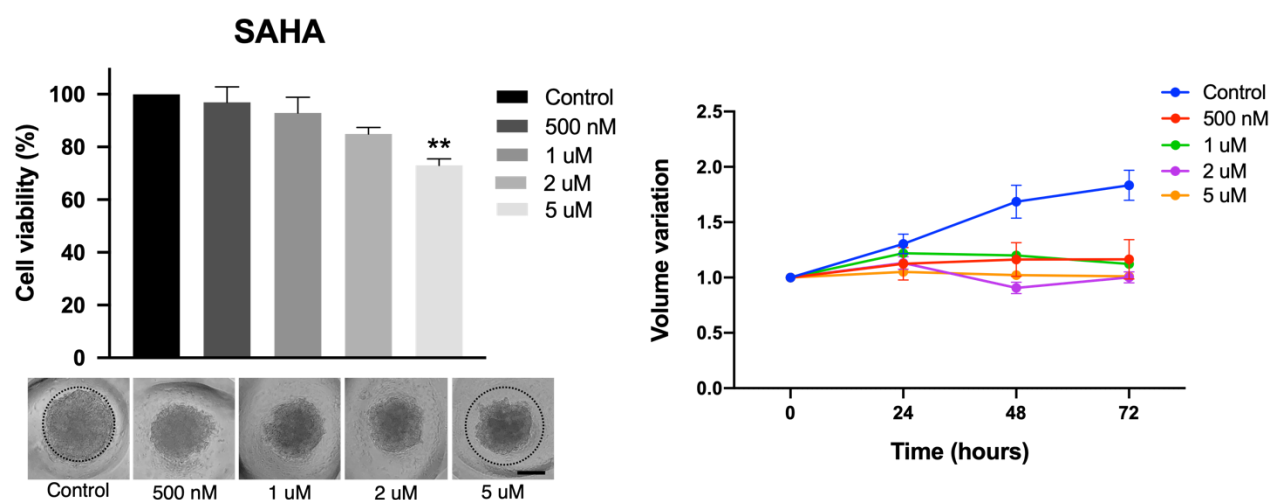
Figure 17: Viability analysis and growth curves of Paclitaxel treated spheroids. Samples were evaluated in triplicate. Each data point indicates mean ± SEM. (Student's t-test indicated that this result was statistically significant; *P < 0.05, **P < 0.01, ***P < 0.001 versus control)

In Paclitaxel-treated microtumors, as shown in ***Figure 17***, slight inhibition was observed for concentrations > 25nM whereas concentration between 50 nM and 250 nM showed similar viability reduction around 50%. This compound also caused a peculiar effect on HCT116 spheroids, borders became ruffled in the final stage acquiring a looser appearance, with cells gradually detached at the edges. Microtumors exhibited an evident decrease in size and spread with Paclitaxel, but the compact central core of the spheroids was easily identifiable and measured for volume analysis during treatment. Untreated spheroids doubled their volume on the contrary treated ones showed a growth inhibition after 72h up to 180% for the highest concentration dose of 250nM.
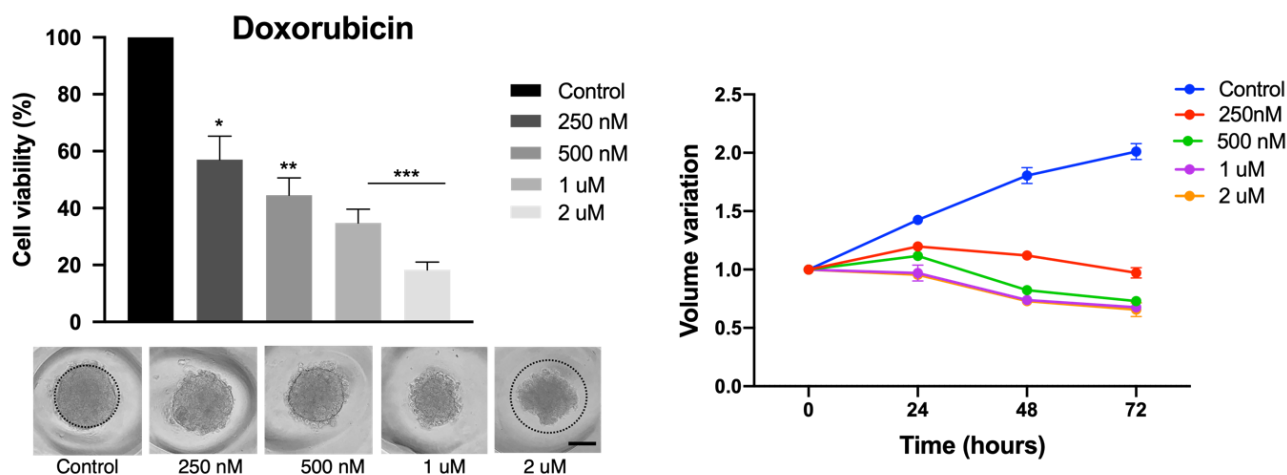
Figure 18: Viability analysis and growth curves of Doxorubicin-treated spheroids. Samples were evaluated in triplicate. Each data point indicates mean ± SEM. (Student's t-test indicated that this result was statistically significant; *P < 0.05, **P < 0.01, ***P < 0.001 versus control)

On the contrary, Doxorubicin treatment showed a dose-dependent reduced viability of HCT116 spheroids indicating that the drug significantly induced cell death in the used colon cancer cell line (**Figure 18**). Image analysis allowed also to observe distinct dose-dependent growth inhibition curves for each concentration dose. The decrease in metabolic activity in the 3D culture correlated with a decrease in spheroid size and more pronounced cell death. 1µM and 2 µM curves showed similarity, after 72h the growth inhibition was only 5% higher in 2 µM compared to 1µM drug concentration (125% and 120% respectively).



Figure 19: **Viability analysis and growth curves of SAHA-treated spheroids**. Samples were evaluated in triplicate. Each data point indicates mean ± SEM. (Student's t-test indicated that this result was statistically significant; *P < 0.05, **P < 0.01, ***P < 0.001 versus control)

Furthermore, SAHA showed to have limited effects on the reduction of the viability (**Figure 19**). A significant viability reduction of 27% ± 2.5 was observed at a concentration of 5 µM. With respect to the controls, the core volume of treated spheroids showed no volume increase remaining at initial volume value. Growth inhibition after 72h for maximum concentration dose of 5 µM was 99%. In conclusion, previous works investigated viability of HCT116 cells treated with HDACs inhibitor in colon cancer cell lines (Weichert et al. 2008; Chen et al. 2015). Wang et al. observed a slight inhibition for concentrations > 0.5 µM for SAHA treatments (H. Wang et al. 2019) and investigation with tumor spheroids have been performed as well (Lobjois et al. 2009). These scientific works emphasize more the suitability of our spheroid generation platform for various compound screening.

## 4.1.5 Development and optimization of live/dead fluorescence assay

Cell viability measurement is a common biological readout used to evaluate drug responses in 3D cell cultures. Specifically, existing live/dead staining methods are used to evaluate the live

and dead cell distribution after drug exposure and investigate the compound penetration into the compact structure of the spheroids. Generally, this procedure is only used as final read out without a specific quantification of the dyes fluorescence signals in relation to the type of drug or concentration. Additionally, standard staining and observation procedures required spheroid harvesting or new well transfer (Kang et al. 2015; Virgone-Carlotta et al. 2017; Cho et al. 2020). Cho et al. 2020). In this research work, it was demonstrated that it was possible to perform a live/dead cell staining directly into the PDMS inserts thanks to the transparency and thinness of the platform substrates. The distribution of live and dead cells after drug administration was observed, live spheroids cultured in PDMS device were directly stained with fluorescein diacetate in green and with Propidium Iodide in red for identifying live and apoptotic cells respectively. Moreover, the purpose was to employ this assay as on-device read-out to determine differential dose responses of a high number of 3D colon cancer microtumors in the developed culture platform. Furthermore, after spheroids imaging using epifluorescence, images were analyzed with customized MATLAB script to estimate spheroids volume, cell viability and dead cells distribution on generated spheroid culture. Then, in order to keep most of the cells of the diffuse layer, the device surface was embedded gently in agarose low melting point after staining cells (3.2.7). This method allowed easier handling during staining and offered the possibility to let the spheroids grow after imaging. Additionally, supported sample observation from below with an inverted microscope ensuring an adequate optical path or allowed face-up sample analysis through a thin layer of agarose with straight microscope, as in this case. Consequently, different types of microscopes can be used to achieve the same image quality. Preliminary experiments showed that it was possible to analyze single spheroids in epifluorescence without recovery (**Figure *20***). Information was obtained on the distribution of live and dead cells, and it was observed that control spheroids cultured over 13 days of culture showed high cell viability. Furthermore, regular media exchange on spheroids culture allowed to discard PI-stained cells from spheroids outer layer implying that changing the media was required for cultivating cell spheroids on the array. As consequence the microwell dimensions (400 µm of diameter and 300 µm of depth) accommodated enough cells while also protecting the formed spheroids from direct exposure to the medium exchange.
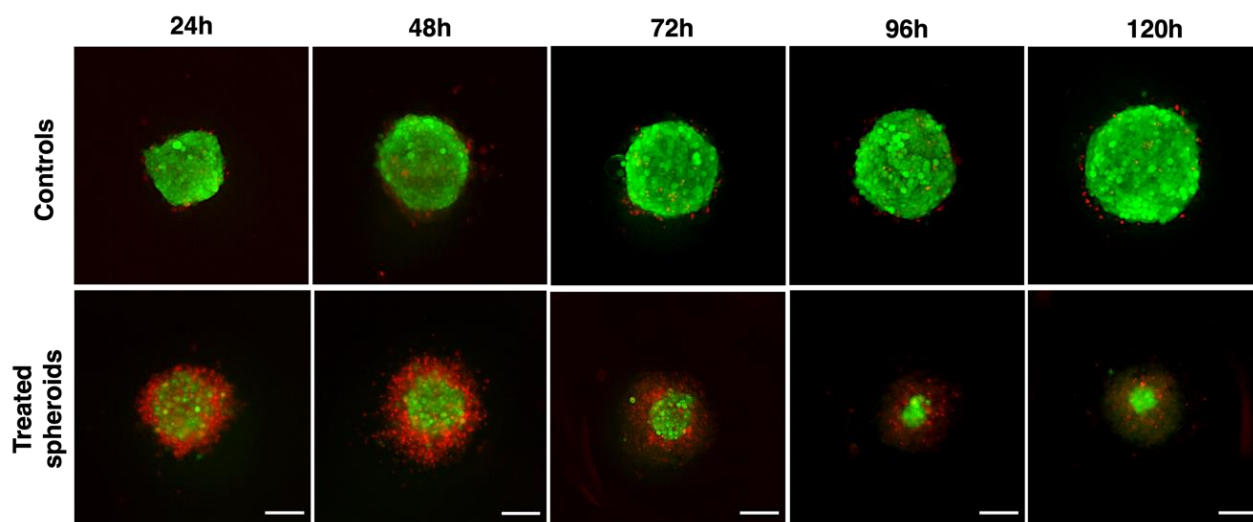
Figure 20: Live/dead staining images of control and drug treated HCT116 tumor spheroids. Fluorescein diacetate (FDA, green) and propidium iodide (PI, red) allow observation of viable and dead cells in the cancer spheroid. After a 3-days initiation, spheroids were treated with 100nM of PTX for 5 days, at each time point spheroids were stained with FDA and PI. Medium was changed every other day. Images of single spheroids were acquired with *Nikon Eclipse 80i* fluorescence microscope. Scale bar:100 μm.

Spheroids of HCT116 cell line were exposed to Paclitaxel for three days and fluorescence signal intensity and spheroids morphology were imaged directly in the device with a semi-automated image-based segmentation analysis. As shown in *Figure 21* during first 24 hours, spheroids treated with 25nM of PTX showed irregular shape and at the highest concentration of 50nM increasing presence of dead cells (PI+) was detected. A tooth-shaped morphology on the edge of the spheroid and dramatically incompact architecture were also observed. After additional 24 hours appeared a diffuse outer layer of dead cells in both conditions. Finally, after 72h a central viable central core was detected, with a pronounced increase in levels of dead and apoptotic cells in the peripheral layer of the spheroid. On the contrary, control spheroids did not present this diffuse layer and did not change in shape. Additionally, several conclusions could be drawn from the developed MATLAB segmentation analysis. *Figure 21* B shows data mean data of relative fluorescence intensity of PI+ cells of > 60 spheroid per condition. First, it was observed a dose dependent increase in PI fluorescence intensity over time. This response most closely matched those measured with MTT assay. Moreover, with respect to the control the volume of FDA+ core gradually decreased as a function of the PTX concentration, while was still present even at the PTX concentration of 50nM after 72h (*Figure 21* C). This observation may be correlated to the limited effects on the reduction of cell viability with MTT assay. PTX caused cell death in the superficial layer of HCT116 spheroids.
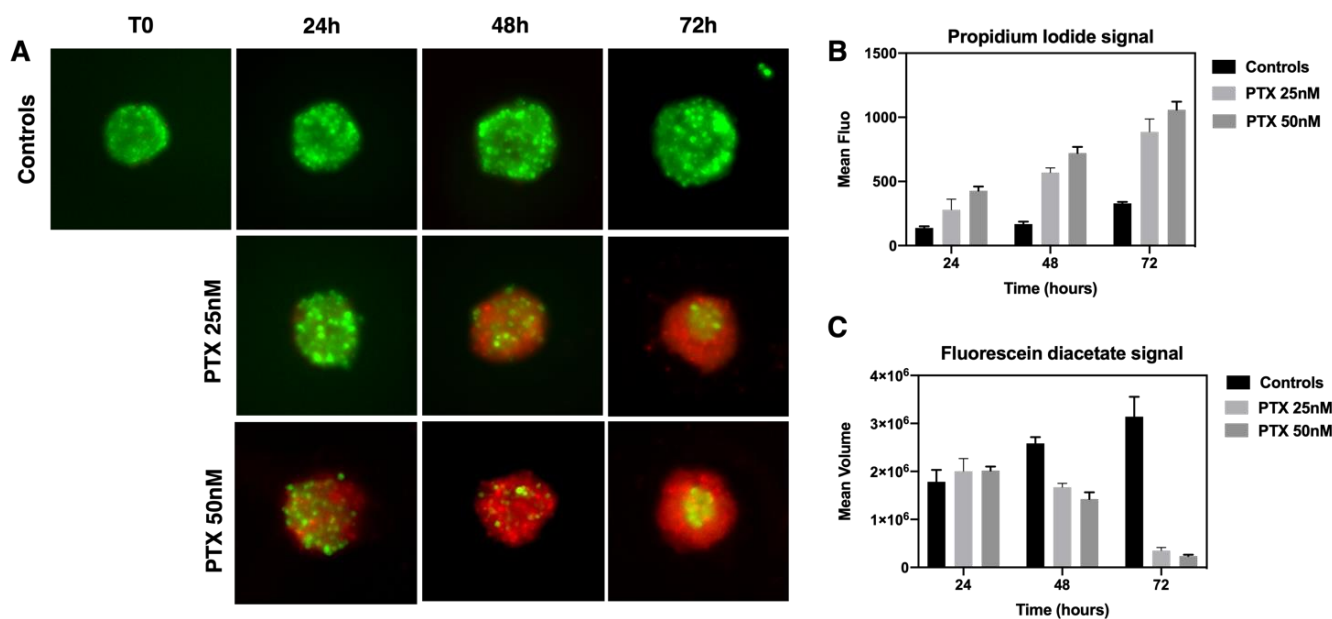
Figure 21: Live/dead staining images of drugs treated HCT116 spheroids. (A) Images of single spheroids control and treated with different concentrations of PTX for 24h,48h,72h and then stained with FDA and PI. Histograms were stretched equally for each channel for display purposes. (B) Normalized mean fluorescence intensity relative to propidium iodide signal. (C) Normalized mean volume calculated from FDA-signal segmentation. Histograms represents mean data of >60 spheroids per condition

To conclude, live/dead analysis provided complementary information regarding how the drug induced apoptosis within spheroids and provided data relative to fluorescence intensity and morphology parameters derived from signal segmentation. In accordance with the drop-in metabolic activity, an increase in cell death was observed in PTX treated spheroids. In fact, MTT assay showed that PTX was more effective at 50nM, but the inhibition did not reach 50% even at this highest concentration of the drug.

4.1.6 Prototype device comparison with commercial 3D culture plates

Several studies have shown that 3D spatial arrangement of cell-cell, cell-ECM, and cell-microenvironment interactions can affect a variety of cellular functions, including cell growth, organization, and responses to external stimuli, resulting in the generation of several features that are distinct of tumor spheroids (Zanoni et al. 2016). These characteristics are expected to differ not just between 2D and 3D environments, but also between 3D cell cultures generated using various methods. As a result, the morphology characteristics and growth/metabolism of spheroids formed using two different commercial systems were evaluated first, and then cytotoxicity was assessed. The cell spheres produced by prototype device were compared with: Elplasia® 24-wells plate with round bottom wells (Corning, Life Science) and Spherical plate 5D 24-well plate (Kugelmeiers®). Two commercial plates technologies were used for a comparative analysis of 3D spheroids generated by microstructured plates. These platforms were chosen as both presented the same well inserts dimensions, micropatterned surface technology and were frequently used

as ready-made 3D culture plates. The HCT116 colon cancer cell line was used as a model. The morphological features of the spheroids, cell growth behavior, metabolism, and response to treatment with the anticancer drug Paclitaxel were evaluated in the three methods. HCT116 cells started aggregating on day 1 in all three platforms used for spheroid generation. Preliminary experiments were performed to determine optimal cell seeding for each platform to generate spheroids of similar dimensions. Afterwards, the cell-seeding density used was calculated in order to seed 150 cells/microwell, and the resulting spheroids were imaged starting from day 1 and followed up until day 7 in culture. Phase contrast images obtained at day 1, 3 and 7 are shown in **Figure 22** A. Spheroids presented a round-type morphology and appeared more compact after day 1. The different culture wells did not show statistically significant changes in spheroids growth. After seven days of culture spheroids generated by prototype device reached 202±2.4 µm of diameter while Elplasia plate and Spherical plate 5D generated spheroids of 190±1.9 and 186±4.2 µm of diameter (**Figure 22**).
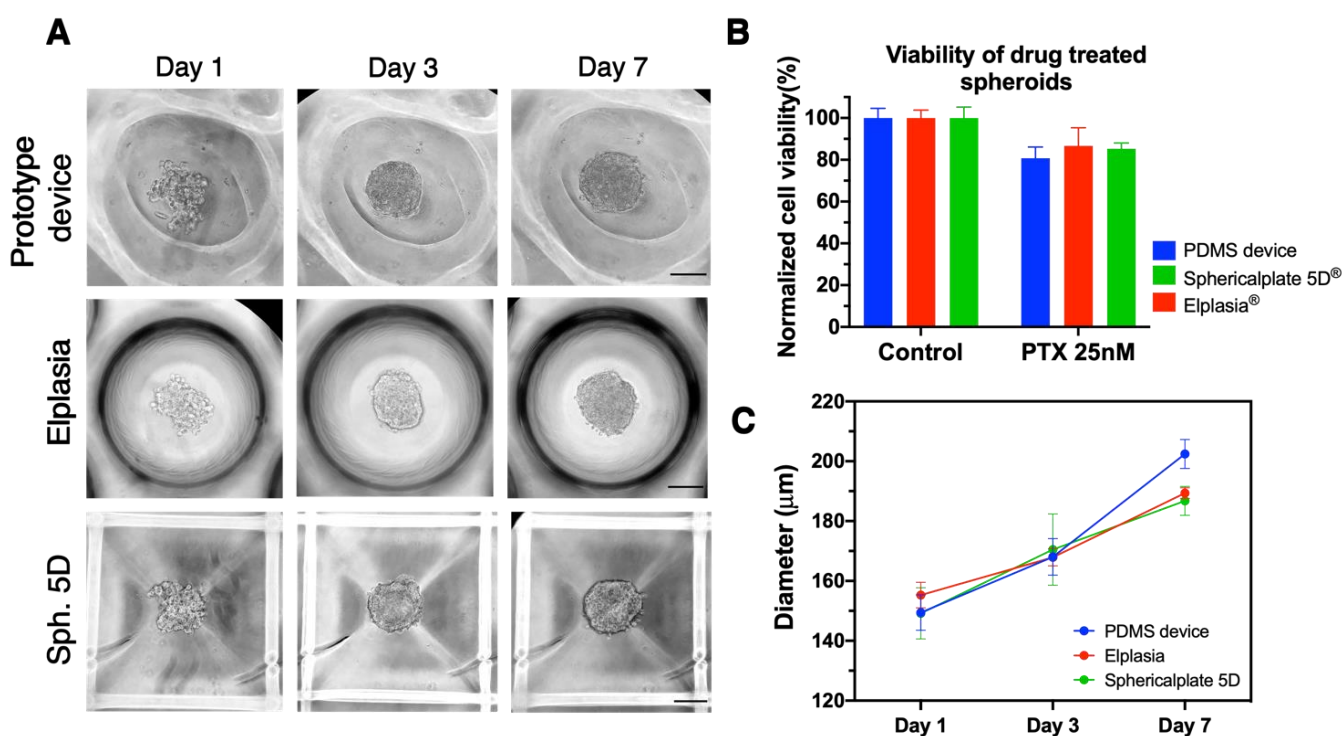

Figure 22: Comparison of HCT116 spheroids produced with prototype device and commercial culture plates. (A) Phase contrast images of HCT116 spheroids initiated with 150 cells/microwell on the three platforms, scale bar: 100 µm. (B) Effect of Paclitaxel treatment on viability and of colon cancer spheroids. HCT116 spheroids demonstrated reduced viability in response to Paclitaxel treatment. The viability of treated spheroids did not change significantly depending on the culture platform (one-way ANOVA). Viability within spheroids was measured using MTT assay and normalized to untreated control spheroids generated on the same platform. (C) Diameter measurement of HCT116 spheroids generated on prototype device, Elplasia and Spherical plate 5D. Curves represent quadruplicate biological repeats and are displayed as mean ± SEM (n = 4).

Spheroid's growth rate was around 20% with all three platforms. The displacement of the spheroids after few days of culture was found particularly with Spherical plate 5D. Additionally, was investigated if Paclitaxel-sensitivity of spheroids varied depending on the method of spheroid generation. The viability of PTX treated spheroids was measured using MTT assay and

normalized to control untreated spheroids generated on the same platform. Viability data indicated that regardless of method of spheroid generation, the PTX treatment reduced viability of the 20% in all three spheroids population analyzed.

### 4.1.7 In situ immunofluorescence in the device

High-content imaging plates with a single spheroid within a well are generally used for fluorescence studies of 3D cell cultures (i.e., ULA 96-348 wells plates)(Kochanek et al. 2019; Mittler et al. 2017). Here, is described an alternative method of simultaneous immunostaining more than 400 spheroids in one single microstructured device without recovery. Because of the flexible nature of the PDMS microwells, all immunostaining experimental steps (i.e., PBS rinsing, medium exchange, sample fixation and antibody incubation) could be performed in the same multi-well plate with no sample manipulation, resulting in the treatment and labeling of multiple spheroids at the same time. Samples could be imaged with high-resolution optical microscopy such as confocal fluorescence microscopy without using glass bottom multiwell and with straight widefield fluorescence microscopes. The advantage is that a high yield spheroid harvesting can be achieved with this method. Moreover, it is possible to monitor the growth of the same spheroids and then precisely localize them after immunofluorescence staining in the device array. *Figure 23* showed more than ten spheroids within the same focal plane, giving access to easy parallelization of 3D spheroids imaging.
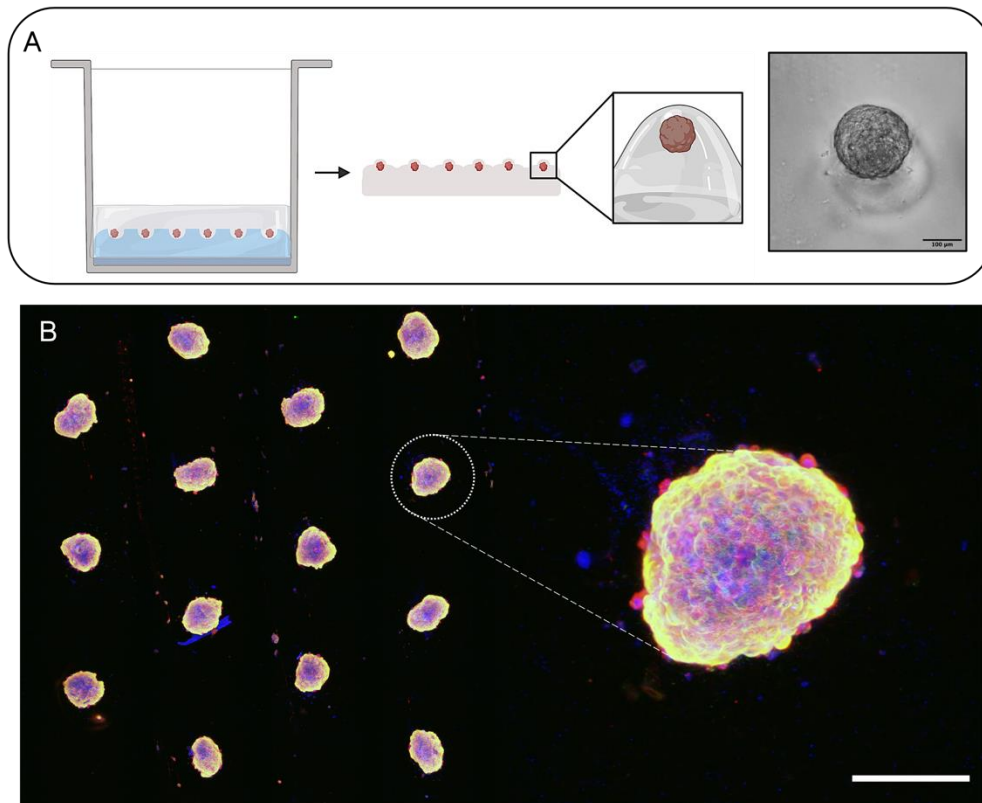
Figure 23 Method for image analysis of a high number of spheroids while maintaining sample position array. (A) Illustration depicting method for spheroids embedding and harvesting. (B) Maximal Image Projection (MIP) of confocal fluorescence images of spheroids in prototype device microsystem labelled for actin (green), tubulin (red) and nuclei (blue) (20X magnification) and an enlarged MIP of one of the spheroids (40X magnification, scale bar 100 um)

This is an added value of the system considering that the state-of-the-art method for imaging requires sample transfer to specific microscopy plates for high resolution imaging (Singh et al. 2015; Becatti et al. 2020). Spheroid collection and the numerous washing and centrifugations needed for standard immunostaining protocols may lead to sample fusion, damaging and deformations.

A two-photon microscope featured with Insight X3 laser was employed for larger acquisition field. The system delivered high average and peak power levels across the laser tuning range, including the critical NIR wavelengths above 900 nm, which allowed for the deepest penetration imaging. With a continuous scanning procedure, twenty-one spheroids were imaged, each image was merged and arranged in a single one with image-stitching (**Figure *24***).
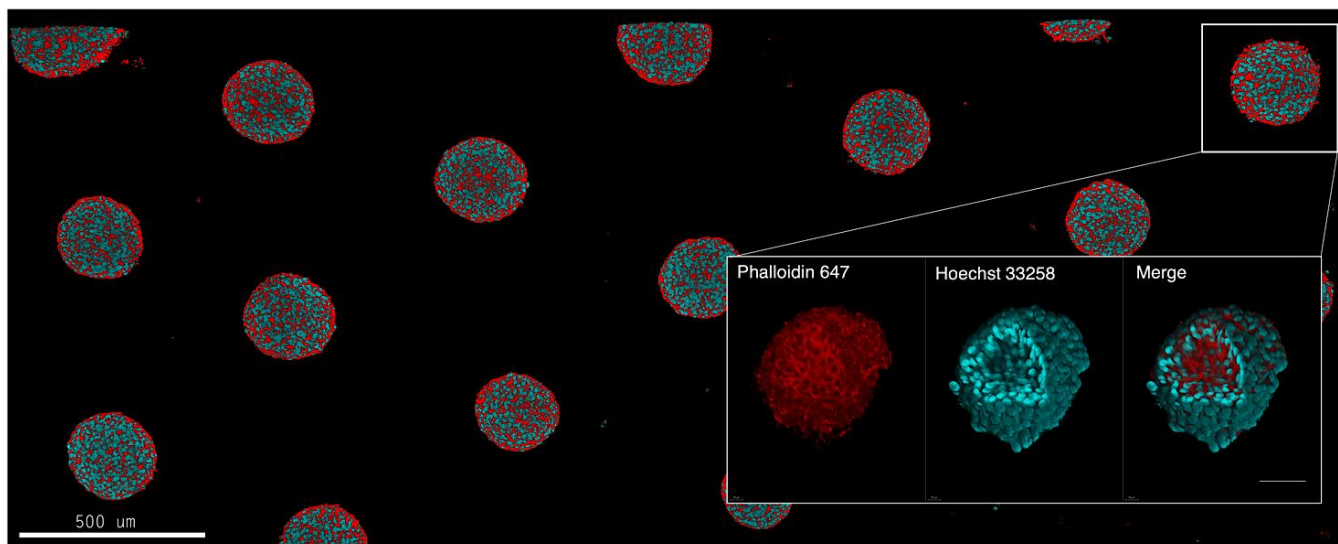
Figure 24: Two-photon images of spheroids cultured in prototype devices. The image in the background was obtained from device area containing 21 HCT116 spheroids. Image was cropped for presentation purpose (40X magnification; scale bar: 500µm). The red emission is due to phalloidin 488 (to maximize contrast) while the blue emission is from Hoechst 33258. Image in the bottom represents a 3D reconstruction of a single spheroid, sectioned (Scale bar: 100µm).

It was observed that no sample sliding or undesired movements during acquisition period. Then, for other image analysis, low-melting-point agarose can be subsequently melted in order to recover previously stained spheroids. This method allowed deep penetration imaging of the spheroids architecture and overcome the general procedure of performing immunofluorescence of frozen or paraffin-embedded sections that are usually applied for complex and thick tissue structures (Lobjois et al. 2009; Laurent et al. 2013; Chambers et al. 2014; Kabadi et al. 2017). To our knowledge, very few works in the literature have exploited such a similar approach. Goodarzi et al. used a agarose-based device to assess nanoparticle penetration within spheroids and immunostaining with a confocal microscope (Goodarzi et al. 2020). In our work, on the other hand, the direct imaging of spheroids cultured in prototype devices was demonstrated, allowing identification of the fragile outer layer of the spheroids without any harvesting of the spheroids. The possibility of removing the still-assembled spheroid array from the culture multi-well plate enables high-resolution high-throughput imaging in a comparatively simple way.

4.1.8 Characterization of the physical properties of spheroids cultured in prototype device

For numerous applications such as cancer research, tissue engineering, and regenerative medicine, detailed information on the mass density, shape, size, and weight of cells or cell aggregates are essential. Methods for physical cytometry and standardization of three-dimensional heterogeneous models are currently lacking, despite the fact that few technical solutions for single cell analysis have been given (1.1.1). With the purpose of obtaining additional

information regarding morphology characteristics and mass density of spheroids produced with the prototype device, an innovative flow-based method was used. The aim was also to test the homogeneity of the produced 3D cell culture with alternative methods of analysis and to compare populations of treated and control spheroids investigating relative mass densities. The W8 Physical Cytometer (https://celldynamics.it/w8/; Cell Dynamics isrl, Bologna) technology has been employed to perform quality control of 3D cell culture and quantitatively analyze *in vitro* tests from a physical point of view, with an automatic data analysis. Spheroid mass is computed from the terminal velocity each microobject acquires when moving in a channel in free-fall. Specifically, the samples for the analysis consisted of 2 test conditions of live spheroids population: control SKOV-3 spheroids and SKOV-3 spheroids treated with PTX 25nM. Spheroids were cultured and harvested from PDMS devices (as previously described in 3.2.1). After two PBS washings, spheroids were collected in a 15 ml tube containing 1mL of W8 analysis solution (**Figure 25**).
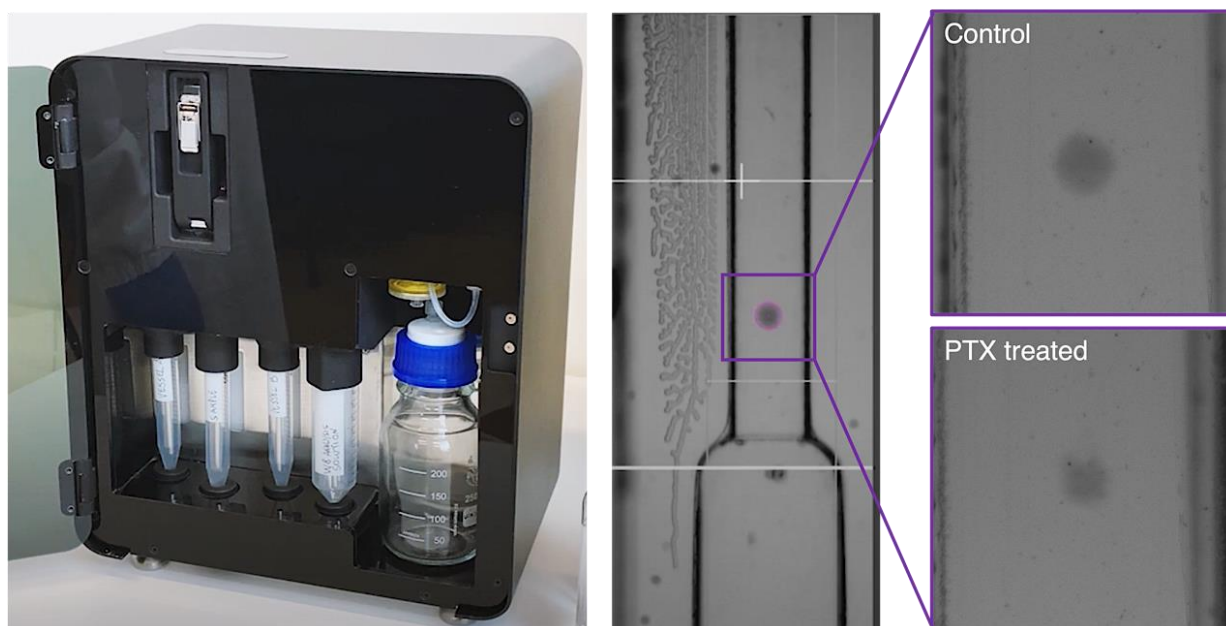
Figure 25: W8 automated platform and fluidic core-chip. Samples can be monitored any time while the instrument is running. On the right are reported example images of frames collected for two representative samples. A large and rounded control spheroid on top right and a medium sized treated spheroid on down right, showing a slight deviation from sphericity.

Results are relative to the analysis of 24 spheroids per condition. Each spheroid was analyzed twice. Two acquisitions contributed to the measurement of the spheroid mass density (MD), weight (W) and diameter (D). The mean value and standard deviation (SD) of these three parameters (MD, W, D) were then calculated for each sample. As shown in **Figure 26**, it was observed that the PTX treatment influenced spheroid mass density, a statistical difference was found between control (1031.1 ± 2.2 fg/ μm^3) and treated spheroids (1022.2 ± 3.0 fg/ μm^3) of the SKOV-3 cell line. The diameter evaluation of the spheroid culture generated in PDMS devices

confirmed the morphological data discussed previously. In fact, control spheroids were characterized by a diameter of 227 ± 11 µm and a narrow size distribution range. Additionally, as expected, it was observed that diameter of PTX treated spheroids was reduced of around 50 µm but sample presented a broader values range of 174 ± 27 µm. Finally, was evaluated a statistical difference was found between the weights values of the two spheroids population. Control spheroids resulted to weight 6.3 ± 09 µg, on the contrary, the weight of treated spheroids decreased up to 3.0 ± 1.2 µg.
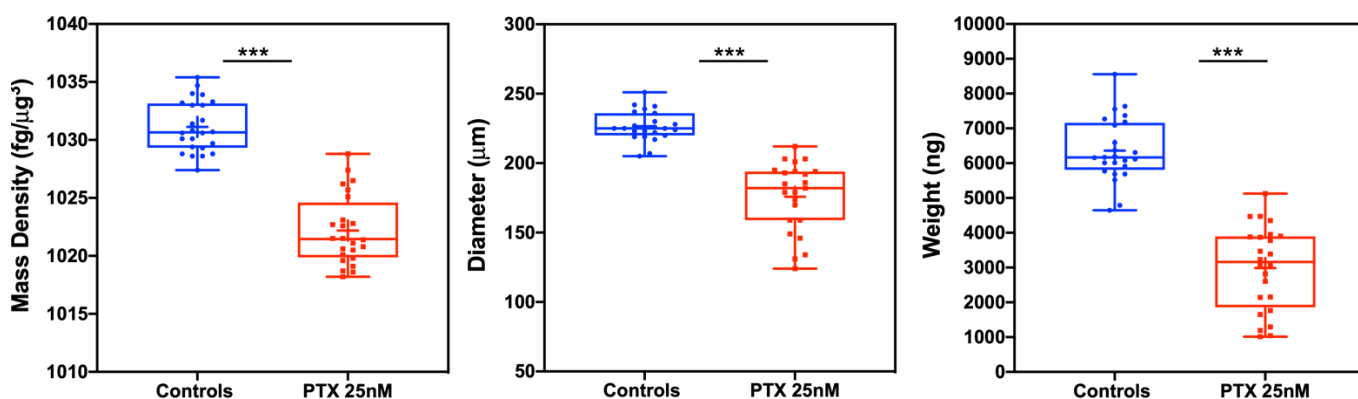

Figure 26: Box-and-whisker plots exhibiting the distribution of mass density, diameter and weight for every condition under testing. The lines, extending from the boxes, indicate variability outside the upper and lower quartiles. Results are expressed as the mass density (fg/μm^3, left graph), diameter (mm, central graph) and weight (ng, right graph). The mean value and SD of these three parameters (MD, W, D) are calculated for each sample. Student's t-test (two-tailed and heteroscedastic) was used to assess statistical significance between the two data sets: p-value < 0.001 (***).

In conclusion, this flow-based alternative method allowed to acquire accurate information on physical properties of the spheroids cultured in the devices. The results confirmed the morphological analyzes previously carried out; the generated spheroids were homogeneous and significant differences were found on PTX-treated spheroids regarding mass density, diameter, and weight. In comparison with the diameter values of our control spheroids, in previous works more dispersed sample dimensions were observed (using W8 Physical Cytometer). Cristaldi et al. generated spheroids with ULA plates and observed diameter variations between 95 ± 2 and 195 ± 10 µm in 72 live SW620 spheroids (Cristaldi et al. 2020). Additionally, with the same method, Cianciosi et al. showed dimensions of control spheroids with higher values dispersion compared with our model. Control spheroids had an average diameter of 160 ± 22 µm while spheroids produced with prototype device had average diameter of 227 ± 11 µm (Cianciosi et al. 2022).

4.1.9 Method for single spheroid disruption and cell counting

Flow cytometry is widely used for the analysis of single-cells dissociated from 3D cultures due to the ample cell number. Spheroids can be treated, stained with apoptosis markers, and flow cytometry analysis can be conducted as an endpoint assay. As a result, spheroid culture must be dissociated, a procedure and method that requires substantial training to master (Grässer et al. 2018). Currently, spheroids generated even with highly sophisticated techniques are entirely collected and dissociated for this type of analysis (Patra et al. 2016). Hence, we wanted to investigate if it was possible to harvest one single spheroid from the prototype device and estimate how many cells it was composed of. Since it is possible to count the number of cells positioned at the bottom of each microwell, it would be interesting to evaluate how many cells form a single spheroid at different days of growth. Hence, preliminary attempts were directed to develop a cell counting method to harvest, disrupt, and count cells deriving from a single spheroid cultured in a prototype device (**Figure 27**). A glass capillary (1 mm of diameter) was used to collect a single spheroid in a small drop of FBS-free culture medium containing trypsin. The capillary was placed between two cover glasses, and the edges were sealed with parafilm to avoid solution leaks. Images of the spheroid were acquired at different perspectives (by rotating the capillary) to evaluate the volume. Then, after capillary ultrasonication, a single-cell number was counted within the capillary deriving from the disrupted spheroid. Preliminary results showed that, for neurospheres samples, every cell occupies a volume of a cube with a side of 12 µm.

Spheroid	Volume	# single cells
1	$3,8 \times 10^6 \, \mu m^3$	2205
2	$3,2 \times 10^6 \, \mu m^3$	1855
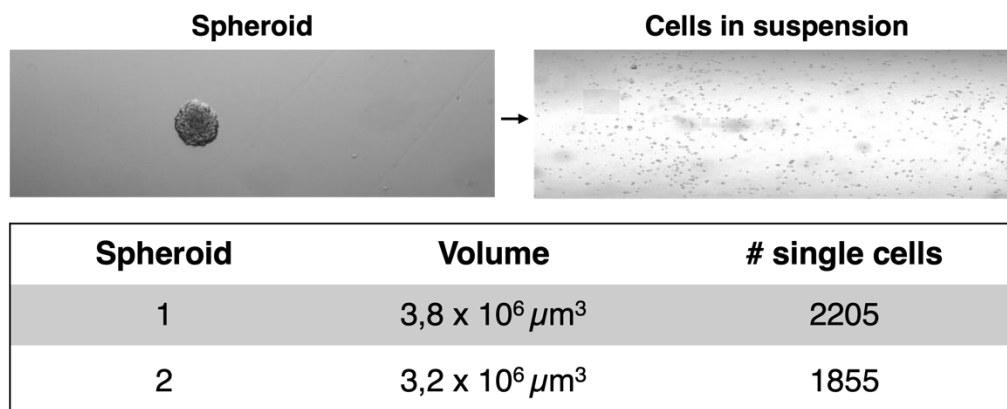
Figure 27: Method for estimating spheroid cells number. Images of a spheroid sample before and after ultrasonication, volume and relative cell number are reported

In conclusion, preliminary results helped understand the correlation between the size of the spheroid and the relative number of cells. In addition, a fluorescent staining (FDA/PI) would undoubtedly facilitate the segmentation of individual cells inside the capillary for automatic counting and would provide quantification of live/dead cells at the level of the single spheroid.

4.1.10 Conclusions and observations

In recent years micro-techniques have been widely used to generate spheroids from different cell lines (Verjans et al. 2018; Bērziņa et al. 2021). We described an effective method for producing a large number of 3D spheroids from established cancer cell lines. Nevertheless, our approach is fully compatible with non-cancer cells (i.e., neural stem cells). The developed technology is suitable for different applications, and devices can be assembled on conventional multi-well plates. We demonstrated that it is possible to characterize the formation and morphometry of the spheroids produced. The device was designed to form highly uniform, numerous, and medium-sized spheroids. In general, our method generated spheroids with a satisfactory compact and circular shape, especially for SKOV-3 and HCT116, when compared to results reported in the literature (Raghavan et al. 2015; Zoetemelk et al. 2019; Kulesza et al. 2021). Furthermore, results indicated that PDMS devices coated with PVA allowed easier and faster spheroid formation than conventional systems. In addition, this platform supported larger media volumes of up to 500µl, enabling the growth of spheroids without significant media depletion over 13 days.

Furthermore, this study investigated system adaptability for spheroids generation with different materials (device production with PDMS and agarose) and conditions (scaffold-free and scaffold-based culture). Geltrex™ was employed to develop 3D compact cell mass cultures with MCF-7 and HeLa cell lines composed of a specific combination matrix comprising laminin, collagen IV, entactin, and heparin sulfate proteoglycan predominantly. Spheroids grow as compact cell agglomerates. A significant difference in circularity was observed depending on the method of spheroids generation, indicating that combined use of Geltrex during seeding promoted spheroid formation in PDMS devices. System characteristics offered the exciting possibility of fabricating both scaffold-free and scaffold-based microtissues, generating multiple spheroids with uniform size by controlling the depth and diameter of microwells array. This peculiarity represented an added value of the system with respect to the standard 3D culture methods developed.

Once more, an essential aspect of in vitro tumor model is the identification of treatment response along with the formation of 3D MTSs. This method enabled a reproducible generation of homogeneous tumor-like structures grown separately in an array disposition and subsequently used to evaluate different compounds' drug effects. Spheroids were treated under the same condition, which is advantageous for drug applications. We demonstrated an in vitro chemosensitivity assay using conventional chemotherapeutic agents and compounds (DOX, PTX, SAHA) to ascertain if a difference in size resulted in a difference in drug sensitivity. When

comparing the untreated control spheroids generated with the three methods, there were significant differences in the cell viability after 72h of spheroid growth. The sign of the effect could also vary depending on the drug. Our results showed that micropatterned technology can be used to conduct single spheroid growth kinetic analysis and standard viability assay to assess drug treatments effect. The developed method was compared with two different commercial plates with similar principles. We did not observe differences in the growth behavior and morphology of the spheroids, resulting in similar growth and treatments response in the three different techniques. Further, the purpose of this study was to demonstrate that the prototype system may integrate several assays into one single experiment. It was performed direct correlation with morphological changes in response to treatment, viability assays, and comparison of different compound concentration profiles with specific live/dead cell staining (*Figure 28*).
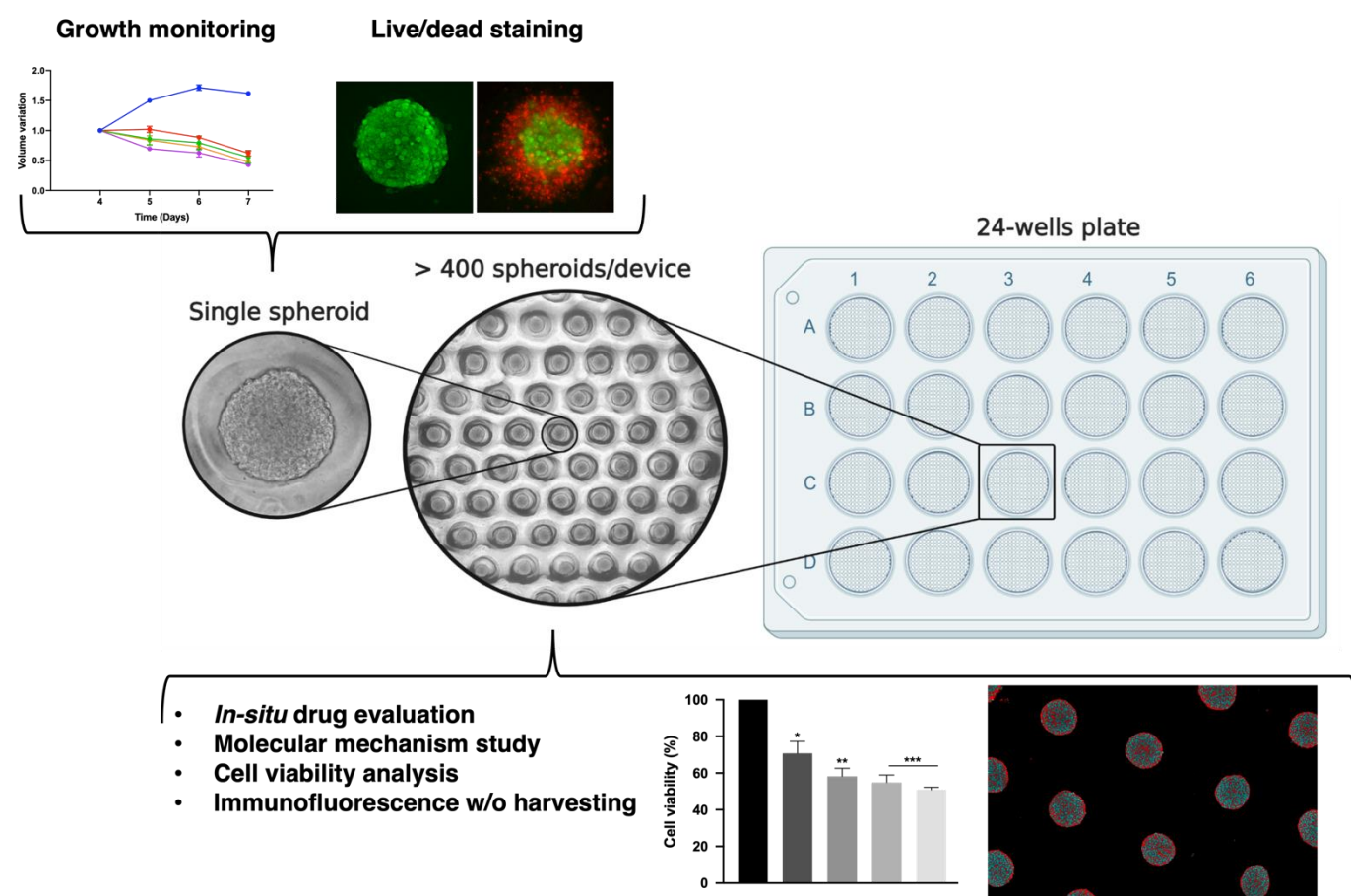
Figure 28: Graphic representation of the principal applications provided by prototype device for 3D cultures. When developing the microstructured device the goal was to create a 3D cell culture platform to produce high-quality, homogenous, standardized, and size-controlled spheroids. At the same time, the plate allows real-time imaging and monitoring within the platform, both at the single spheroid level and the entire culture population level.

We performed direct FDA/PI staining of live spheroids. We demonstrated on-chip imaging of spheroids cultured in prototype devices, allowing identification of the most fragile spheroid's outer layer without any recovery. Standard live/dead staining approaches often do not utilize automatic

procedures to segment, quantify and interpret fluorescence signals to form metabolic dyes. We used a customized MATLAB script to semi-automatically individuate, segment, and analyze more than 60 single spheroids per condition. Of note, the prototype device application was validated for *in situ* immunofluorescence. This method provides a fast and straightforward process for immunostaining hundreds of spheroids and allowed easy transfer on coverslips for image acquisition using confocal and two-photon microscopy. Simultaneously, the plate provided for real-time imaging and monitoring within the platform, as well as being scalable and simple to use. Preliminary analysis showed that our system is compatible with standard automation units (Incucyte®,Sartorous - Lionheart FX, Agilent- Cytosmart Omni®), this aspect is particularly promising and advantageous given the increasing interest over high-throughput drug screenings (Kondo et al. 2019; Schumacher et al. 2019). The proposed technique will have broader utility in the manufacture of other microtissues and cancer models as well as in a situation where conventional methods are not practicable. To conclude, we believe this method could be helpful for preclinical screening and assessment of anticancer drugs for a variety of tumors, able to provide relevant information at the level of the whole spheroid population and at the single spheroid level.

4.2   Microfluidic device to investigate microglia activation

The work presented here illustrates an alternative approach of advanced cell culture methods. Microfluidics systems allow culturing cells in controlled microscale conditions and have been used as an effective analytical tool for many biomedical fields. The Ph.D. project focused on developing alternative culture methods characterized by targeted drug delivery controlled by flow regulation. Unlike the culture method previously used, the field of microfluidics offered numerous capabilities like easy usage with minimal human intervention and fine control concentration of sample in both space and time. Thus, a microfluidic platform represented the ideal approach for drug screening. Nevertheless, our approach can be fully compatible with cancer cells. In our case, the developed system was employed on an ongoing research project. The cellular model, a murine microglia cell line (N9), was already used in previous experiments in collaboration with *the Cellular Neurobiology* laboratory (FaBiT), led by Prof. Barbara Monti, in the context of the project financed by Amyotrophic Lateral Sclerosis Association (ALSA). The project objective was to investigate the regulation system of microglia activation pathways to obtain a greater understanding of neuroinflammation and neurodegeneration mechanisms.

As previously mentioned (1.3.3), recent evidence suggests that extracellular vesicles (EVs) secreted by neurons, glia, and microglia play a key role in the propagation of neuroinflammation, carrying mRNA, microRNA, and regulatory proteins. The molecules contained within these vesicles could therefore be critical pharmacological targets for reducing the progress of the neuroinflammatory and neurodegenerative state. In fact, neurodegenerative diseases are often accumulated by the presence of a neuroinflammatory state. To fully understand the mechanisms of activation and regulation of microglia, it is necessary to investigate in depth the phenomena of cellular communication. *In vitro* models are essential for understanding the fundamental processes of microglial-mediated neuroprotection, as well as for identifying potentially effective neuroprotective compounds and designing innovative techniques in a gene therapy setup. In previous works, the *Cellular Neurobiology* laboratory has developed *in vitro* methods to study microglia cell activation, conditioned media analysis and EVs isolation (Massenzio et al. 2018). Current *in vitro* research is carried out with standard culture dishes, and it requires a strict schedule timing to perform seeding, media exchange, and LPS treatment (***Figure 29***).
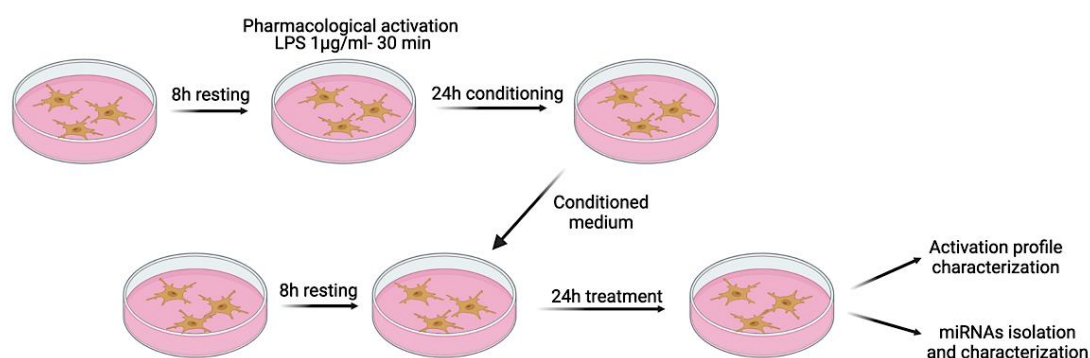
Figure 29: Experimental scheme of microglia activation through extracellular vesicles isolated from microglia culture previously treated with LPS (1μg/ml)

Additionally, our laboratory contributed by developing a DNA nanostructure for delivery of DNAzymes to block microglial activation spreading through vesicles. Tetrahedral DNA nanostructures of different architectures and sizes were designed and characterized. For this purpose, the microfluidic platform can be employed as *in vitro* tool for testing developed nanostructures, replicating standard experiments with an additional fine control over the parameters and flows direction. The PDMS-glass prototype device was characterized by two separate culture chambers which can be put in communication throughout the regulation and direction of media flows. Flow controls regulate when and for how long the two cultures can be in contact. In this way, the cell line cultured in parallel could be maintained in culture in two distinct

chambers and then a single chamber could be exposed to a diversified treatment. Subsequently, it was possible to put the two chambers in communication, to observe morphological differences and phenotypic status regarding different responses to these agents and their subsequent remote communication phase.

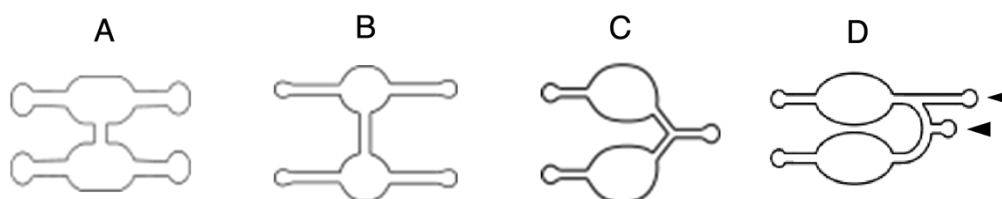### 4.2.1 Microfluidic device chambers design

The main purpose was to design a fluidic tool that allowed investigation of signals released by microglia cells at a certain phenotypic state. Specifically, the aim was to detect the effect of a paracrine signal released in the culture medium by microglia cells in an activated proinflammatory state (M1) towards another microglia culture in an inactive or resting state (M0). *In vitro* experiments are currently being performed manually with standard 35mm dishes. The aim was to develop a more practical and effective method for microglia activation studies. To do this, a system was first developed which supported microglia culture in two separate chambers and allowed directional flows regulation of culture media. The designed system provided control on flows diffusion and direction and maintained separation or connection of the two chambers at specific times. Additionally, this tool allowed the simultaneous observation of the two cultures in the different experimental phases and at the same time provided a fine control over the molecules and particles diffusion of secreted in the different phenotypic states.

For this reason, the idea of developing a microfluidic device for the culture of N9 cell line could ensure fine control over the paracrine interactions between the different phenotypic states and an automatic and continuous monitoring of culture morphological changes.

For the development of the microfluidics chip were evaluated different materials properties. The chip was made of PDMS, chosen for its biocompatibility, plasticity, and optical properties. In the literature, this material is widely used for microfluidics, especially when coupled to glass surfaces (Kuncová-Kallio et al., 2006; Nikolakopoulou et al., 2020). In fact, glass provides a flat surface, resistant, optically transparent, and compatible with cell growth. The possibility of covalently joining the PDMS and the glass through a plasma treatment (*bonding*) allows to fully exploit the REM possibilities for the fabrication of microstructured chambers. For this purpose, several tests were carried out to validate the optimal setting of the plasma machine, present in the laboratory, to covalently fix the two materials by varying different power and time settings.

Originally, different fluidic chambers were designed with a variety of shapes and structures. *Figure 30* depicts different prototyped configurations with various placement of the chamber communication channels; C and D were the final structures used. Specifically, the device was fabricated to host two culture chambers connected through a narrow channel, in which the flows

could be controlled in terms of how, when and for how long the two cell cultures should be in communication. The design has been modified several times to obtain a geometry that ensured the passage of solutions from one cell to another only when required, trying to eliminate any possible passage of unwanted fluids, due to unstable flows. With the aim to precisely regulate the fluidics, the shared channel between the chambers was modified in a "Y" shaped branch proximal to the *inlet.* With this outline, the maintenance flow prevented communication between the two cells, and, through the change of inputs and outputs (*outlets*), to also work individually on one chamber. The last configuration (**Figure 30** D) was designed to improve flow directionality.


Figure 30: Different chambers design for microfluidic chip. (C) First design used for testing glia culture (D) Design implementation with two *inlets* (arrows)

In fact, the final structure with a rounded central *inlet* and more elliptical shaped chambers, provided the correct mixing of the culture media flowed inside the individual cells. In addition, a second *inlet* was added in correspondence of only one of the two cells to keep the flows even more separated when activating N9 culture in one chamber. It was observed experimentally that the presence of another tube increased the probability of air infiltration in the chip, compromising the cell culture, so both *inlets* have always been used during treatments.

4.2.2 Syringe pump

The design and fabrication of a syringe pump were essential steps for the functioning of the entire microfluidic system. In fact, the operating conditions required several steps to be performed in the cell incubator at controlled temperature and humidity. Commercial syringe pumps are equipped with power supply cables which needs to be connected out of the incubator, the laboratory equipment was not suited for external cable connection, for this reason we had to undertake the development of a battery-powered portable syringe pump. With fast prototyping technologies (i.e., 3D printing and Arduino) it was possible to quickly develop a protype system overcoming problems of cost and size (**Figure 31**).
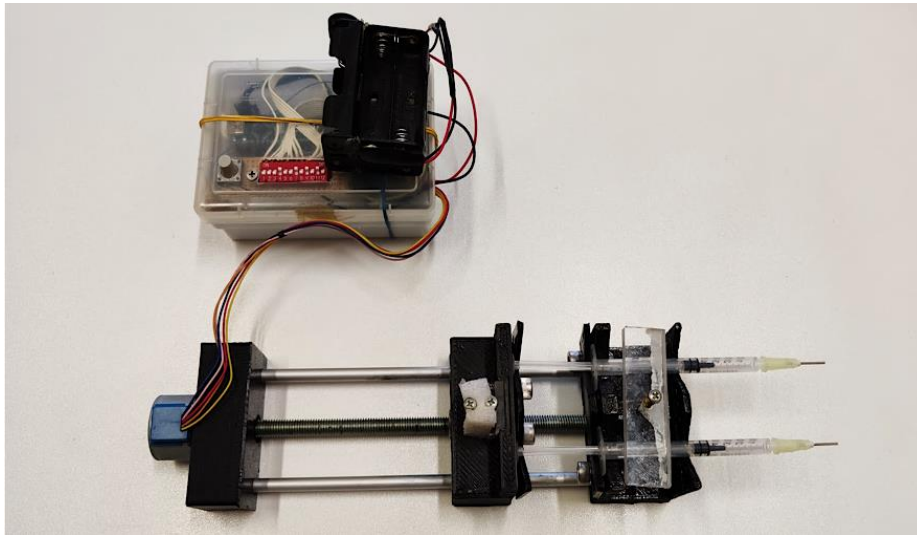
Figure 31: Fabricated syringe pump. Small, battery-powered syringe pump used for all experimental procedures

The capacity to independently program the pump allowed to preset working parameters not obtainable from a commercial syringe pump and to optimize them for the microfluidic system used. Firstly, the volumes moved by different syringe types (1 mL, 2.5 mL, 5 mL, 10 mL) were calculated for each complete motor rotation, which are determined by the syringe diameter and the pitch of the screw used. In this way, a specific parameter to the different types of syringes was obtained, necessary to establish how many microliters a motor pitch corresponded to. Different ranges of volumes, pumping speeds and operating modes were subsequently set throughout a DIP switch. A multiplexer was used to increase the number of Arduino pins and thus to read and control more switches at a time. The pumping modes set allowed working in withdraw or ejection, in continuous flow or in pulses. The modifications of the pump flow parameters made it possible to adapt the instrument to the operational needs during subsequent experiments. Since the goal was to develop a battery-powered instrument, it was necessary to optimize the program in order to reduce energy consumption, for this reason the system's *sleep* functions were used instead of simple pauses during pause times between sequential pulses. 6 batteries of 2450 mAh were necessary to dispense a difference potential of 7.2V which provided an autonomy of at least one week without the need to recharge. The possibility of pumping flows every one or two hours made it possible to keep the cell culture in the most static environment possible but at the same time, programming an impulse setting, to perform media exchange necessary to maintain optimal culture conditions. In this way, the cell culture was not undergoing continuous stress due to constant media flows, while at the same time ensuring nutrients supply throughout a defined time. Software and DOS script are described in the *APPENDIX.*
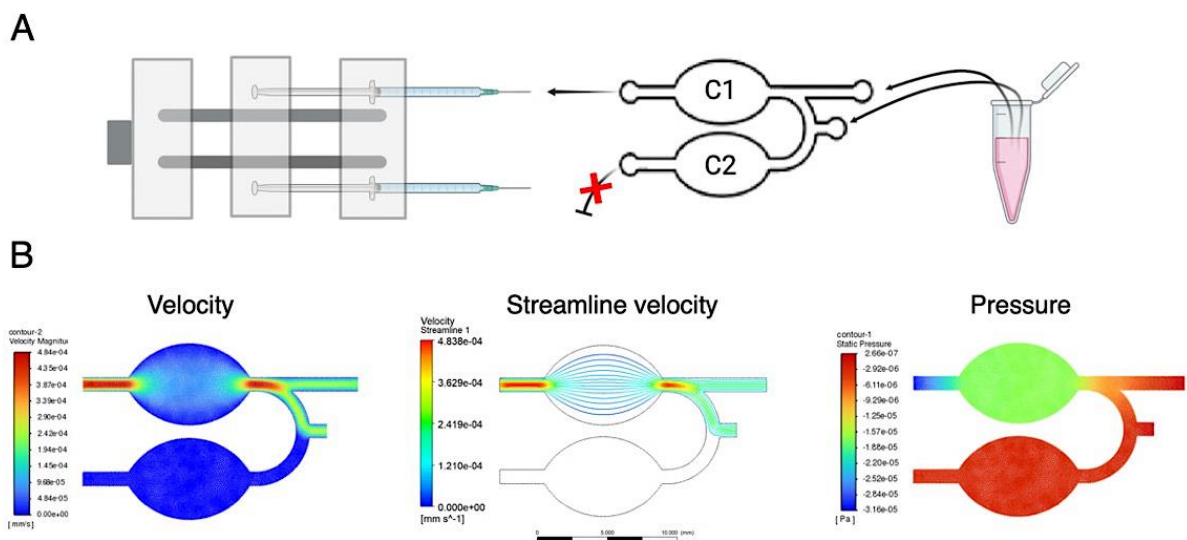
4.2.3 Fluid dynamics simulations

For the validation of the design used for the microfluidic culture chip, simulations were carried out *in silico* and using solutions. Thanks to the support of Dr. F. Rahbar Kouibaran, *Ansys workbench 2019 R3* software suit was used to obtain data on flow predictions within the chosen fluidic design. The analysis was carried out by examining the different flow configurations that the system could support (i.e., cell culture maintenance, cross-communication, differential treatments). The data obtained from *in silico* simulations showed aqueous liquids flow lines within the microfluidic chip, the pressure differences and flow rates in the different areas of the system. In addition to the design and dimensions of the system, it was necessary to determine the type of flow passing through the device. For this, Reynolds' equation was used ($Re = vL = \rho vL \ v\mu$). Considering the reduced flow velocities (µl/h or µl/min) and the thickness of the prototyped chip (100 µm), the Reynolds' number obtained was extremely low. Thus, the flows of aqueous solutions during the experimental simulations performed were assumed as laminar. Through fluid dynamics simulations, the different *inlet* and *outlet* configurations were evaluated. Cell culture maintenance, differential treatment and cross-activation configuration were investigated. The setting used for cell culture maintenance consisted of two different *inlets* and *outlets* that worked at negative pressure developed by the syringe pump set in withdrawal mode. This type of configuration (***Figure 32*** A) was then analyzed through fluid dynamics simulation which provided data on the direction of the flows, the speed, and the partial pressures to which the device was subjected. The flow rate in the *outlets* was set at 200 µl/h, the same value was used for maintaining the culture. The simulation results (***Figure 32*** B) showed a defined separation of the N9 cell culture in the two chambers, this was defined by the absence of flow lines passing from one chamber to another. It was possible to notice a slight pressure difference between the two chambers. On the other hand, the flow lines are sparse, synonymous with a very slow flow, but it was still observed that the flows are directional towards the chambers and do not mix between one chamber and another. The speed of the flow lines is much lower inside the culture chambers than in the channels; at the same time, a central stream is evident, which has a higher speed than that of the peripheral stream. The distribution of the flow lines showed an extensive surface covered within the culture chambers; this indicated a correct mixing of the incoming fresh media with the exhausted media present in the chambers.
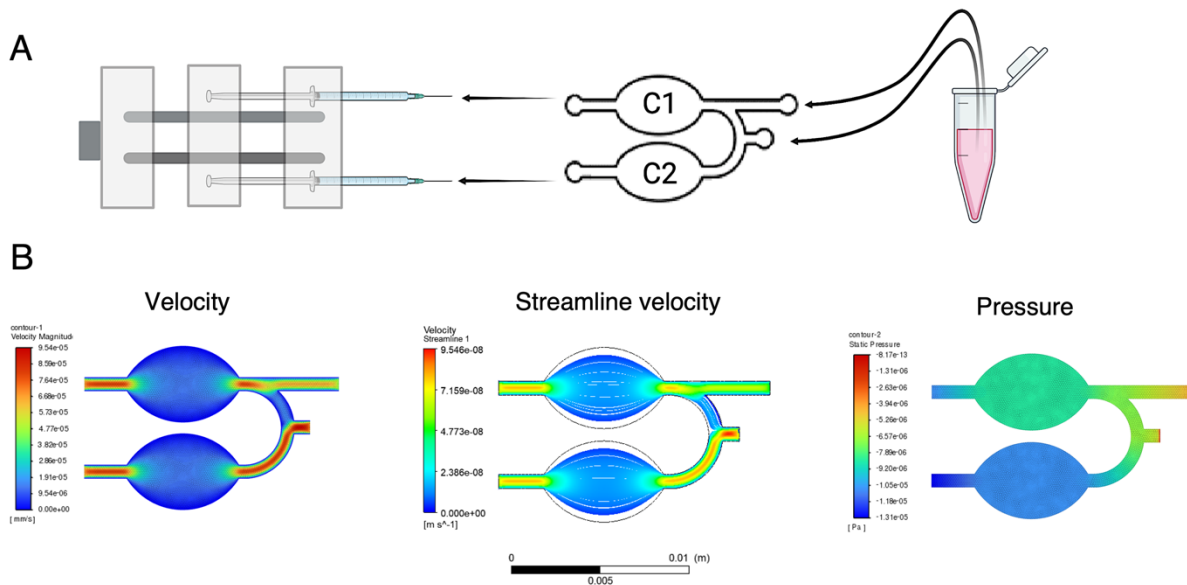
Figure 32: Culture maintenance configuration. (A) Configuration scheme showing reservoir and syringe pump positioning corresponding to inlets and outlets. (B) Fluid dynamics simulation of culture maintenance at a flow rate of 200 µl/h

The configuration used for treating differentially the two culture chambers involved the presence system's one *inlet* and *outlet*, corresponding to C1 chamber (***Figure 33*** A). This simulation was carried out by setting the syringe pump in withdrawal mode at a speed of 20 µl/min. From the results obtained (***Figure 33*** B) it was possible to observe how the flow lines were directed exclusively into one chamber. A slight partial negative pressure was observed in the isolated chamber which was higher than the one present in the operating chamber, promoting a preferential flow path in the treated culture chamber.

Figure 33: Configuration for selective activation of one chamber. (A) Configuration scheme showing reservoir and syringe pump positioning corresponding to inlets and outlets. (B) Fluid dynamics simulation of C1chamber LPS-treatment at a flow rate of 20 µl/min

Finally, the cross-activation configuration was simulated, necessary for the intercommunication of the two chambers (*Figure 34* A). This configuration, designed to transfer conditioned culture media from the cellular products of C1 to C2 culture chamber required the use only of an *inlet* and an *outlet*, while blocking others present in the device. Also, in this case the simulation was carried out assuming withdrawal at a speed of 200 µl/h. The flow lines showed homogeneity between the two cells and the flow speeds were comparable to those showed in the culture maintenance configuration (*Figure 34* B). In the cross-activation, the partial pressures inside both cultivation cells were homogeneous showing a positive pressure (still lower than the pressure present in the *inlet*) in the cell connected with the *inlet* tube, in line with the negative pressure pumping activity. The flow covered an extensive surface of the culture chambers. This was necessary to obtain a correct media transfer between C1 and C2, providing an adequate mixing into the chambers. The media covering the surface of C2 chamber reveled essential to bring all the cell culture in contact with the factors released by N9 cells cultured in C1 chamber.
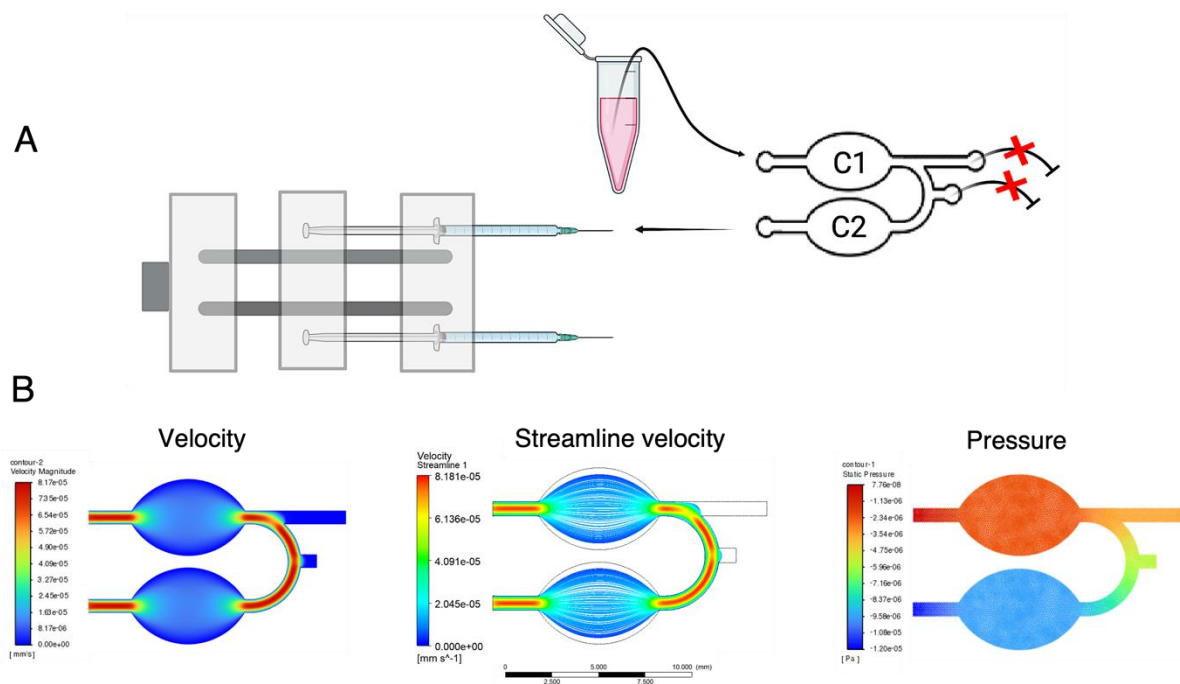

Figure 34: Cross-activation configuration. (A) Configuration scheme showing reservoir and syringe pump positioning corresponding to inlets and outlets. (B) Fluid dynamics simulation of chambers cross-activation at a flow rate of 200 µl/h

To conclude, simulations showed controlled and stable flow trends within the entire fluidics. The pressures inside the chambers were homogeneous and the flow rates were moderate to not compromise cell culture within the prototype device, causing stress and cell detachment. To

confirm results obtained *in silico*, tests of fluidics and their respective configurations were carried out using aqueous solutions dyed with phenol red and methylene blue (

Figure 35).
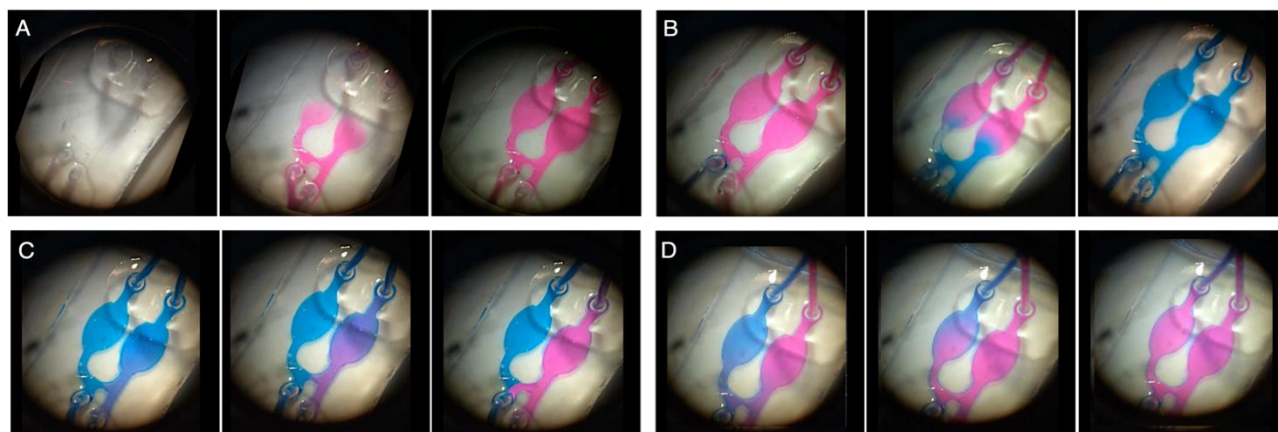
Figure 35: Validation of the different fluidic configurations with colored solutions. (A) Seeding simulation at a flow rate of 200 µl/min. (B) Fresh medium renewal for culture maintenance at a flow rate of 200 µl/h. (C) Selective treatment of a single chamber, flow rate of 200 l/h. (D) Cross-activation at a flow rate of 200 µl/h

The aim was to observe the flow directions inside the device, and, thanks to the use of a microscope, *time-lapse* images were obtained to monitor the fluidic trends. The observations were coherent to those obtained from *in silico* simulations: the flows were well-established and controlled in line with the type of configuration. It can therefore be concluded that the microfluidic system can be effectively stable and adjustable over time according to the operator's needs.

4.2.4 Microglia culture in microfluidic device

The cell line used for the experimental procedures was a murine microglia cell line (N9). To define the cell number to perform cell seeding, calculations were made regarding the surface to be covered and the volumetric capacity of the chambers. The estimated cell density was between 100.000 cells/ml and 300.000 cells/ml depending on the type of assay to be performed. Firstly, N9 growth within the microfluidic system was determined, the cell culture was successfully maintained for 120 hours in culture after seeding a cell suspension of 160.000 cells/ml (*Figure 36* A). To quantitatively estimate cell growth, images of the same device areas were acquired every 24 hours for three days using 10X and 20X magnifications. N9 single cells were counted each day, as shown in

Figure *36* B, displayed an exponential growth trend of the culture. The fold increase was determined as the average growth value of the individual device areas considered; results showed a significant increase each day compared to the previous 24h.
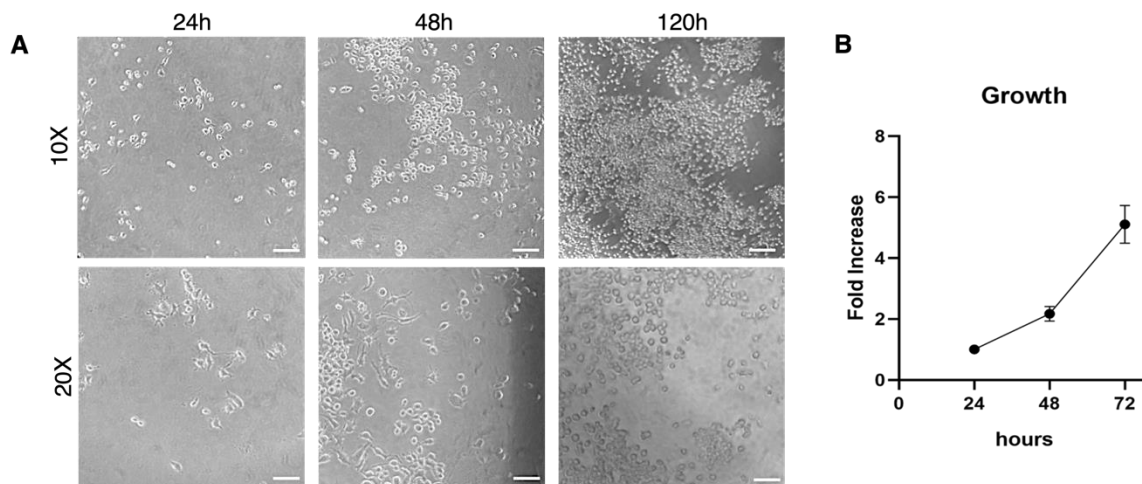
Figure 36: N9 cell culture growth within prototype device. (A) Culture area monitored for 5 days, images acquired at 10X and 20X magnification, scale bar 100 μm and 50 μm respectively. (B) Growth curve obtained from cell count of four different device areas

The cell morphology was identical to N9 cells grown in standard culture dishes (***Figure 37***). The N9 culture was characterized by cells with a small body and extensive ramifications in the resting phase. The presence of cellular debris was also observed in both culture conditions suggesting that culturing N9 cells in the prototype device did not alter culture morphology.
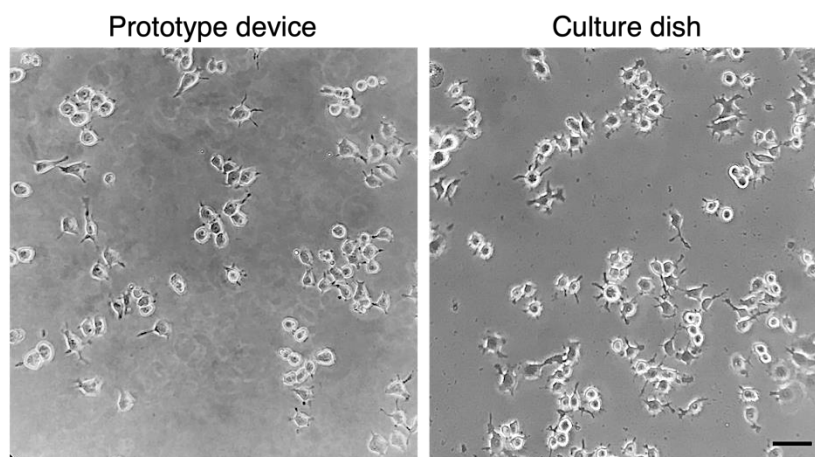
Figure 37: Image comparison of N9 cell morphology cultured in microfluidic device and in standard culture dishes. Scale bar: 50 μm

Additionally, the cell distribution within the microfluidic system was not extremely homogeneous, this was probably due to the flow lines distribution within the culture chambers that guided cells mainly along the chambers margins. This phenomenon was also predicted from *in silico* fluidic simulations. Thus, we adapted the seeding procedure by pausing the syringe pump for two hours before flowing fresh medium into the microfluidic device in order to facilitate cell

distribution on the entire chambers surface. To conclude, cell viability was verified with FDA staining, which allows the evaluation of the cellular enzymatic activity characteristic of healthy cells. N9 cell line cultured in microfluidics showed a high intense fluorescence after treatment with FDA as proof of the effective activity of cytoplasmic esterase and consequently of the active metabolic functions.

4.2.5 Immunofluorescence analysis within microfluidic device

Immunostaining for cytoskeletal proteins was performed to validate the practical possibility of performing cell assays within the designed microfluidic system. Immunofluorescence assays on these two cellular components are highly widespread in 2D cell cultures for structural and morphological observations. Therefore, we tried to optimize and adapt it on the developed microfluidic device, starting from a well-validated protocol. The purpose was to perform differential staining of the two culture chambers to determine the possibility of working selectively on one single chamber. The assay was performed on N9 cell line cultured in the fluidic platform. The cells, grown within the culture system for 24 hours, were fixed and stained as described in 3.3.7. Chamber 1 (C1) was treated with the β-actin primary antibody, while chamber 2 (C2) was treated with α-tubulin primary antibody. After incubation, a solution containing the two secondary antibodies was simultaneously flowed in both cells. The images acquired with a fluorescence microscope were analyzed to determine and compare the fluorescence values. As shown in *Figure 38,* the β-actin signal was detected in sample areas corresponding to C1 chamber, which was treated with the specific Ab-I for this marker while the α-tubulin signal was absent.
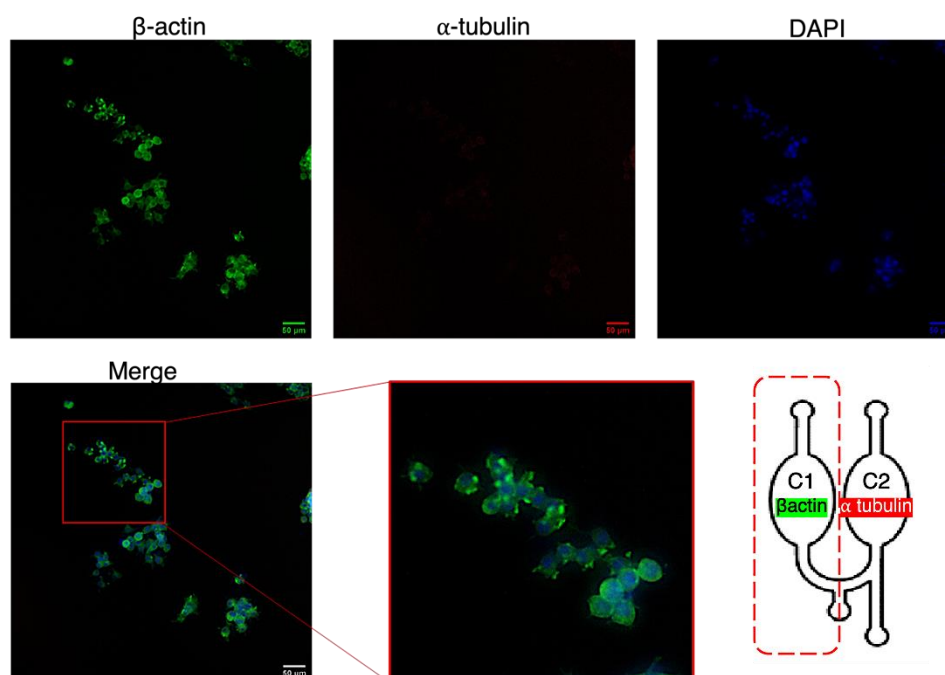
Figure 38: Fluorescence microscope images of chamber 1 treated with the specific Ab-I for β-actin. β-actin (FITC-green), α-tubulin (Cy3, red) and nuclei staining in DAPI (blue). Merge of the three channels (20X objective, scale bar 50 µM)

On the contrary, in chamber 2 the specific α-tubulin signal was detected while the β-actin was absent (***Figure 39***). The fluorescence intensity of single cells corresponding to different areas of the two culture chambers was then converted into a quantitative value expressed in arbitrary units (AUs) determined by the number of photons captured by the camera at the emission wavelength of the respective fluorophores used. Then, the average fluorescence of both frequency intervals (FITC and Cy3) was calculated relating to the cell populations present in the two respective device chambers. The light exposure time and intensity were maintained standard for image acquisitions procedures.
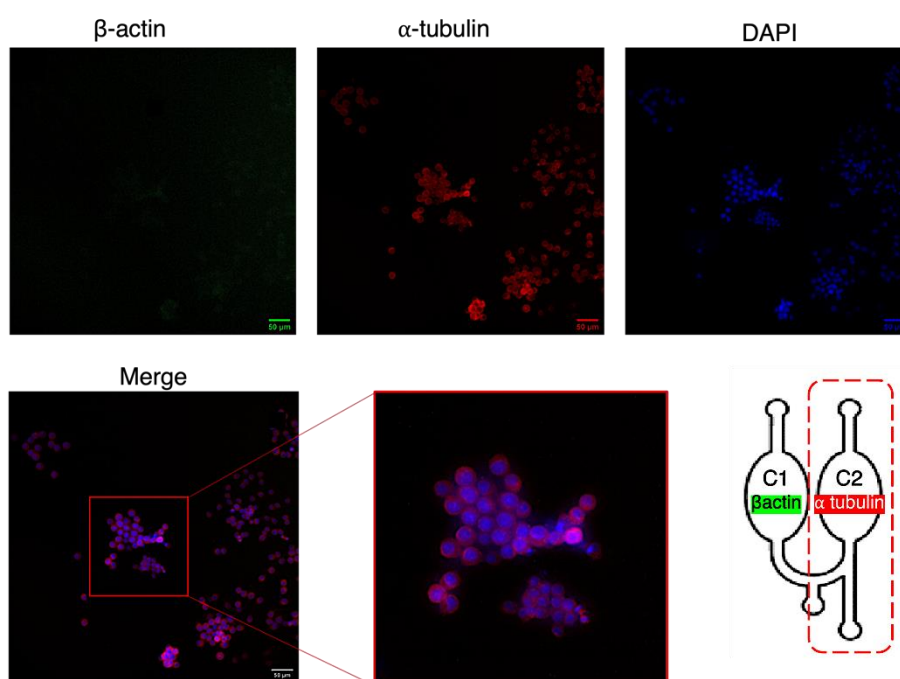
Figure 39: Fluorescence microscope images of chamber 2 treated with the specific Ab-I for α-tubulin. β-actin (FITC-green), α-tubulin (Cy3, red) and nuclei staining in DAPI (blue). Merge of the three channels (20X objective, scale bar 50 µM)

Figure 40 represents the average fluorescence values (after background subtraction) of the pixels relative to the single cells in both fluorescence channels. Fluorescence values were evaluated using customized MATLAB script which allowed fast single cell segmentation, background subtraction and specific signal analysis. The results obtained for each channel in the two distinct chambers were related to the fluorescence intensity derived from actin and tubulin staining.

84
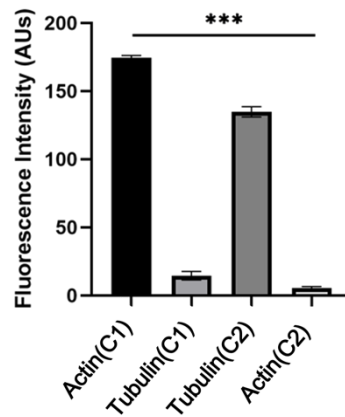
Figure 40: Mean fluorescence values β-actin and α-tubulin of the single cells cultured in the microfluidic device. Actin (C1) and Tubulin (C1) refer to the mean fluorescence values of the cells grown in chamber1. Actin (C2) and Tubulin (C2) correspond to the average fluorescence values of the cells cultured in chamber 2. Data normalized to cell number, One-way Anova test, p-value <0.001 (***)

Specifically, in chamber 1, treated with the primary Ab for β-actin, the average fluorescence value was significantly higher than the same signal deriving from α-tubulin staining. N9 culture in chamber 1 was treated only with the primary antibody for β-actin. Results were in line with the immunostaining performed. Equally, stained cells in chamber 2, treated with the α-tubulin primary Ab, showed significantly higher signals compared to the β-actin signal. Therefore, it can be assumed that it was possible to selectively carry out an immunostaining in the two device chambers. In fact, the corresponding labeling of the sample has been verified regarding the primary antibody used, and therefore, different treatments can be performed separately in the device chambers.

4.2.6 N9 activation: iNOS immunostaining

Previously, it was demonstrated that our prototype device could be successfully used as culturing platform for N9 cell line, allowing to treat the two culture chambers separately and carrying out immunofluorescence directly in the device. The research work has consequently focused on testing methods of investigation for discrimination markers for microglia activated state in comparison with controls. Standard *in vitro* experimental design considers, as final end-point test, western blot analysis and relative quantification of iNOS and TREM2 proteins. Standard experiments used 3.5 mm or 6 mm dishes to have adequate sample quantities for the analysis. For the microfluidic platform developed, containing a modest cell number, immunostaining was used as the main readout for studying microglia activation. Firstly, since microglial cells change morphology when shifting from pro-inflammatory M0 resting state to the M1 phenotypic states (1.3.3) immunofluorescence of cytoskeletal proteins was used as end-point analysis to determine

and discern activated glia cells in one chamber and resting cells in the other chamber. N9 cells were seeded in the device chambers and maintained for 24h in culture with FBS-free medium. Subsequently, C1 chamber was treated with LPS for 30 minutes and then fresh medium was flowed in both device chambers. After 24h, the cells were fixed directly into the device and immunostaining with β-actin and α-tubulin Abs-I as performed. Contrary to the immunofluorescence performed to demonstrate that device chambers can be separately treated, an immunofluorescence was attempted flowing a solution containing both primary antibodies in the device chambers. The purpose was to find morphological differences between the two microglia cultures. M0 resting microglia (in chamber C2) should present a branched morphology with numerous protrusions that branch off from the cell body, M1 LPS-activated microglia should be characterized by a more circular shape without the presence of protrusions. Results showed no morphological differences between the two microglia cultures. This may be because microglial culture consists of a heterogeneous population made of cells with different morphologies. Consequently, with the aim of concretely evaluate differences between the pro-inflammatory M0 resting and M1 phenotypic states, the iNOS immunofluorescence assay was applied. iNOS is transcriptionally induced in response to bacterial endotoxins, such as LPS and proinflammatory cytokines, in macrophages and various other cell types. In this study, N9 cells were stained for the iNOS used as differentiation marker for activated microglia along with negative controls. For these preliminary experiments, cells were seeded on coverslip slides and a standard immunofluorescence was performed. The LPS incubation timing was extended up to 24h to observe a stronger iNOS signal. Images were acquired with the fluorescence microscope using the same settings and light exposure for all images. LPS-activated cells showed increased iNOS-expression compared to the controls (*Figure 41*).
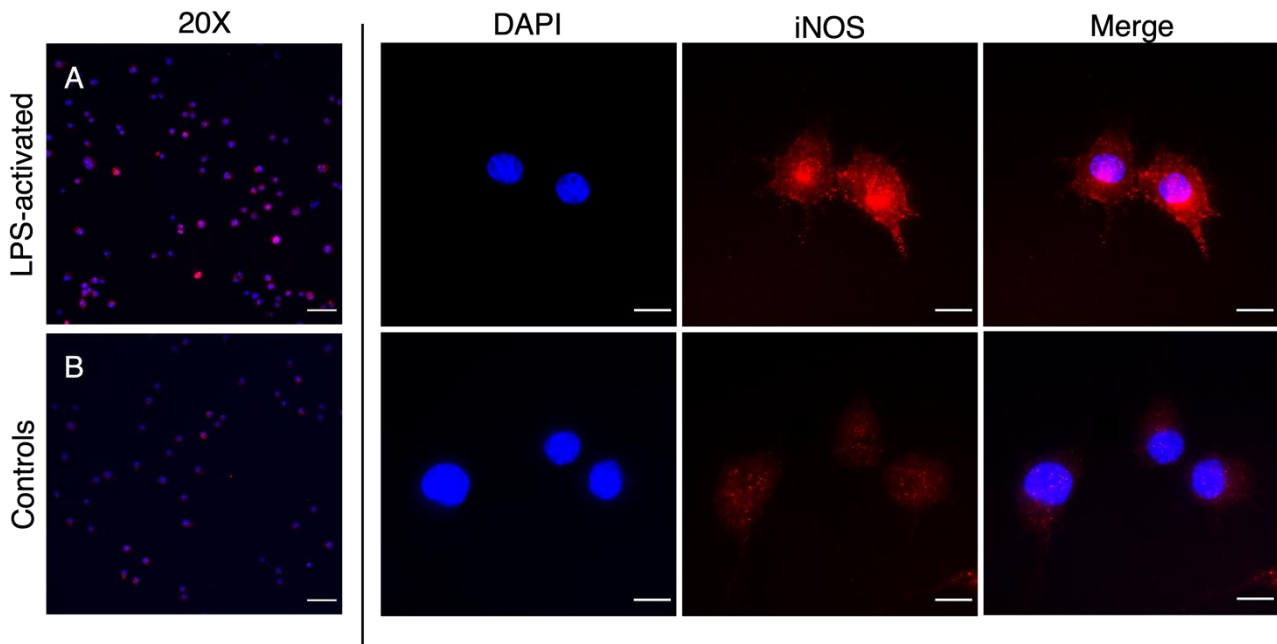
Figure 41: Immunofluorescence staining of iNOS in N9 cells. (A) LPS-activated cells, nuclei staining (blue) and an apparent increase of iNOS expression level (red). Left image acquired with 20X (scale bar: 50 µm), right images with 100X magnification. (B) The expression level of iNOS (red) in N9 control cells was lower. Histograms were stretched equally for each channel for display purposes (scale bar: 10 µm)

Next, with a customized MATLAB script for single cell segmentation, a quantitative analysis of iNOS expression levels was evaluated (6). Corrected integrated pixel density was used as an indicator of signal intensity. In *Figure 42*, the mean of the relative values of the integral cell fluorescence of controls and LPS-activated N9 cells from 3 repeated experiments are represented. For each replicate, 50 cells were evaluated. Results showed a significant difference in fluorescence values among the two groups.
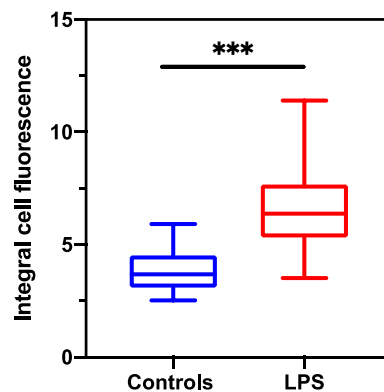
Figure 42: Box plot of the integral cell fluorescence of iNOS signal comparing controls and LPS-activated cells. Student's T test p value < 0.001 (***)

In conclusion, it can be said that iNOS has provided results that lead to discrimination between the activated or resting cell population. Nevertheless, this marker is the same one used for western blot analysis in standard *in vitro* experiments. Future steps will involve immunostaining experiments within the prototype device (as already performed with cytoskeletal protein staining)

in order to define a signal difference between the N9 culture grown in the two separate chambers, one control and one LPS-activated.

4.2.7 Conclusions and observations

The fabricated prototype has proved functional for culturing N9 murine microglia and is suitable for other cell types. The results obtained so far have shown that the microfluidic chip could provide an optimal microenvironment for the growth and proliferation of a microglial cell line. Similarly, the system could be used as a tool for different types of analysis. It was demonstrated that it is possible to perform viability analysis (FDA) and immunofluorescence staining (cytoskeletal proteins) within the device. Additionally, it was shown that the flows directed to each culture chamber could be selectively controlled to activate only one cell population within the device. Regarding this, it was initially performed LPS activation (LPS – 1000ng/ml; 30min) of only one culture chamber and then it was carried out an immunofluorescence analysis to determine an N9 different phenotypic state through another organization of actin and tubulin signals between activated and control cells. Since we obtained no significant results with this method, a marker of the microglia activated state was used; iNOS. iNOS marker was tested with standard immunofluorescence techniques on fixed N9 cells adherent to cover-slip slides. Results analysis demonstrated statistically significant differences between quiescent and activated N9 cells (LPS – 1000ng/ml; 24h). The next step will concern performing the same experiments within the device to prove significant difference between cells cultured in control chambers and LPS activated cells. Furthermore, it will be possible to conduct cross-activation analyses within the system using two microglial cultures in different phenotypic states. In fact, numerous chip devices can be produced at the same time while maintaining N9 cell cultures in parallel and carry out simultaneous activation experiments in more than one microfluidic platform.

4.3 Standard Operating Procedures

The methods developed in this research work have been organized into SOPs in order to be available to external personnel requests. The most recent versions of the files can be found at the following link: http://nanobionano.unibo.it/people/ottaviatartagni.html or requested to: ottavia.tartagni3@unibo.it.

5. CONCLUSIONS AND FUTURE PERSPECTIVES

The overall work consisted of developing and testing advanced *in vitro* methods for compound screening. Specifically, the project was focused on fabricating a microstructured device for the generation of uniform 3D cell structures and a microfluidic platform for the study of microglia role in the propagation of neurodegenerative diseases.

Firstly, we designed a microstructured device to generate and maintain more than 400 highly homogeneous spheroids in culture. The population of spheroids produced by 3D cell culture techniques is often fairly dispersed in terms of size and shape, which can strongly influence the outcome of drug efficacy and toxicity studies. The development of standardized spheroid fabrication procedures could potentially reduce data variability and enhance the clinical significance of experimental data derived from spheroid systems. The fabricated device was employed as a culturing platform for different cell lines and was confirmed to be a suitable system for drug testing. We monitored single spheroid growth and morphology over time and investigated drugs effects on 3D cell architecture. We paid special attention to developing a versatile system; within the same device the following characterizations can be performed: spheroid growth kinetic analysis, metabolic activity assay, and live-dead staining without harvesting 3D cell culture from microwells. Thus, the system allows the tracking and analysis of the single spheroid and the entire 3D culture within the device. Furthermore, microwells arrangement and dimensions are entirely customizable. The information obtained and the experiments performed led then to the development of immunofluorescence protocols for direct immunostaining of the spheroids within the device. More investigations would be required, and the adaptation of the immunostaining with drug-treated spheroids would surely further enlighten the suitability of the method for deeper characterization of the compound effects.

Our contribution helped the development of a custom-made device with alternative methods of handling and *in situ* analysis of homogeneous spheroid culture (manuscript in preparation). In addition, implementing the mold number for massive device production would allow fast plate fabrication for conducting more experiments in parallel. Compared to previously reported techniques, this method is more straightforward in fabrication. It can produce 3D culture devices of different biocompatible materials. It is a versatile platform for generating spheroids both in the presence and absence of biological matrices and spheroids are assayed in the same plate where they are seeded, with no need for sample transfer at any stage. Even if we proved that our method could be used as a screening platform, the system needs optimization with a wide range of compounds and cell lines to return reliable results. Interlaboratory collaborations with drug screening expertise would also implement data obtained with our system and contribute to

validating and comparing our results. Our model may be a promising approach for high-throughput spheroids screening and characterization since the production of devices for 96-wells plate format is feasible. In future studies, co-culturing MTSs with cancer-related cells or surrounding non-malignant cells will be used to develop the 3D tumor model for better modeling of *in vivo* solid tumors and microenvironments.

Further, the second topic of the Ph.D. project concerned the development of a microfluidic system to provide separation and interaction of two different cell populations cultured in the chip. Different technologies have been developed for the generation of microfluidic platforms; our system is characterized by ease of production and design simplicity. The main objective was to create a tool to emulate, in a highly automated system, in vitro experiments conducted with standard techniques. Our work illustrates a microfluidic chip design, validation, and implementation. Our results showed that the platform allowed culturing a microglia cell line in two separate areas and selectively treating one single chamber through fine regulation of the flows. Fluid dynamics simulation showed that it is possible to change flows directions and velocity, direct flows in one chamber precisely, and then put the two chambers in communication. We demonstrated that N9 cells could be successfully cultured and immuno-stained within the platform, and the optical transparency of the materials made the system suitable for microscopy analysis. Since we showed the possibility of performing immunostaining within the device, we faced methods for fluorescence analysis of microglial activation. Preliminary experiments with cytoskeletal proteins did not support the hypothesis of finding differences in actin and tubulin cell organization between activated and resting cell populations. However, the immunofluorescence of iNOS mAb provided interesting preliminary results as a specific marker of glial activation. iNOS marker is currently used for western blot analysis in N9 cultures activated according to the standard method. We will test it on our microfluidic system after activating the N9 cell population in a chamber. This will allow us to observe differences between the activated and control culture chamber, replicating the immunostaining analyses on N9 cultured on coverslips.

Compared to other reported microfluidic platforms, this method is more accessible in fabrication, allows real-time cell detection, and is undoubtedly open to further improvements and optimization. Time-lapse imaging could be beneficial for conducting growth analyses with the support of more complex and automated microscopy equipment such as the *Phasefocus Livecyte system* (https://www.phasefocus.com/livecyte), which was available at our Department. Preliminary tests were carried out within this high-content tool, highlighting the potential compatibility with our microfluidic system (***Figure 43***).
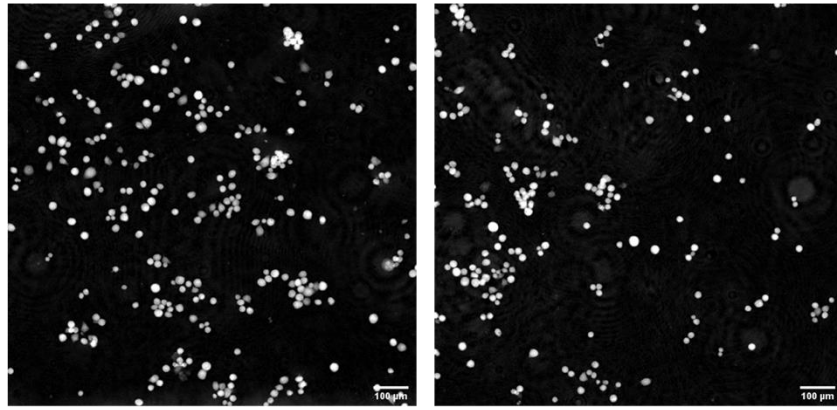
Figure 43: Livecyte images relative of N9 culture within microfluidic device. 10X objective, scale bar 100 μm

It was possible to insert the microfluidic chip inside the *Livecyte* apparatus by creating a gasket obtained in 3D printing that allowed the tubes to exit out of the incubation chamber of the instrument. In this way time-lapse images of the N9 cell culture were obtained inside the microfluidic device. Future perspectives regarding *Livecyte* analysis will include an in-depth investigation of evaporation and air bubbles formation drawbacks. These issues may compromise long-term experiments, one of the main potentials of the apparatus. The combined use of high-content data, like those provided with *Livecyte,* and molecular assays within the microfluidic system, could make it a platform for targeted studies on various types of cellular interaction or assays for drug testing. Lastly, the system successfully maintained a cell culture with finely medium regulation that limited the need for manipulation by the operator for prolonged periods while preserving constant nutrients supply essential to the culture. This aspect could allow prolonged investigations on morphological changes and cellular interaction necessary for the in-depth study of cell dynamics in neurodegenerative pathological contexts. Additionally, we can not exclude the possibility of fabricating more complex microfluidic multi-chip systems. Multiple cell culture chambers are fluidically connected and put into communication, adapting fluid configurations to large-scale experiments. A preliminary attempt was also made in the direction of supporting 3D cell culture in microfluidics, which is already proving to be widely used in many fields of biomedical research (***Figure* 44***).* Flow perfusion techniques can better culture tumor cells in environments that more nearly simulate *in vivo* tumor progression conditions and presence of the complex tumor microenvironment. The possibility of combining and complementing the microfluidic and 3D culture systems would allow making a further step forward concerning *in vitro* models, getting closer to a physiological and similar culture *in vivo* context.

Figure 44: Prototype of a PDMS microfluidic device for 3D cell cultures

We can conclude that there are countless uses in the biomedical and biotechnology field that can be obtained starting from these culturing platforms. Cell structure size and shape can be modified using techniques like micropatterning and microfluidic platforms. Microtechnology solutions can be used to increase the reproducibility of spheroids, as well as to deliver and exchange nutrients, create mechanical stimuli, and monitor growth in real time. Microtechnology also adapts itself to large production, which is necessary for drug testing and commercial applications. Even though microtechnology has enabled spheroids development, their full potential has yet to be investigated. The future of microtechnology-assisted 3D cultures will be determined by how successfully many spheroids can be combined into a single platform to mimic the complex cell-cell milieu observed *in vivo*. For this reason, focusing on these new technologies could allow overcoming many obstacles and limitations imposed by classic culture models, providing results that can be translated more effectively to *in vivo* models.

6. APPENDIX

Detailed information, regarding customized MATLAB scripts and syringe pump hardware and software components used in this work, can be found at the following link:

http://nanobionano.unibo.it/people/ottaviatartagni.html

7. REFERENCES

Agarwal A, Josue Adrian Gossa, Alexander Choa, Megan Laura McCaina, and Kevin Kit Parker. 2011. "Microfluidic Heart on a Chip for Higher Throughput Pharmacological Studies." *Bone* 23 (1): 1–7.

Ahmed, Enas M. 2015. "Hydrogel: Preparation, Characterization, and Applications: A Review." *Journal of Advanced Research* 6 (2): 105–21.

Akther, Fahima, Shazwani Binte Yakob, Nam-Trung Nguyen, and Hang T. Ta. 2020. "Surface Modification Techniques for Endothelial Cell Seeding in PDMS Microfluidic Devices." *Biosensors* 10 (11): 182.

Alemany-Ribes, Mireia, and Carlos E. Semino. 2014. "Bioengineering 3D Environments for Cancer Models." *Advanced Drug Delivery Reviews* 79: 40–49.

Amaral, Robson L.F., Mariza Miranda, Priscyla D Marcato, and Kamilla Swiech. 2017. "Comparative Analysis of 3D Bladder Tumor Spheroids Obtained by Forced Floating and Hanging Drop Methods for Drug Screening." *Frontiers in Physiology* 8 (AUG): 605.

Andersson, Helene, and Albert Van den Berg. 2003. "Microfluidic Devices for Cellomics: A Review." *Sensors and Actuators, B: Chemical* 92 (3): 315–25.

Auner, Alexander W., Kazi M. Tasneem, Dmitry A. Markov, Lisa J. McCawley, and M. Shane Hutson. 2019. "Chemical-PDMS Binding Kinetics and Implications for Bioavailability in Microfluidic Devices." *Lab on a Chip* 19 (5): 864–74.

Barralet, J. E., L. Wang, M. Lawson, J. T. Triffitt, P. R. Cooper, and R. M. Shelton. 2005. "Comparison of Bone Marrow Cell Growth on 2D and 3D Alginate Hydrogels." *Journal of Materials Science: Materials in Medicine* 16 (6): 515–19.

Bauer, Sophie, Charlotte Wennberg Huldt, Kajsa P Kanebratt, Isabell Durieux, Daniela Gunne, Shalini Andersson, Lorna Ewart, et al. 2017. "Functional Coupling of Human Pancreatic Islets and Liver Spheroids On-a-Chip: Towards a Novel Human Ex Vivo Type 2 Diabetes Model." *Scientific Reports* 7 (1).

Bauleth-Ramos, Tomás, Tália Feijão, André Gonçalves, Mohammad Ali Shahbazi, Zehua Liu, Cristina Barrias, Maria José Oliveira, Pedro Granja, Hélder A. Santos, and Bruno Sarmento. 2020. "Colorectal Cancer Triple Co-Culture Spheroid Model to Assess the Biocompatibility and Anticancer Properties of Polymeric Nanoparticles." *Journal of Controlled Release* 323 (December 2019): 398–411.

Becatti, Matteo, Victoria Barygina, Tingting Yu, Richard P Visconti, Veronica Romano, Rüdiger Rudolf, von E Molitor, et al. 2020. "Routine Optical Clearing of 3D-Cell Cultures: Simplicity Forward." *Cell Cultures: Simplicity Forward. Front. Mol. Biosci* 7: 20.

Bershteyn, Marina, Tomasz J. Nowakowski, Alex A. Pollen, Elizabeth Di Lullo, Aishwarya Nene, Anthony Wynshaw-Boris, and Arnold R. Kriegstein. 2017. "Human IPSC-Derived Cerebral Organoids Model Cellular Features of Lissencephaly and Reveal Prolonged Mitosis of Outer Radial Glia." *Cell Stem Cell* 20 (4): 435-449.e4.

Bērziņa, Santa, Alexandra Harrison, Valérie Taly, and Wenjin Xiao. 2021. "Technological Advances in Tumor-on-Chip Technology: From Bench to Bedside." *Cancers*. Cancers (Basel).

Bhang, Suk Ho, Seung Woo Cho, Wan Geun La, Tae Jin Lee, Hee Seok Yang, Ah Young Sun, Sang Hong Baek, Jong Won Rhie, and Byung Soo Kim. 2011. "Angiogenesis in Ischemic Tissue Produced by Spheroid Grafting of Human Adipose-Derived Stromal Cells." *Biomaterials* 32 (11): 2734–47.

Bhatia, Sangeeta N., and Donald E. Ingber. 2014. "Microfluidic Organs-on-Chips." *Nature Biotechnology* 32 (8): 760–72.

Boehnke, Karsten, Philip W. Iversen, Dirk Schumacher, María José Lallena, Rubén Haro, Joaquín Amat, Johannes Haybaeck, et al. 2016. "Assay Establishment and Validation of a High-Throughput Screening Platform for Three-Dimensional Patient-Derived Colon Cancer Organoid Cultures." *Journal of Biomolecular Screening* 21 (9): 931–41.

Bonafede, Roberta, and Raffaella Mariotti. 2017. "ALS Pathogenesis and Therapeutic Approaches: The Role of Mesenchymal Stem Cells and Extracellular Vesicles." *Frontiers in Cellular Neuroscience*. Frontiers Media SA.

Bruns, Thomas, Sarah Schickinger, Rainer Wittig, and Herbert Schneckenburger. 2012. "Preparation Strategy and Illumination of Three-Dimensional Cell Cultures in Light Sheet–Based Fluorescence Microscopy." *Journal of Biomedical Optics* 17 (10): 1015181.

Bryan, Andrea K., Alexi Goranov, Angelika Amon, Scott R. Manalis, and Marc W Kirschner. 2010. "Measurement of Mass, Density, and Volume during the Cell Cycle of Yeast." *Proceedings of the National Academy of Sciences* 107 (3): 999–1004.

Campenot, R. B. 1977. "Local Control of Neurite Development by Nerve Growth Factor." *Proceedings of the National Academy of Sciences of the United States of America* 74 (10): 4516–19.

Chambers, Karen F., Eman M.O. O Mosaad, Pamela J. Russell, Judith A. Clements, and Michael R. Doran. 2014. "3D Cultures of Prostate Cancer Cells Cultured in a Novel High-Throughput Culture Platform Are More Resistant to Chemotherapeutics Compared to Cells Cultured in Monolayer." *PLoS ONE* 9 (11).

Chatzinikolaidou, Maria. 2016. "Cell Spheroids: The New Frontiers in in Vitro Models for Cancer Drug Validation." *Drug Discovery Today* 21 (9): 1553–60.

Chelobanov, Boris, Julia Poletaeva, Anna Epanchintseva, Anastasiya Tupitsyna, Inna Pyshnaya, and Elena Ryabchikova. 2020. "Ultrastructural Features of Gold Nanoparticles Interaction with Hepg2 and Hek293 Cells in Monolayer and Spheroids." *Nanomaterials* 10 (10): 1–23.

Chen, Chun Han, Chia Hwa Lee, Jing Ping Liou, Che Ming Teng, and Shiow Lin Pan. 2015. "Molecular Mechanisms Underlying the Antitumor Activity of (E)-N-Hydroxy-3-(1-(4-Methoxyphenylsulfonyl)-1,2,3,4- Tetrahydroquinolin-6-Yl)Acrylamide in Human Colorectal Cancer Cells in Vitro and in Vivo." *Oncotarget* 6 (34): 35991–2.

Chen, Yongli, Dan Gao, Hongxia Liu, Shuo Lin, and Yuyang Jiang. 2015. "Drug Cytotoxicity and Signaling Pathway Analysis with Three-Dimensional Tumor Spheroids in a Microwell-Based

Microfluidic Chip for Drug Screening." *Analytica Chimica Acta* 898 (October): 85–92.

Chen, Yu-Chih, Xia Lou, Zhixiong Zhang, Patrick Ingram, and Euisik Yoon. 2015. "High-Throughput Cancer Cell Sphere Formation for Characterizing the Efficacy of Photo Dynamic Therapy in 3D Cell Cultures." *Scientific Reports* 5 (June): 1–12.

Cho, Chin-Yi, Tzu-Hsiang Chiang, Li-Hung Hsieh, Wen-Yu Yang, Hsiang-Hao Hsu, and Chih-Kuang Yeh. 2020. "Development of a Novel Hanging Drop Platform for Engineering Controllable 3D Microenvironments."

Cianciosi, Danila, Tamara Y. Forbes-Hernández, Lucia Regolo, José M. Alvarez-Suarez, Denise Quinzi, Azzurra Sargenti, Weibin Bai, Lingmin Tian, Francesca Giampieri, and Maurizio Battino. 2022. "Manuka Honey in Combination with 5-Fluorouracil Decreases Physical Parameters of Colonspheres Enriched with Cancer Stem-like Cells and Reduces Their Resistance to Apoptosis." *Food Chemistry* 374 (November 2021): 131753.

Clayton, Natasha P., Alanna Burwell, Heather Jensen, Barbara F. Williams, Quashana D. Brown, Pamela Ovwigho, Sreenivasa Ramaiahgari, Tonia Hermon, and Darlene Dixon. 2018. "Preparation of Three-Dimensional (3-D) Human Liver (HepaRG) Cultures for Histochemical and Immunohistochemical Staining and Light Microscopic Evaluation." *Toxicologic Pathology* 46 (6): 653–59.

Cristaldi, Domenico Andrea, Azzurra Sargenti, Simone Bonetti, Francesco Musmeci, Cecilia Delprete, Francesco Bacchi, Simone Pasqua, et al. 2020. "A Reliable Flow-Based Method for the Accurate Measure of Mass Density, Size and Weight of Live 3D Tumor Spheroids." *Micromachines* 11 (5).

Cui, X, Y Hartanto, and H Zhang. 2017. "Advances in Multicellular Spheroids Formation." *Journal of the Royal Society Interface*.

Dabrowska, Sylwia, Anna Andrzejewska, Barbara Lukomska, and Miroslaw Janowski. 2019. "Neuroinflammation as a Target for Treatment of Stroke Using Mesenchymal Stem Cells and Extracellular Vesicles." *Journal of Neuroinflammation* 16 (1).

Dadgar, Neda, Alan M. Gonzalez-Suarez, Pouria Fattahi, Xiaonan Hou, John S. Weroha, Alexandre Gaspar-Maia, Gulnaz Stybayeva, and Alexander Revzin. 2020. "A Microfluidic Platform for Cultivating Ovarian Cancer Spheroids and Testing Their Responses to Chemotherapies." *Microsystems and Nanoengineering* 6 (1).

Dai, Xiao jing, Na Li, Le Yu, Zi yang Chen, Rong Hua, Xia Qin, and Yong Mei Zhang. 2015. "Activation of BV2 Microglia by Lipopolysaccharide Triggers an Inflammatory Reaction in PC12 Cell Apoptosis through a Toll-like Receptor 4-Dependent Pathway." *Cell Stress & Chaperones* 20 (2): 321–31.

Däster, Silvio, Nunzia Amatruda, Diego Calabrese, Robert Ivanek, Eleonora Turrini, Raoul A. Droeser, Paul Zajac, et al. 2017. "Induction of Hypoxia and Necrosis in Multicellular Tumor Spheroids Is Associated with Resistance to Chemotherapy Treatment." *Oncotarget* 8 (1): 1725–36.

Dekkers, Johanna F, Cornelis K Van Der Ent, and Jeffrey M Beekman. 2013. "Rare Diseases Novel Opportunities for CFTR-Targeting Drug Development Using Organoids."

Dixit, Chandra K, and Ajeet Kaushik. 2016. *Microfluidics for Biologists.*

Durymanov, Mikhail, Christian Kroll, Anastasia Permyakova, Elizabeth O'Neill, Raed Sulaiman, Michael Person, and Joshua Reineke. 2019. "Subcutaneous Inoculation of 3D Pancreatic Cancer Spheroids Results in Development of Reproducible Stroma-Rich Tumors." *Translational Oncology* 12 (1): 180–89.

Edmondson, Rasheena, Jessica Jenkins Broglie, Audrey F. Adcock, and Liju Yang. 2014. "Three-Dimensional Cell Culture Systems and Their Applications in Drug Discovery and Cell-Based Biosensors." *Assay and Drug Development Technologies.* Mary Ann Liebert Inc.

El-Ali, Jamil, Peter K. Sorger, and Klavs F. Jensen. 2006. "Cells on Chips." *Nature* 442 (7101): 403–11.

Fedorovich, Natalja E., Wouter Schuurman, Hans M. Wijnberg, Henk Jan Prins, P. René Van Weeren, Jos Malda, Jacqueline Alblas, and Wouter J.A. Dhert. 2012. "Biofabrication of Osteochondral Tissue Equivalents by Printing Topologically Defined, Cell-Laden Hydrogel Scaffolds." *Tissue Engineering - Part C: Methods* 18 (1): 33–44.

Fehlauer, Fabian, Martina Muench, Dirk Rades, Lukas J.A. Stalpers, Sieger Leenstra, Paul Van Der Valk, Ben Slotman, Ernst J. Smid, and Peter Sminia. 2005. "Effects of Irradiation and Cisplatin on Human Glioma Spheroids: Inhibition of Cell Proliferation and Cell Migration." *Journal of Cancer Research and Clinical Oncology* 131 (11): 723–32.

Fennema, Eelco, Nicolas Rivron, Jeroen Rouwkema, Clemens van Blitterswijk, and Jan De Boer. 2013. "Spheroid Culture as a Tool for Creating 3D Complex Tissues." *Trends in Biotechnology* 31 (2): 108–15.

Ferreira, L. P., V. M. Gaspar, and J. F. Mano. 2018. "Design of Spherically Structured 3D in Vitro Tumor Models -Advances and Prospects." *Acta Biomaterialia* 75: 11–34.

Firth, Amy L., Tushar Menon, Gregory S. Parker, Susan J. Qualls, Benjamin M. Lewis, Eugene Ke, Carl T. Dargitz, et al. 2015. "Functional Gene Correction for Cystic Fibrosis in Lung Epithelial Cells Generated from Patient IPSCs." *Cell Reports* 12 (9): 1385–90.

Fontoura, Julia C., Christian Viezzer, Fabiana G. dos Santos, Rosane A. Ligabue, Ricardo Weinlich, Renato D. Puga, Dyeison Antonow, Patricia Severino, and Cristina Bonorino. 2020. *Comparison of 2D and 3D Cell Culture Models for Cell Growth, Gene Expression and Drug Resistance. Materials Science and Engineering C.* Vol. 107. Elsevier Ltd.

Friedrich, Juergen, Claudia Seidel, Reinhard Ebner, and Leoni A. Kunz-Schughart. 2009. "Spheroid-Based Drug Screen: Considerations and Practical Approach." *Nature Protocols* 4 (3): 309–24.

Gay, Nicholas J., Martyn F. Symmons, Monique Gangloff, and Clare E. Bryant. 2014. "Assembly and Localization of Toll-like Receptor Signalling Complexes." *Nature Reviews Immunology.* Nat Rev Immunol.

Geiger, Benjamin, Joachim P. Spatz, and Alexander D. Bershadsky. 2009. "Environmental Sensing through Focal Adhesions." *Nature Reviews Molecular Cell Biology 2009 10:1* 10 (1): 21–33.

Gencoglu, Maria F., Lauren E. Barney, Christopher L. Hall, Elizabeth A. Brooks, Alyssa D. Schwartz, Daniel C. Corbett, Kelly R. Stevens, Shelly R. Peyton, and ID Maria F. Gencoglu†, Lauren E. Barney†, Christopher L. Hall†, Elizabeth A. Brooks†, Alyssa D. Schwartz†, Daniel C. Corbett‡, Kelly R. Stevens‡, and Shelly R. Peyton*,†. 2018. "Comparative Study of Multicellular Tumor Spheroid Formation Methods and Implications for Drug Screening." *ACS Biomater Sci Eng* 4 (2): 410–20.

Goodarzi, Saba, Audrey Prunet, Fabien Rossetti, Olivier Tillement, Erika Porcel, Sandrine Lacombe, Ting-Di Wu, et al. 2020. "Quantifying Nanotherapeutics Penetration Using Hydrogel Based Microsystem as a New 3D In-Vitro Platform." *BioRxiv* 1: 29.

Grässer, Ute, Monika Bubel, Daniela Sossong, Martin Oberringer, Tim Pohlemann, and Wolfgang Metzger. 2018. "Dissociation of Mono- and Co-Culture Spheroids into Single Cells for Subsequent Flow Cytometric Analysis." *Annals of Anatomy* 216: 1–8.

Gray, SophieC C., KerriJ J. Kinghorn, and NathanielS S. Woodling. 2020. "Shifting Equilibriums in Alzheimer's Disease: The Complex Roles of Microglia in Neuroinflammation, Neuronal Survival and Neurogenesis." *Neural Regeneration Research* 15 (7): 1208.

Groebe, Karlfried, and Wolfgang Mueller-Klieser. 1996. "On the Relation between Size of Necrosis and Diameter of Tumor Spheroids." *International Journal of Radiation Oncology Biology Physics* 34 (2): 395–401.

Gross, Pamela G., Emil P. Kartalov, Axel Scherer, and Leslie P. Weiner. 2007. "Applications of Microfluidics for Neuronal Studies." *Journal of the Neurological Sciences* 252 (2): 135–43.

Guan, Yuan, Dan Xu, Phillip M. Garfin, Ursula Ehmer, Melissa Hurwitz, Greg Enns, Sara Michie, et al. 2017. "Human Hepatic Organoids for the Analysis of Human Genetic Diseases." *JCI Insight* 2 (17).

Hardelauf, Heike, Jean Philippe Frimat, Joanna D. Stewart, Wiebke Schormann, Ya Yu Chiang, Peter Lampen, Joachim Franzke, et al. 2011. "Microarrays for the Scalable Production of Metabolically Relevant Tumour Spheroids: A Tool for Modulating Chemosensitivity Traits." *Lab on a Chip* 11 (3): 419–28.

Hassell, Bryan A., Girija Goyal, Esak Lee, Alexandra Sontheimer-Phelps, Oren Levy, Christopher S. Chen, and Donald E. Ingber. 2017. "Human Organ Chip Models Recapitulate Orthotopic Lung Cancer Growth, Therapeutic Responses, and Tumor Dormancy In Vitro." *Cell Reports* 21 (2): 508–16.

Hayashi, Kentaro, and Yasuhiko Tabata. 2011. "Preparation of Stem Cell Aggregates with Gelatin Microspheres to Enhance Biological Functions." *Acta Biomaterialia* 7 (7): 2797–2803.

Hickman, Suzanne, Saef Izzy, Pritha Sen, Liza Morsett, and Joseph El Khoury. 2018. *Microglia in Neurodegeneration*. Vol. 21. Nature Publishing Group.

Ho, Wan Yong, Swee Keong Yeap, Chai Ling Ho, Raha Abdul Rahim, and Noorjahan Banu Alitheen. 2012. "Development of Multicellular Tumor Spheroid (MCTS) Culture from Breast Cancer Cell and a High Throughput Screening Method Using the MTT Assay." *PLoS ONE* 7 (9): 44640.

Hockemeyer, Dirk, and Rudolf Jaenisch. 2016. "Induced Pluripotent Stem Cells Meet Genome

Editing." *Cell Stem Cell* 18 (5): 573–86. https://doi.org/10.1016/j.stem.2016.04.013.

Hosmane, Suneil, In Hong Yang, April Ruffin, Nitish Thakor, and Arun Venkatesan. 2010. "Circular Compartmentalized Microfluidic Platform: Study of Axon-Glia Interactions." *Lab on a Chip* 10 (6): 741–47.

Huang, Bu Wei, and Jian Qing Gao. 2018. "Application of 3D Cultured Multicellular Spheroid Tumor Models in Tumor-Targeted Drug Delivery System Research." *Journal of Controlled Release* 270: 246–59.

Huang, Qiong, Xingbin Hu, Wanming He, Yang Zhao, Shihui Hao, Qijing Wu, Shaowei Li, Shuyi Zhang, and Min Shi. 2018. "Fluid Shear Stress and Tumor Metastasis." *Am J Cancer Res*. Vol. 8.

Huang, Yi Ching, Chih Chieh Chan, Wei Ting Lin, Hsien Yi Chiu, Ren Yeu Tsai, Tsung Hua Tsai, Jung Yi Chan, and Sung Jan Lin. 2013. "Scalable Production of Controllable Dermal Papilla Spheroids on PVA Surfaces and the Effects of Spheroid Size on Hair Follicle Regeneration." *Biomaterials* 34 (2): 442–51.

Hughes, Chris S., Lynne M. Postovit, and Gilles A. Lajoie. 2010. "Matrigel: A Complex Protein Mixture Required for Optimal Growth of Cell Culture." *PROTEOMICS* 10 (9): 1886–90.

Huh, Dongeun, Benjamin D. Matthews, Akiko Mammoto, Martin Montoya-Zavala, Hong Yuan Hsin, and Donald E. Ingber. 2010. "Reconstituting Organ-Level Lung Functions on a Chip." *Science (New York, N.Y.)* 328 (5986).

Inamdar, Niraj K., and Jeffrey T. Borenstein. 2011. "Microfluidic Cell Culture Models for Tissue Engineering." *Current Opinion in Biotechnology* 22 (5): 681–89.

Ivanov, Delyan P., Terry L. Parker, David A. Walker, Cameron Alexander, Marianne B. Ashford, Paul R. Gellert, and Martin C. Garnett. 2014. "Multiplexing Spheroid Volume, Resazurin and Acid Phosphatase Viability Assays for High-Throughput Screening of Tumour Spheroids and Stem Cell Neurospheres." *PLoS ONE* 9 (8): 1–14.

Ivanov, Delyan P, and Anna M Grabowska. 2017. "Spheroid Arrays for High-Throughput Single-Cell Analysis of Spatial Patterns and Biomarker Expression in 3D." *Scientific Reports* 7.

Jang, Kyung Jin, Ali Poyan Mehr, Geraldine A. Hamilton, Lori A. McPartlin, Seyoon Chung, Kahp Yang Suh, and Donald E. Ingber. 2013. "Human Kidney Proximal Tubule-on-a-Chip for Drug Transport and Nephrotoxicity Assessment." *Integrative Biology (United Kingdom)* 5 (9): 1119–29.

Janova, Hana, Chotima Böttcher, Inge R. Holtman, Tommy Regen, Denise van Rossum, Alexander Götz, Anne Sophie Ernst, et al. 2016. "CD14 Is a Key Organizer of Microglial Responses to CNS Infection and Injury." *Glia* 64 (4): 635–49.

Jeon, Joong won, Seung Hwan Lee, Donghyun Kim, and Jong Hwan Sung. 2021. "In Vitro Hepatic Steatosis Model Based on Gut–Liver-on-a-Chip." *Biotechnology Progress* 37 (3).

Jiang, Tao, Jose Munguia-Lopez, Salvador Flores-Torres, Joel Grant, Sanahan Vijayakumar, Antonio de Leon-Rodriguez, and Joseph M. Kinsella. 2018. "Bioprintable Alginate/Gelatin Hydrogel 3D in Vitro Model Systems Induce Cell Spheroid Formation." *Journal of Visualized Experiments* 2018 (137): 1–11.

Jin, Jong Shiaw, Tang Yi Tsao, Pei Chang Sun, Cheng Ping Yu, and Ching Tzao. 2012. "SAHA Inhibits the Growth of Colon Tumors by Decreasing Histone Deacetylase and the Expression of Cyclin D1 and Survivin." *Pathology and Oncology Research* 18 (3): 713–20.

Joshi, Jyotsna, Gautam Mahajan, and Chandrasekhar R. Kothapalli. 2018. "Three-Dimensional Collagenous Niche and Azacytidine Selectively Promote Time-Dependent Cardiomyogenesis from Human Bone Marrow-Derived MSC Spheroids." *Biotechnology and Bioengineering* 115 (8): 2013–26.

Joshi, Pranav, Akshata Datar, Kyeong Nam Yu, Soo Yeon Kang, and Moo Yeal Lee. 2018. "High-Content Imaging Assays on a Miniaturized 3D Cell Culture Platform." *Toxicology in Vitro* 50: 147–59.

Kabadi, Pranita K, Marguerite M Vantangoli, April L Rodd, Elizabeth Leary, Samantha J Madnick, Jeffrey R Morgan, Agnes Kane, and Kim Boekelheide. 2017. "Into the Depths: Techniques for in Vitro Three-Dimensional Microtissue Visualization." *Physiology & Behavior* 176 (3): 139–48.

Kamei, Ken ichiro, Momoko Yoshioka, Shiho Terada, Yumie Tokunaga, and Yong Chen. 2019. "Three-Dimensional Cultured Liver-on-a-Chip with Mature Hepatocyte-like Cells Derived from Human Pluripotent Stem Cells." *Biomedical Microdevices* 21 (3).

Kang, Ah Ran, Hye In Seo, Bong Geun Chung, and Sang Hoon Lee. 2015. "Concave Microwell Array-Mediated Three-Dimensional Tumor Model for Screening Anticancer Drug-Loaded Nanoparticles." *Nanomedicine: Nanotechnology, Biology, and Medicine* 11 (5): 1153–61.

Kim, Hyung Joon, Jeong Won Park, Jae Woo Park, Jae Hwan Byun, Behrad Vahidi, Seog Woo Rhee, and Noo Li Jeon. 2012. "Integrated Microfluidics Platforms for Investigating Injury and Regeneration of CNS Axons." *Annals of Biomedical Engineering* 40 (6): 1268–76.

Kleinman, Hynda K., and George R. Martin. 2005a. "Matrigel: Basement Membrane Matrix with Biological Activity." *Seminars in Cancer Biology* 15 (5): 378–86.

Kleinman, Hynda K, and George R Martin. 2005b. "Matrigel: Basement Membrane Matrix with Biological Activity." *Seminars in Cancer Biology* 15: 378–86.

Kochanek, Stanton J., David A. Close, and Paul A. Johnston. 2019. "High Content Screening Characterization of Head and Neck Squamous Cell Carcinoma Multicellular Tumor Spheroid Cultures Generated in 384-Well Ultra-Low Attachment Plates to Screen for Better Cancer Drug Leads." *Assay and Drug Development Technologies* 17 (1): 17–36.

Kondo, Jumpei, Tomoya Ekawa, Hiroko Endo, Kanami Yamazaki, Norio Tanaka, Yoji Kukita, Hiroaki Okuyama, et al. 2019. "High-throughput Screening in Colorectal Cancer Tissue-originated Spheroids." *Cancer Science* 110 (1): 345.

Kratochvil, Michael J., Alexis J. Seymour, Thomas L. Li, Sergiu P. Paşca, Calvin J. Kuo, and Sarah C. Heilshorn. 2019. *Engineered Materials for Organoid Systems*. *Nature Reviews Materials*. Vol. 4.

Kulesza, Jolanta, Monika Pawłowska, and Ewa Augustin. 2021. "The Influence of Antitumor Unsymmetrical Bisacridines on 3d Cancer Spheroids Growth and Viability." *Molecules* 26

(20).

Kuncová-Kallio, Johana, and Pasi J. Kallio. 2006. "PDMS and Its Suitability for Analytical Microfluidic Devices." *Annual International Conference of the IEEE Engineering in Medicine and Biology - Proceedings*, 2486–89.

Lambert, Bieke, Leo De Ridder, Filip De Vos, Guido Slegers, Virginie De Gelder, Christophe Van De Wiele, and Hubert Thierens. 2006. "Assessment of Supra-Additive Effects of Cytotoxic Drugs and Low Dose Rate Irradiation in an in Vitro Model for Hepatocellular Carcinoma." *Canadian Journal of Physiology and Pharmacology* 84 (10): 1121–28.

Laschke, Matthias W., and Michael D. Menger. 2017. "Life Is 3D: Boosting Spheroid Function for Tissue Engineering." *Trends in Biotechnology* 35 (2): 133–44.

Laurent, Jennifer, Céline Frongia, Martine Cazales, Odile Mondesert, Bernard Ducommun, and Valérie Lobjois. 2013. "Multicellular Tumor Spheroid Models to Explore Cell Cycle Checkpoints in 3D."

Law, Andrew M K, Laura Rodriguez de la Fuente, Thomas J Grundy, Guocheng Fang, Fatima Valdes-Mora, and David Gallego-Ortega. 2021. "Advancements in 3D Cell Culture Systems for Personalizing Anti-Cancer Therapies." *Frontiers in Oncology* 11.

Leary, Elizabeth, Claire Rhee, Benjamin T. Wilks, and Jeffrey R. Morgan. 2018. "Quantitative Live-Cell Confocal Imaging of 3D Spheroids in a High-Throughput Format." *SLAS Technology* 23 (3): 231–42.

Lee, Jungwoo, Meghan J. Cuddihy, and Nicholas A. Kotov. 2008. "Three-Dimensional Cell Culture Matrices: State of the Art." *Tissue Engineering - Part B: Reviews* 14 (1): 61–86.

Lee, Jungwoo, Daniel Lilly, Christopher Doty, Paul Podsiadlo, and Nicholas Kotov. 2009. "In Vitro Toxicity Testing of Nanoparticles in 3D Cell Culture." *Small* 5 (10): 1213–21.

Lee, Seung A., Da Yoon No, Edward Kang, Jongil Ju, Dong Sik Kim, and Sang Hoon Lee. 2013. "Spheroid-Based Three-Dimensional Liver-on-a-Chip to Investigate Hepatocyte-Hepatic Stellate Cell Interactions and Flow Effects." *Lab on a Chip* 13 (18): 3529–37.

Leonard, Fransisca, and Biana Godin. 2016. "3D in Vitro Model for Breast Cancer Research Using Magnetic Levitation and Bioprinting Method." In *Methods in Molecular Biology*, 1406:239–51.

Li, Yingjun, Ying Wang, Chong Shen, and Qin Meng. 2020. "Non-Swellable F127-DA Hydrogel with Concave Microwells for Formation of Uniform-Sized Vascular Spheroids." *RSC Advances* 10 (72): 44494–502.

Lin, Hongxin, Taojian Fan, Jian Sui, Guangxing Wang, Jianxin Chen, Shuangmu Zhuo, and Han Zhang. 2019. "Recent Advances in Multiphoton Microscopy Combined with Nanomaterials in the Field of Disease Evolution and Clinical Applications to Liver Cancer." *Nanoscale* 11 (42): 19619–35.

Lin, Ruei-Zhen Zhen, and Hwan-You You Chang. 2008. "Recent Advances in Three-Dimensional Multicellular Spheroid Culture for Biomedical Research." *Biotechnology Journal* 3 (9–10): 1172–84.

Lobjois, Valérie, Céline Frongia, Suzanne Jozan, Isabelle Truchet, and Annie Valette. 2009. "Cell Cycle and Apoptotic Effects of SAHA Are Regulated by the Cellular Microenvironment in HCT116 Multicellular Tumour Spheroids." *European Journal of Cancer* 45 (13): 2402–11.

Lu, Hongxu, and Martina H. Stenzel. 2018. "Multicellular Tumor Spheroids (MCTS) as a 3D In Vitro Evaluation Tool of Nanoparticles." *Small* 14 (13): 1–26.

Luk, Vivienne N., Gary Ch Mo, and Aaron R. Wheeler. 2008. "Pluronic Additives: A Solution to Sticky Problems in Digital Microfluidics." *Langmuir* 24 (12): 6382–89.

Lukashev, Matvey E., and Zena Werb. 1998. "ECM Signalling: Orchestrating Cell Behaviour and Misbehaviour." *Trends in Cell Biology* 8 (11): 437–41.

Madou, Marc J. 2002. *Fundamentals of Microfabrication : The Science of Miniaturization*. Second edition. Boca Raton, Fla. : CRC Press, [2002] ©2002.

Massenzio, Francesca, Emiliano Peña-Altamira, Sabrina Petralla, Marco Virgili, Giampaolo Zuccheri, Andrea Miti, Elisabetta Polazzi, Ilaria Mengoni, Deborah Piffaretti, and Barbara Monti. 2018. "Microglial Overexpression of FALS-Linked Mutant SOD1 Induces SOD1 Processing Impairment, Activation and Neurotoxicity and Is Counteracted by the Autophagy Inducer Trehalose." *Biochimica et Biophysica Acta (BBA) - Molecular Basis of Disease* 1864 (12): 3771–85.

Mathur, Lukas, Martine Ballinger, Ramesh Utharala, and Christoph A Merten. 2020. "Microfluidics as an Enabling Technology for Personalized Cancer Therapy." *Small*.

Mehesz, A. Nagy, J. Brown, Z. Hajdu, W. Beaver, J. V.L. Da Silva, R. P. Visconti, R. R. Markwald, and V. Mironov. 2011. "Scalable Robotic Biofabrication of Tissue Spheroids." *Biofabrication* 3 (2).

Mirbagheri, Marziye, Vahid Adibnia, Bethany R. Hughes, Stephen D. Waldman, Xavier Banquy, and Dae Kun Hwang. 2019. "Advanced Cell Culture Platforms: A Growing Quest for Emulating Natural Tissues." *Materials Horizons* 6 (1): 45–71.

Mittler, Frédérique, Patricia Obeïd, Anastasia V. Rulina, Vincent Haguet, Xavier Gidrol, and Maxim Y. Balakirev. 2017. "High-Content Monitoring of Drug Effects in a 3D Spheroid Model." *Frontiers in Oncology* 7 (DEC): 293.

Moerkens, Renée, Joram Mooiweer, Sebo Withoff, and Cisca Wijmenga. 2019. *Celiac Disease-on-Chip: Modeling a Multifactorial Disease in Vitro*. Vol. 7.

Moor, Lise De, Idriz Merovci, Sarah Baetens, Julien Verstraeten, Paulina Kowalska, Dmitri V. Krysko, Winnok H. De Vos, and Heidi Declercq. 2018. "High-Throughput Fabrication of Vascularized Spheroids for Bioprinting." *Biofabrication* 10 (3).

Moscona, A. 1957. "The Development In Vitro Of Chimeric Aggregates Of Dissociated Embryonic Chick And Mouse Cells." *Proceedings of the National Academy of Sciences* 43 (1): 184–94.

Mysior, Margaritha M., and Jeremy C. Simpson. 2021. "Cell3: A New Vision for Study of the Endomembrane System in Mammalian Cells." *Bioscience Reports* 0 (November): 1–11.

Nath, Sritama, and Gayathri R. Devi. 2016. "Three-Dimensional Culture Systems in Cancer

Research: Focus on Tumor Spheroid Model." *Pharmacology and Therapeutics*. Elsevier Inc.

Naz, Asia, Yi Cui, Christopher J. Collins, David H. Thompson, and Joseph Irudayaraj. 2017. "PLGA-PEG Nano-Delivery System for Epigenetic Therapy." *Biomedicine and Pharmacotherapy* 90: 586–97.

Neurohr, Gabriel E., and Angelika Amon. 2020. "Relevance and Regulation of Cell Density." *Trends in Cell Biology* 30 (3): 213–25.

Nie, Jing, Qing Gao, Yidong Wang, Jiahui Zeng, Haiming Zhao, Yuan Sun, Jian Shen, et al. 2018. "Vessel-on-a-Chip with Hydrogel-Based Microfluidics." *Small* 14 (45): 1–14.

Nikolakopoulou, Polyxeni, Rossana Rauti, Dimitrios Voulgaris, Iftach Shlomy, Ben M. Maoz, and Anna Herland. 2020. "Recent Progress in Translational Engineered in Vitro Models of the Central Nervous System." *Brain : A Journal of Neurology* 143 (11): 3181–3213.

Norberg, K. J., X. Liu, C. Fernández Moro, C. Strell, S. Nania, M. Blümel, A. Balboni, B. Bozóky, R. L. Heuchel, and J. M. Löhr. 2020. "A Novel Pancreatic Tumour and Stellate Cell 3D Co-Culture Spheroid Model." *BMC Cancer* 20 (1): 1–13.

Pampaloni, Francesco, Roli Richa, and Ernst H.K. Stelzer. 2014. "Live Spheroid Formation Recorded with Light Sheet-Based Fluorescence Microscopy." *Methods in Molecular Biology* 1251: 43–57.

Park, Jaewon, Hisami Koito, Jianrong Li, and Arum Han. 2009. "A Multi-Compartment CNS Neuron-Glia Co-Culture Microfluidic Platform."

Park, Jeong Won, Behrad Vahidi, Anne M. Taylor, Seog Woo Rhee, and Noo Li Jeon. 2006. "Microfluidic Culture Platform for Neuroscience Research." *Nature Protocols* 1 (4): 2128–36.

Park, Joseph, Isaac Wetzel, Ian Marriott, Didier Dréau, Carla D'Avanzo, Doo Yeon Kim, Rudolph E. Tanzi, et al. 2018. "A 3D Human Tri-Culture System Modeling Neurodegeneration and Neuroinflammation in Alzheimer's Disease." *Nat Neurosci* 21 (7): 941–51.

Patra, Bishnubrata, Chien Chung Peng, Wei Hao Liao, Chau Hwang Lee, and Yi Chung Tung. 2016. "Drug Testing and Flow Cytometry Analysis on a Large Number of Uniform Sized Tumor Spheroids Using a Microfluidic Device." *Scientific Reports* 6 (January): 1–12.

Petralla, Sabrina, Francesca De Chirico, Andrea Miti, Ottavia Tartagni, Francesca Massenzio, Eleonora Poeta, Marco Virgili, Giampaolo Zuccheri, and Barbara Monti. 2021. "Epigenetics and Communication Mechanisms in Microglia Activation with a View on Technological Approaches." *Biomolecules* 11 (2): 306.

Phan, Nhan, Jenny J Hong, Bobby Tofig, Matthew Mapua, David Elashoff, Neda A Moatamed, Jin Huang, Sanaz Memarzadeh, Robert Damoiseaux, and Alice Soragni. 2019. "A Simple High-Throughput Approach Identifies Actionable Drug Sensitivities in Patient-Derived Tumor Organoids." *Communications Biology* 2 (1).

Pignatta, Sara, Isabella Orienti, Mirella Falconi, Gabriella Teti, Chiara Arienti, Laura Medri, Michele Zanoni, et al. 2015. "Albumin Nanocapsules Containing Fenretinide: Pre-Clinical Evaluation of Cytotoxic Activity in Experimental Models of Human Non-Small Cell Lung Cancer." *Nanomedicine: Nanotechnology, Biology, and Medicine* 11 (2): 263–73.

Porto, Daniel A, Tel M Rouse, Adriana San-Miguel, and Hang Lu. 2016. "Microfluidic Platforms for Quantitative Biology Studies in Model Organisms." In *Microfluidic Methods for Molecular Biology*, 1–18. Cham: Springer International Publishing.

Pratiwi, Feby Wijaya, Chien Chung Peng, Si Han Wu, Chiung Wen Kuo, Chung Yuan Mou, Yi Chung Tung, and Peilin Chen. 2021. "Evaluation of Nanoparticle Penetration in the Tumor Spheroid Using Two-Photon Microscopy." *Biomedicines* 9 (1): 1–14.

Quan, Yi, Miao Sun, Zhaoyi Tan, Jan C T Eijkel, Albert van den Berg, Andries van der Meer, and Yanbo Xie. 2020. "Organ-on-a-Chip: The next Generation Platform for Risk Assessment of Radiobiology." *RSC Advances* 10 (65): 39521–30.

Raff, Martin C, Alan V Whitmore, and John T Finn. 2002. "Neurodegeneration" 296 (May).

Raghavan, Shreya, Maria R. Ward, Katelyn R. Rowley, Rachel M. Wold, Shuichi Takayama, Ronald J. Buckanovich, and Geeta Mehta. 2015. "Formation of Stable Small Cell Number Three-Dimensional Ovarian Cancer Spheroids Using Hanging Drop Arrays for Preclinical Drug Sensitivity Assays." *Gynecologic Oncology* 138 (1): 181–89.

Rane, Tushar D., and Andrea M. Armani. 2016. "Two-Photon Microscopy Analysis of Gold Nanoparticle Uptake in 3D Cell Spheroids." *PLoS ONE* 11 (12).

Reichen, Marcel, Farlan Singh Veraitch, and Nicolas Szita. 2013. "Development of a Multiplexed Microfluidic Platform for the Automated Cultivation of Embryonic Stem Cells." *Journal of Laboratory Automation* 18 (6): 519–29.

Rhee, Seog Woo, Anne M. Taylor, Christina H. Tu, David H. Cribbs, Carl W. Cotman, and Noo Li Jeon. 2005. "Patterned Cell Culture inside Microfluidic Devices." *Lab on a Chip* 5 (1): 102–7.

Rolver, Michala G, Line O Elingaard-Larsen, and Stine F Pedersen. 2019. "Assessing Cell Viability and Death in 3d Spheroid Cultures of Cancer Cells." *Journal of Visualized Experiments* 2019 (148): 59714.

Rothbauer, Mario, Helene Zirath, and Peter Ertl. 2018. "Recent Advances in Microfluidic Technologies for Cell-to-Cell Interaction Studies." *Lab on a Chip* 18 (2): 249–70.

Ruppen, Janine, Lourdes Cortes-Dericks, Emanuele Marconi, Golnaz Karoubi, Ralph A. Schmid, Renwang Peng, Thomas M. Marti, and Olivier T. Guenat. 2014. "A Microfluidic Platform for Chemoresistive Testing of Multicellular Pleural Cancer Spheroids." *Lab on a Chip* 14 (6): 1198–1205.

Ruzycka, Monika, Mihaela R Cimpan, Ivan Rios-Mondragon, and Ireneusz P Grudzinski. 2019. "Microfluidics for Studying Metastatic Patterns of Lung Cancer." *J Nanobiotechnol* 17: 71.

Santo, Vítor E., Marta F. Estrada, Sofia P. Rebelo, Sofia Abreu, Inês Silva, Catarina Pinto, Susana C. Veloso, et al. 2016. "Adaptable Stirred-Tank Culture Strategies for Large Scale Production of Multicellular Spheroid-Based Tumor Cell Models." *Journal of Biotechnology* 221: 118–29.

Sargenti, Azzurra, Francesco Musmeci, Francesco Bacchi, Cecilia Delprete, Domenico Andrea Cristaldi, Federica Cannas, Simone Bonetti, et al. 2020. "Physical Characterization of Colorectal Cancer Spheroids and Evaluation of NK Cell Infiltration Through a Flow-Based

Analysis." *Frontiers in Immunology* 11 (December): 1–13.

Schneckenburger, Herbert, and Verena Richter. 2021. "Challenges in 3D Live Cell Imaging." *Photonics* 8 (7).

Schrum, David P., Christopher T. Culbertson, Stephen C. Jacobson, and J. Michael Ramsey. 1999. "Microchip Flow Cytometry Using Electrokinetic Focusing." *Analytical Chemistry* 71 (19): 4173–77.

Schumacher, Dirk, Geoffroy Andrieux, Karsten Boehnke, Marlen Keil, Alessandra Silvestri, Maxine Silvestrov, Ulrich Keilholz, et al. 2019. "Heterogeneous Pathway Activation and Drug Response Modelled in Colorectal-Tumor-Derived 3D Cultures." *PLoS Genetics* 15 (3).

Shariati, Laleh, Yasaman Esmaeili, Shaghayegh Haghjooy Javanmard, Elham Bidram, and Abbas Amini. 2021. "Organoid Technology: Current Standing and Future Perspectives." *Stem Cells*.

Shi, Wentao, Jean Kwon, Yongyang Huang, Jifu Tan, Christopher G. Uhl, Ran He, Chao Zhou, and Yaling Liu. 2018. "Facile Tumor Spheroids Formation in Large Quantity with Controllable Size and High Uniformity." *Scientific Reports* 8 (1): 1–9.

Singh, Manjulata, David A Close, Shilpaa Mukundan, Paul A Johnston, and Shilpa Sant. 2015. "Production of Uniform 3D Microtumors in Hydrogel Microwell Arrays for Measurement of Viability, Morphology, and Signaling Pathway Activation." *Assay and Drug Development Technologies* 13 (9).

Sontheimer-Phelps, Alexandra, Bryan A. Hassell, and Donald E. Ingber. 2019. "Modelling Cancer in Microfluidic Human Organs-on-Chips." *Nature Reviews Cancer* 19 (2): 65–81.

Stockslager, Max A., Seth Malinowski, Mehdi Touat, Jennifer C. Yoon, Jack Geduldig, Mahnoor Mirza, Annette S. Kim, et al. 2021. "Functional Drug Susceptibility Testing Using Single-Cell Mass Predicts Treatment Outcome in Patient-Derived Cancer Neurosphere Models." *Cell Reports* 37 (1): 109788.

Sutherland, R. M., J. A. McCredie, and W. R. Inch. 1971. "Growth of Multicell Spheroids in Tissue Culture as a Model of Nodular Carcinomas." *Journal of the National Cancer Institute* 46 (1): 113–20.

Taghavi, Sahar, Mohammad Ramezani, Mona Alibolandi, Khalil Abnous, and Seyed Mohammad Taghdisi. 2017. "Chitosan-Modified PLGA Nanoparticles Tagged with 5TR1 Aptamer for in Vivo Tumor-Targeted Drug Delivery." *Cancer Letters* 400: 1–8.

Tang, Yu, and Weidong Le. 2016. "Differential Roles of M1 and M2 Microglia in Neurodegenerative Diseases." *Molecular Neurobiology* 53 (2): 1181–94.

Taylor, Anne M., Seog Woo Rhee, Christina H. Tu, David H. Cribbs, Carl W. Cotman, and Noo Li Jeon. 2003. "Microfluidic Multicompartment Device for Neuroscience Research." *Langmuir* 19 (5): 1551–56.

Tentler, John J., Aik Choon Tan, Colin D. Weekes, Antonio Jimeno, Stephen Leong, Todd M. Pitts, John J. Arcaroli, Wells A. Messersmith, and S. Gail Eckhardt. 2012. "Patient-Derived Tumour Xenografts as Models for Oncology Drug Development." *Nature Reviews Clinical*

Oncology 9 (6): 338–50.

Thomas, Gilberto L., Vladimir Mironov, Agnes Nagy-Mehez, and José C.M. Mombach. 2014. "Dynamics of Cell Aggregates Fusion: Experiments and Simulations." *Physica A: Statistical Mechanics and Its Applications* 395: 247–54.

Trantidou, Tatiana, Yuval Elani, Edward Parsons, and Oscar Ces. 2017. "Hydrophilic Surface Modification of Pdms for Droplet Microfluidics Using a Simple, Quick, and Robust Method via Pva Deposition." *Microsystems and Nanoengineering* 3.

Trumpi, Kari, David A Egan, Thomas T Vellinga, Inne H.M. Borel Rinkes, and Onno Kranenburg. 2015. "Paired Image- and FACS-Based Toxicity Assays for High Content Screening of Spheroid-Type Tumor Cell Cultures." *FEBS Open Bio* 5: 85–90.

Tseng, Hubert, Jacob A Gage, Tsaiwei Shen, William L Haisler, Shane K Neeley, Sue Shiao, Jianbo Chen, et al. 2015. "A Spheroid Toxicity Assay Using Magnetic 3D Bioprinting and Real-Time Mobile Device-Based Imaging." *Nature Publishing Group*.

Turksen, Kursad. 2019. *Organoids*. Edited by Kursad Turksen. Vol. 1576. Methods in Molecular Biology. New York, NY: Springer New York.

Uroukov, Ivan S., and David Patton. 2008. "Optimizing Environmental Scanning Electron Microscopy of Spheroidal Reaggregated Neuronal Cultures." *Microscopy Research and Technique* 71 (11): 792–801.

Verjans, Eddy Tim, Jordi Doijen, Walter Luyten, Bart Landuyt, and Liliane Schoofs. 2018. "Three-Dimensional Cell Culture Models for Anticancer Drug Screening: Worth the Effort?" *Journal of Cellular Physiology* 233 (4): 2993–3003.

Vinci, Maria, Sharon Gowan, Frances Boxall, Lisa Patterson, Miriam Zimmermann, William Court, Cara Lomas, Marta Mendiola, David Hardisson, and Suzanne A. Eccles. 2012. "Advances in Establishment and Analysis of Three-Dimensional Tumor Spheroid-Based Functional Assays for Target Validation and Drug Evaluation." *BMC Biology* 10 (1): 29.

Virgone-Carlotta, Angélique, Manon Lemasson, Hichem C. Mertani, Jean-Jacques Jacques Diaz, Sylvain Monnier, Thomas Dehoux, Hélène Delanoë-Ayari, Charlotte Rivière, and Jean-Paul Paul Rieu. 2017. "In-Depth Phenotypic Characterization of Multicellular Tumor Spheroids: Effects of 5-Fluorouracil." Edited by Javier S. Castresana. *PLoS ONE* 12 (11): e0188100.

Walzl, Angelika, Christine Unger, Nina Kramer, Daniela Unterleuthner, Martin Scherzer, Markus Hengstschläger, Dagmar Schwanzer-Pfeiffer, and Helmut Dolznig. 2014. "The Resazurin Reduction Assay Can Distinguish Cytotoxic from Cytostatic Compounds in Spheroid Screening Assays." *Journal of Biomolecular Screening* 19 (7): 1047–59.

Wang, Hao, Chun Hua Chi, Ying Zhang, Bin Shi, Ru Jia, and Ben Jun Wang. 2019. "Effects of Histone Deacetylase Inhibitors on Atp-Binding Cassette Transporters in Lung Cancer A549 and Colorectal Cancer HCT116 Cells." *Oncology Letters* 18 (1): 63–71.

Wang, Jian Zheng, Yu Xia Zhu, Hui Chao Ma, Si Nan Chen, Ji Ye Chao, Wen Ding Ruan, Duo Wang, Feng Guang Du, and Yue Zhong Meng. 2016. "Developing Multi-Cellular Tumor Spheroid Model (MCTS) in the Chitosan/Collagen/Alginate (CCA) Fibrous Scaffold for Anticancer Drug Screening." *Materials Science and Engineering C* 62: 215–25.

Wang, Lin, and Rebecca L. 2011. "Biomimetic Topography: Bioinspired Cell Culture Substrates and Scaffolds." *Advances in Biomimetics*.

Wang, Qian, Shixia Bu, Dedong Xin, Boning Li, Lan Wang, and Dongmei Lai. 2018. "Autophagy Is Indispensable for the Self-Renewal and Quiescence of Ovarian Cancer Spheroid Cells with Stem Cell-like Properties." *Oxidative Medicine and Cellular Longevity* 2018.

Wang, Wendy Wei Wei, Salman R. Khetani, Stacy Krzyzewski, David B. Duignan, and R. Scott Obach. 2010. "Assessment of a Micropatterned Hepatocyte Coculture System to Generate Major Human Excretory and Circulating Drug Metabolites." *Drug Metabolism and Disposition: The Biological Fate of Chemicals* 38 (10): 1900–1905.

Weichert, Wilko, Annika Röske, and Silvia Niesporek. 2008. "Class I Histone Deacetylase Expression Has Independent Prognostic Impact in Human Colorectal Cancer: Specific Role of Class I Histone Deacetylases In Vitro and In Vivo." *Clin Cancer Res* 14: 1669–77.

Weiswald, Louis-Bastien, Dominique Bellet, Virginie Dangles-Marie, Michael Smith Genome, Jean-Paul Driot Transformative Research Grant, and Laurent Bloch Cancer Research Grant. 2014. "Spherical Cancer Models in Tumor Biology." *NEO* 17: 1–15.

Weiswald, Louis Bastien, Dominique Bellet, and Virginie Dangles-Marie. 2015. "Spherical Cancer Models in Tumor Biology." *Neoplasia (United States)* 17 (1): 1–15.

Whatley, Benjamin R., Xiaowei Li, Ning Zhang, and Xuejun Wen. 2014. "Magnetic-Directed Patterning of Cell Spheroids." *Journal of Biomedical Materials Research - Part A* 102 (5): 1537–47.

Wolf, Susanne A., H. W.G.M. Boddeke, and Helmut Kettenmann. 2017. "Microglia in Physiology and Disease." *Annual Review of Physiology*. Annual Reviews.

Xiang, Yunqing, Hui Wen, Yue Yu, Mingqiang Li, Xiongfei Fu, and Shuqiang Huang. 2020. "Gut-on-Chip: Recreating Human Intestine in Vitro." *Journal of Tissue Engineering* 11.

Xie, Jun, Chengqian Zhang, Fu Gu, Yunming Wang, Jianzhong Fu, and Peng Zhao. 2019. "An Accurate and Versatile Density Measurement Device: Magnetic Levitation." *Sensors and Actuators, B: Chemical* 295 (February): 204–14.

Xiong, Xiao Yi, Liang Liu, and Qing Wu Yang. 2016. "Functions and Mechanisms of Microglia/Macrophages in Neuroinflammation and Neurogenesis after Stroke." *Progress in Neurobiology*.

Yakavets, Ilya, Samuel Jenard, Aurelie Francois, Yulia Maklygina, Victor Loschenov, Henri Pierre Lassalle, Gilles Dolivet, and Lina Bezdetnaya. 2019. "Stroma-Rich Co-Culture Multicellular Tumor Spheroids as a Tool for Photoactive Drugs Screening." *Journal of Clinical Medicine* 8 (10).

Yu, Miao, Aria Mahtabfar, Paul Beelen, Yasir Demiryurek, David I. Shreiber, Jeffrey D. Zahn, Ramsey A. Foty, Liping Liu, and Hao Lin. 2018. "Coherent Timescales and Mechanical Structure of Multicellular Aggregates." *Biophysical Journal* 114 (11): 2703–16.

Zanoni, Michele, Filippo Piccinini, Chiara Arienti, Alice Zamagni, Spartaco Santi, Rolando Polico,

Alessandro Bevilacqua, and Anna Tesei. 2016. "3D Tumor Spheroid Models for in Vitro Therapeutic Screening: A Systematic Approach to Enhance the Biological Relevance of Data Obtained." *Scientific Reports* 6 (January): 1–11.

Zaremba, Leszek S., and Włodzimierz H. Smoleński. 2003. "Cell Culture in 3-Dimensional Microfluidic Structure of PDMS." *Annals of Operations Research* 97 (1–4): 131–41.

Zhang, Binbin, Yang Li, Gaoshang Wang, Zhidong Jia, Haiyan Li, Qing Peng, and Yi Gao. 2018. "Fabrication of Agarose Concave Petridish for 3D-Culture Microarray Method for Spheroids Formation of Hepatic Cells." *Journal of Materials Science: Materials in Medicine* 29 (5).

Zhao, Yuliang, Hok Sum Sam Lai, Guanglie Zhang, Gwo Bin Lee, and Wen Jung Li. 2014. "Rapid Determination of Cell Mass and Density Using Digitally Controlled Electric Field in a Microfluidic Chip." *Lab on a Chip* 14 (22): 4426–34.

Zhaohui, Xiao Wan, Li Hua, Ye Zhanfeng Cui, Xiao Wan, Zhaohui Li, Hua Ye, and Zhanfeng Cui. 2016. "Three-Dimensional Perfused Tumour Spheroid Model for Anti-Cancer Drug Screening." *Biotechnology Letters* 38 (8): 1389–95.

Zoetemelk, Marloes, Magdalena Rausch, Didier J. Colin, Olivier Dormond, and Patrycja Nowak-Sliwinska. 2019. "Short-Term 3D Culture Systems of Various Complexity for Treatment Optimization of Colorectal Carcinoma." *Scientific Reports* 9 (1): 1–14.

Zweifel, Larry S., Rejji Kuruvilla, and David D. Ginty. 2005. "Functions and Mechanisms of Retrograde Neurotrophin Signalling." *Nature Reviews Neuroscience* 6 (8): 615–25.